

Introduction to Climate

Tomoaki OSE (MRI/JMA)

Climate Research Department
Meteorological Research Institute (MRI/JMA)

Climate and Climate System

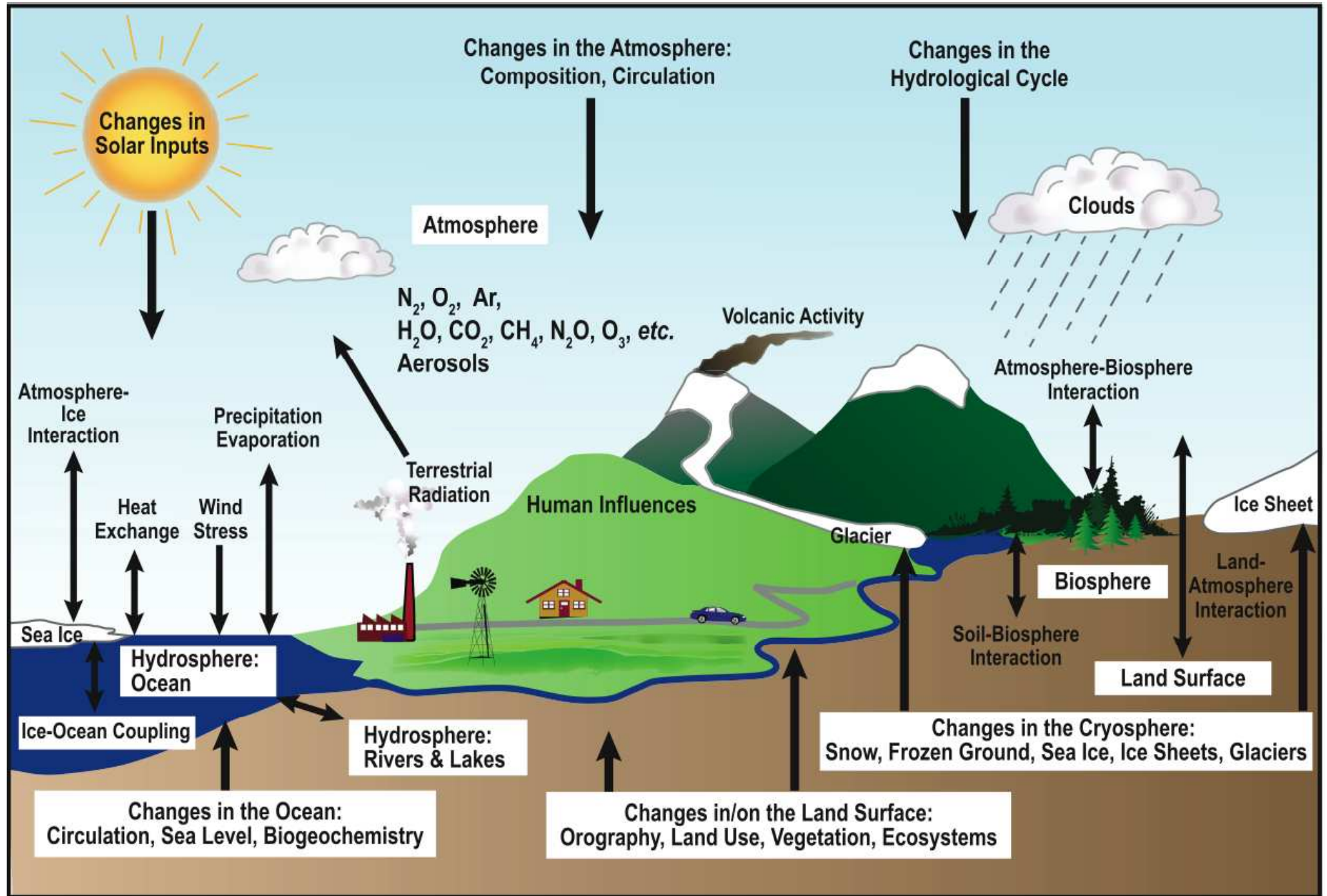
“**Weather** is what is happening to the atmosphere at any given time.

Climate in a narrow sense is the "average weather," the **statistical description** over a period of time.”

Climate is formed in the interactions in **climate system**, consisting of **atmosphere** including composition and circulation, the **ocean**, hydrosphere, land surface, biosphere, **snow and ice**, solar and volcanic activities in its spatial and temporal variability.

Climate System

http://ipcc-wg1.ucar.edu/wg1/FAQ/wg1_faq-1.2.html



Schematic view of the components of the climate system, their processes and interactions.

Radiative Balance



Radiative Balance between Earth and Space

Solar Radiation

■ Solar constant : $S \approx 1370 \text{ Wm}^{-2}$

■ insolation : $\frac{S}{4} \approx 342 \text{ Wm}^{-2}$

■ planetary albedo : $\alpha_p \approx 0.31$

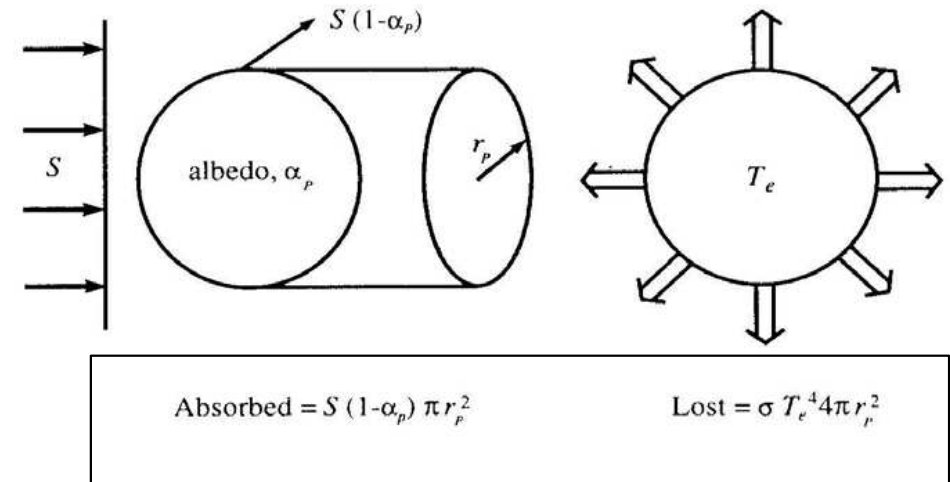
■ absorption : $\frac{S}{4}(1 - \alpha_p) \approx 235 \text{ Wm}^{-2}$

Terrestrial Radiation

■ equilibrium radiative temperature : T_e^*

■ emission : σT_e^{*4}

Earth's temperature observed from the cosmic space



Radiation Balance

■ Balance between absorbed solar radiation and terrestrial emission

$$T_e^* = \sqrt[4]{\frac{S(1 - \alpha_p)}{4\sigma}} \approx 254 \text{ K} \approx -19^\circ \text{ C}$$

Surface Temperature = 15° C

Difference between Equilibrium radiative temperature and Ground Surface Temperature

■ Venus

- Solar constant : 2600 W/m²
- planetary albedo : 0.77
- Equilibrium radiative temperature : - 46° C

■ Earth

- Solar constant : $S \approx 1370 \text{ Wm}^{-2}$
- planetary albedo : $\alpha_p \approx 0.31$
- Equilibrium radiative temperature

$$T_e^* = \sqrt[4]{\frac{S(1-\alpha_p)}{4\sigma}} \approx 254K \approx -19^\circ C$$

■ Mars

- Solar constant : 590 W/m²
- planetary albedo : 0.15
- Equilibrium radiative temperature : -56° C

Surface Temperature

457° C

Surface Pressure

90,000hPa



Surface Temperature

15° C

Surface Pressure

1,000hPa



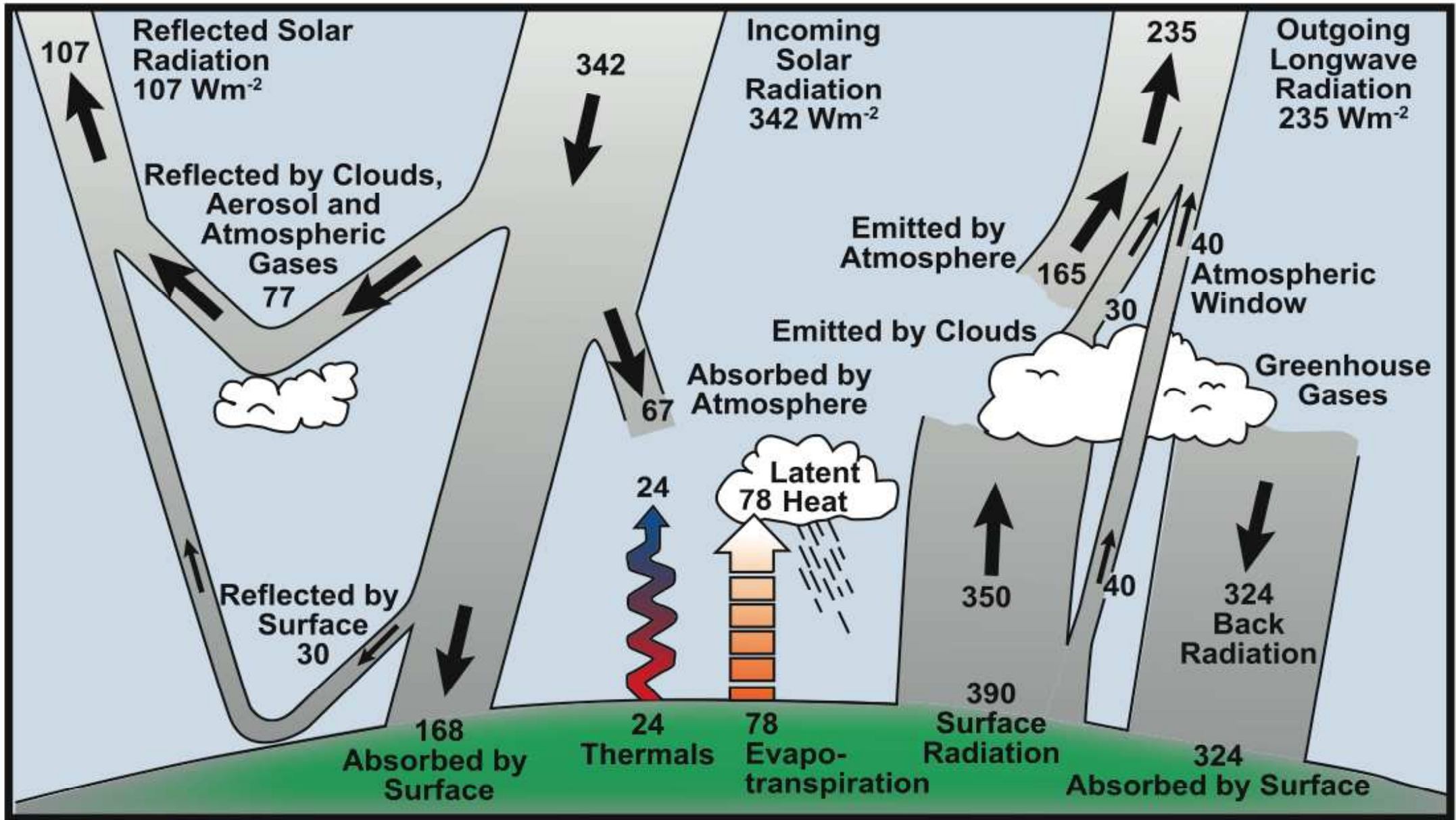
Surface Temperature

-55° C

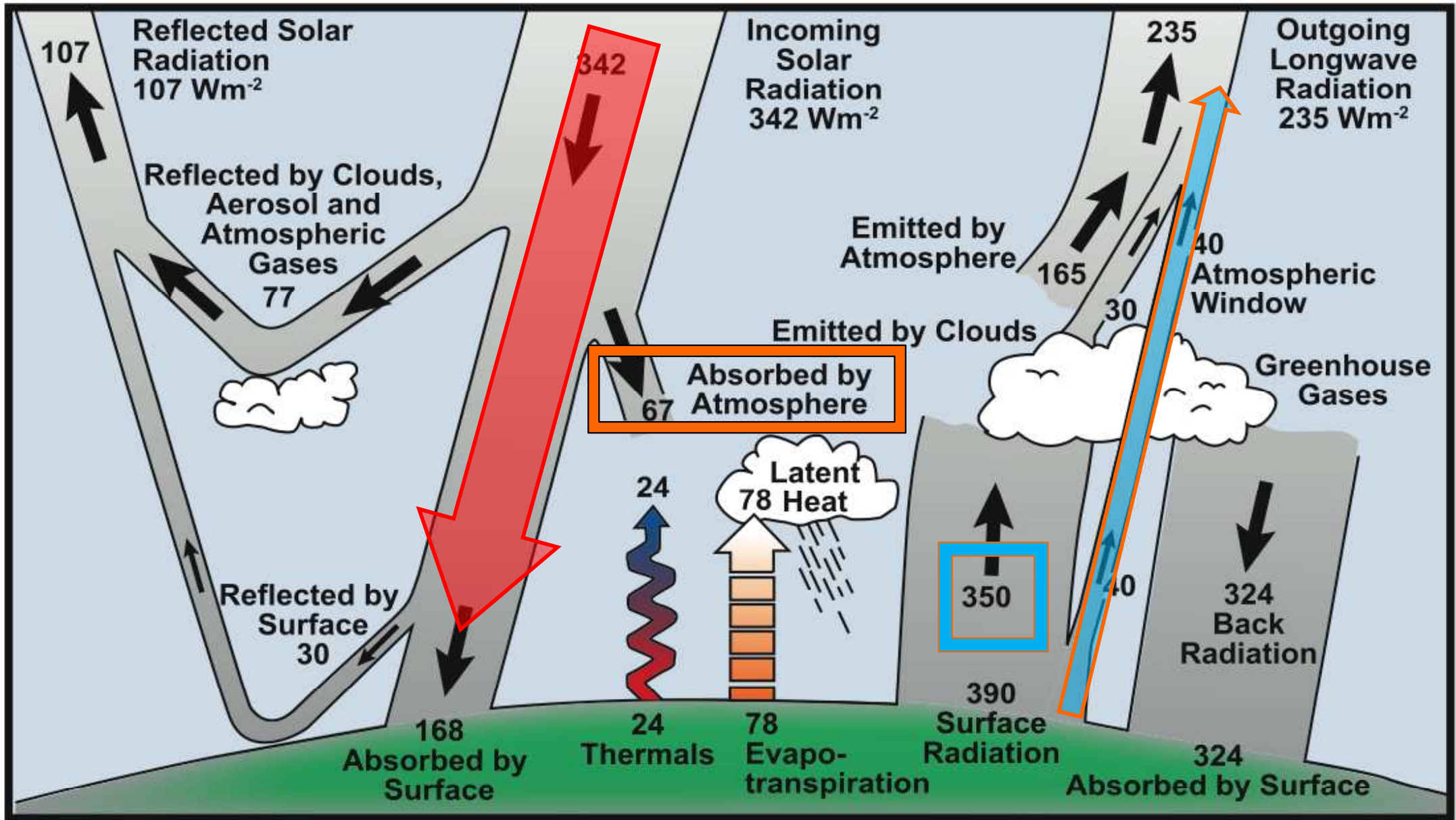
Surface Pressure

10hPa





Estimate of the Earth's annual and global mean energy balance. Over the long term, the amount of incoming solar radiation absorbed by the Earth and atmosphere is balanced by the Earth and atmosphere releasing the same amount of outgoing longwave radiation. About half of the incoming solar radiation is absorbed by the Earth's surface. This energy is transferred to the atmosphere by warming the air in contact with the surface (thermals), by evapotranspiration and by longwave radiation that is absorbed by clouds and greenhouse gases. The atmosphere in turn radiates longwave energy back to Earth as well as out to space. Source: Kiehl and Trenberth (1997).



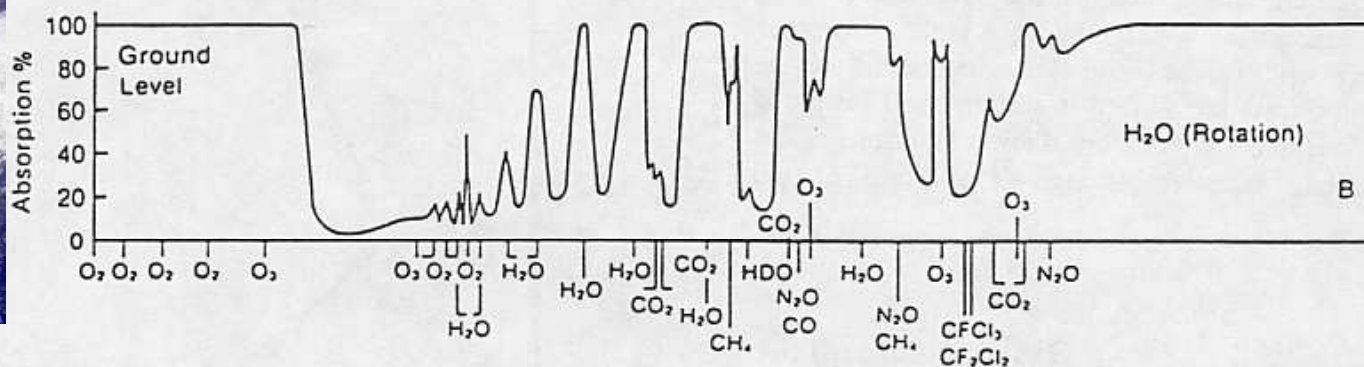
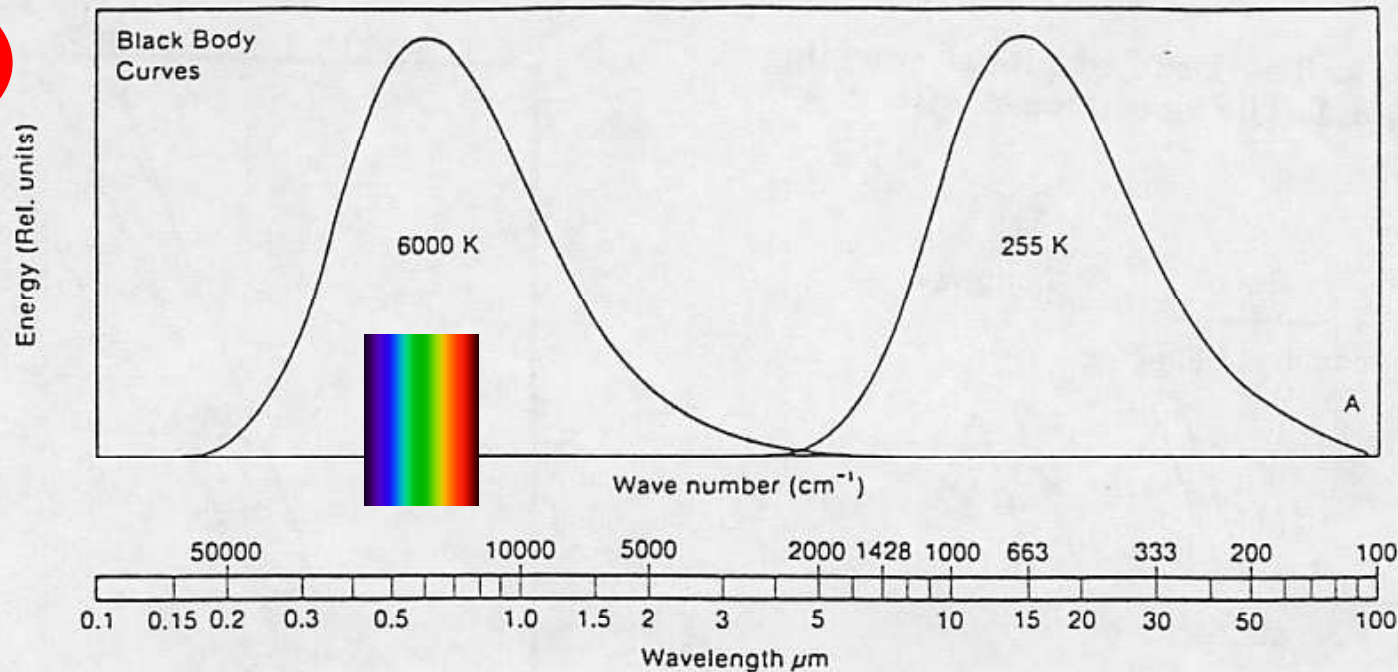
Estimate of the Earth's annual and global mean energy balance. Over the long term, the amount of incoming solar radiation absorbed by the Earth and atmosphere is balanced by the Earth and atmosphere releasing the same amount of outgoing longwave radiation. About half of the incoming solar radiation is absorbed by the Earth's surface. This energy is transferred to the atmosphere by warming the air in contact with the surface (thermals), by evapotranspiration and by longwave radiation that is absorbed by clouds and greenhouse gases. The atmosphere in turn radiates longwave energy back to Earth as well as out to space. Source: Kiehl and Trenberth (1997).

Absorption of Radiation from 6000K and 255K Blackbodies

Solar radiation

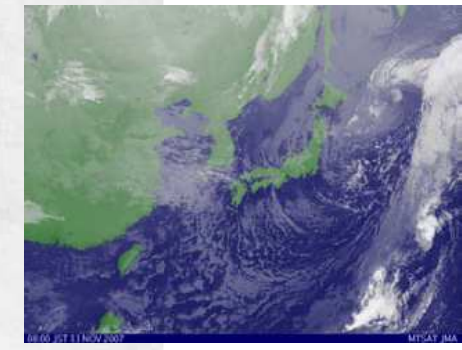
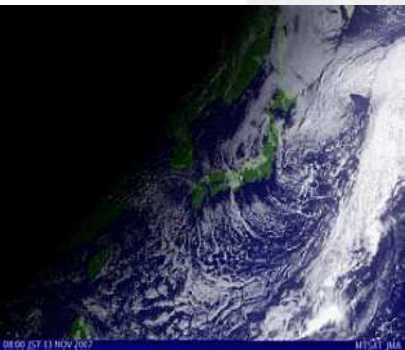


Terrestrial radiation



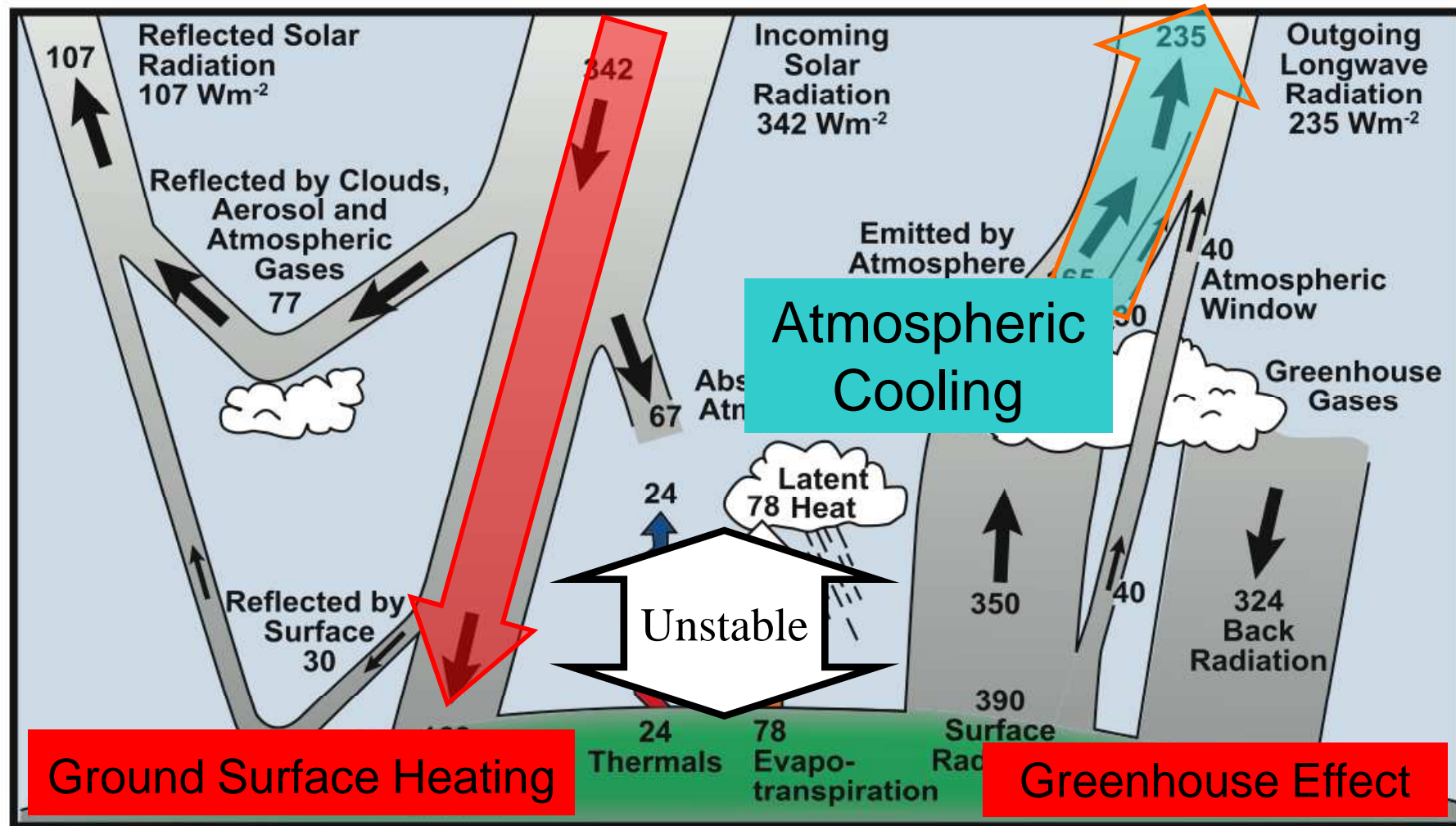
(a) Spectral distribution of long-wave emission from blackbodies at 6000 K and 255 K, corresponding to the mean emitting temperatures of the Sun and Earth, respectively, and (b) percentage of atmospheric absorption for radiation passing from

the top of the atmosphere to the surface. Notice the comparatively weak absorption of the solar spectrum and the region of weak absorption from 8 to 12 μm in the long-wave spectrum [from MacCracken and Luther, 1985].



Radiative heating tends to create vertical instability between heated ground and cooled atmosphere on average

http://ipcc-wg1.ucar.edu/wg1/FAQ/wg1_faq-1.1.html



Estimate of the Earth's annual and global mean energy balance. Over the long term, the amount of incoming solar radiation absorbed by the Earth and atmosphere is balanced by the Earth and atmosphere releasing the same amount of outgoing longwave radiation. About half of the incoming solar radiation is absorbed by the Earth's surface. This energy is transferred to the atmosphere by warming the air in contact with the surface (thermals), by evapotranspiration and by longwave radiation that is absorbed by clouds and greenhouse gases. The atmosphere in turn radiates longwave energy back to Earth as well as out to space. Source: Kiehl and Trenberth (1997).

SYUKURO MANABE AND ROBERT F. STRICKLER

General Circulation Research Laboratory, U. S. Weather Bureau, Washington, D. C.
(Manuscript received 19 December 1963, in revised form 13 April 1964)

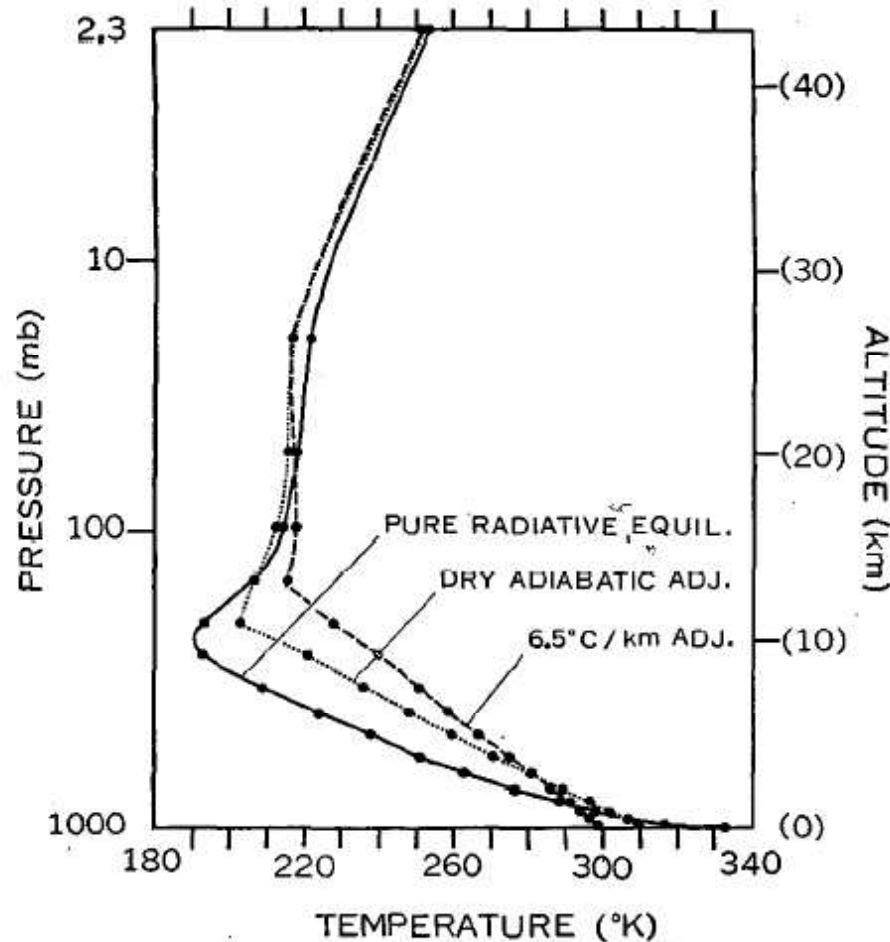


FIG. 4. The dashed, dotted, and solid lines show the thermal equilibrium with a critical lapse rate of 6.5 deg km^{-1} , a dry-adiabatic critical lapse rate (10 deg km^{-1}), and pure radiative equilibrium.

Typical condition at 35N in April

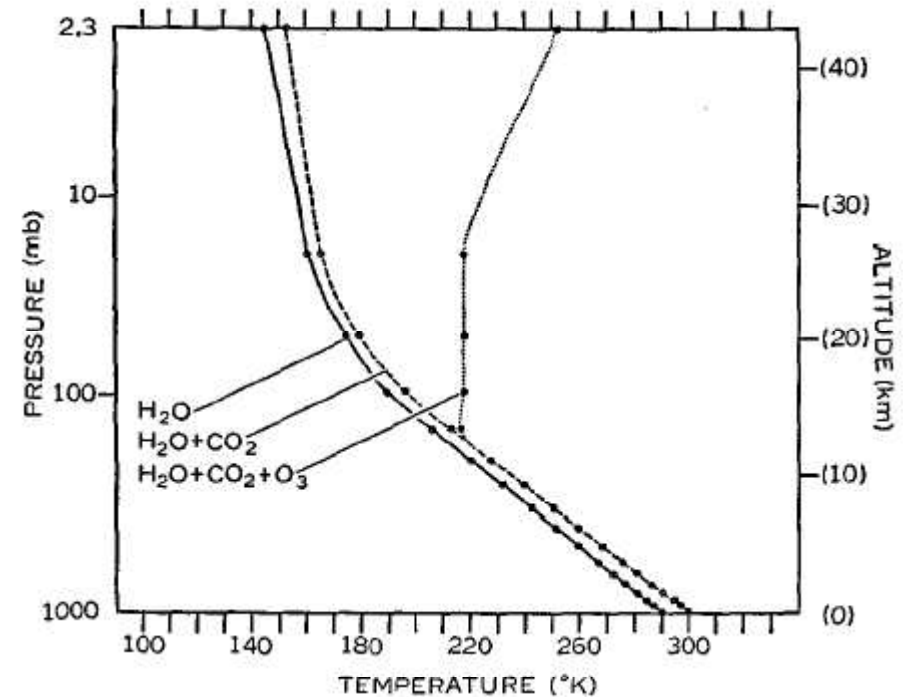


FIG. 6c. Thermal equilibrium of various atmospheres which have a critical lapse rate of 6.5 deg km^{-1} . Vertical distributions of gaseous absorbers at 35N, April, were used. $S_e = 2 \text{ ly min}^{-1}$, $\cos \bar{\mu} = 0.5$, $r = 0.5$, no clouds.

Observed Temperature

1-D model Simulations for each latitudes

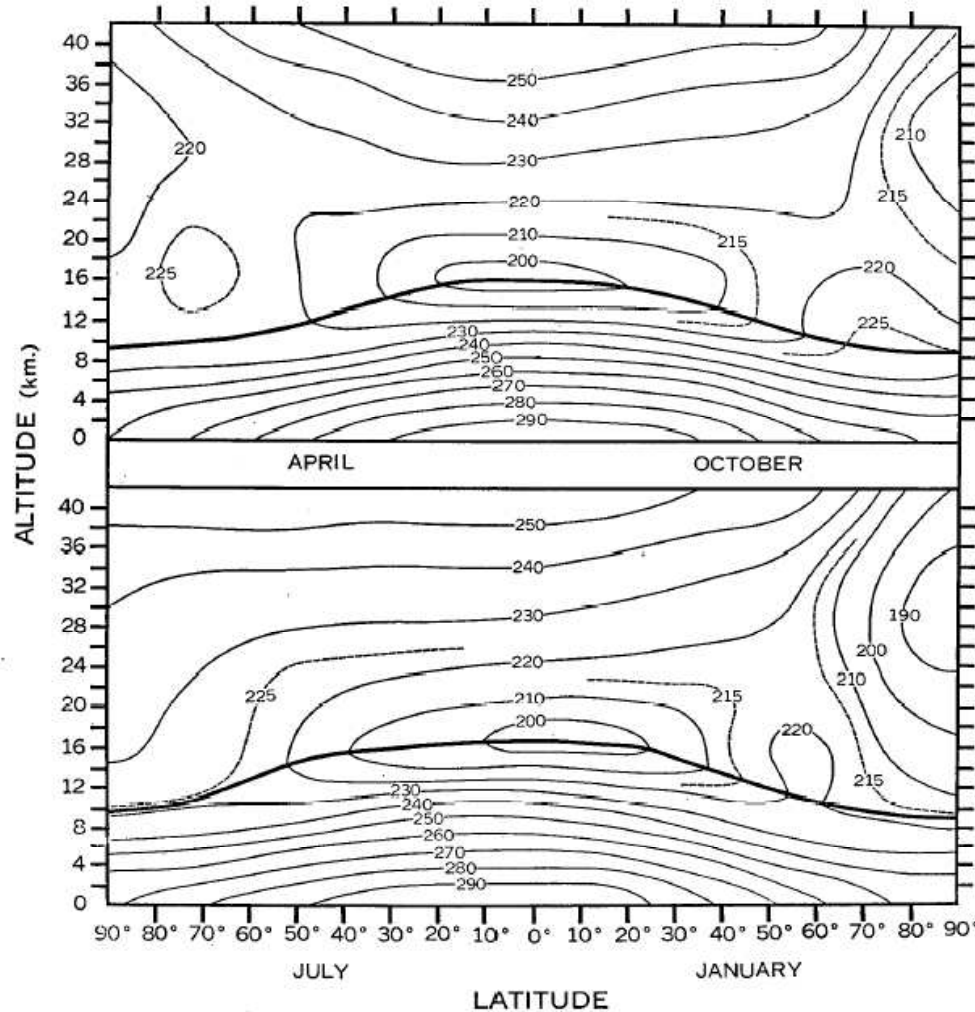


FIG. 12. Distribution of the observed temperature (deg k) in the northern hemisphere for different seasons. From J. London (1956).

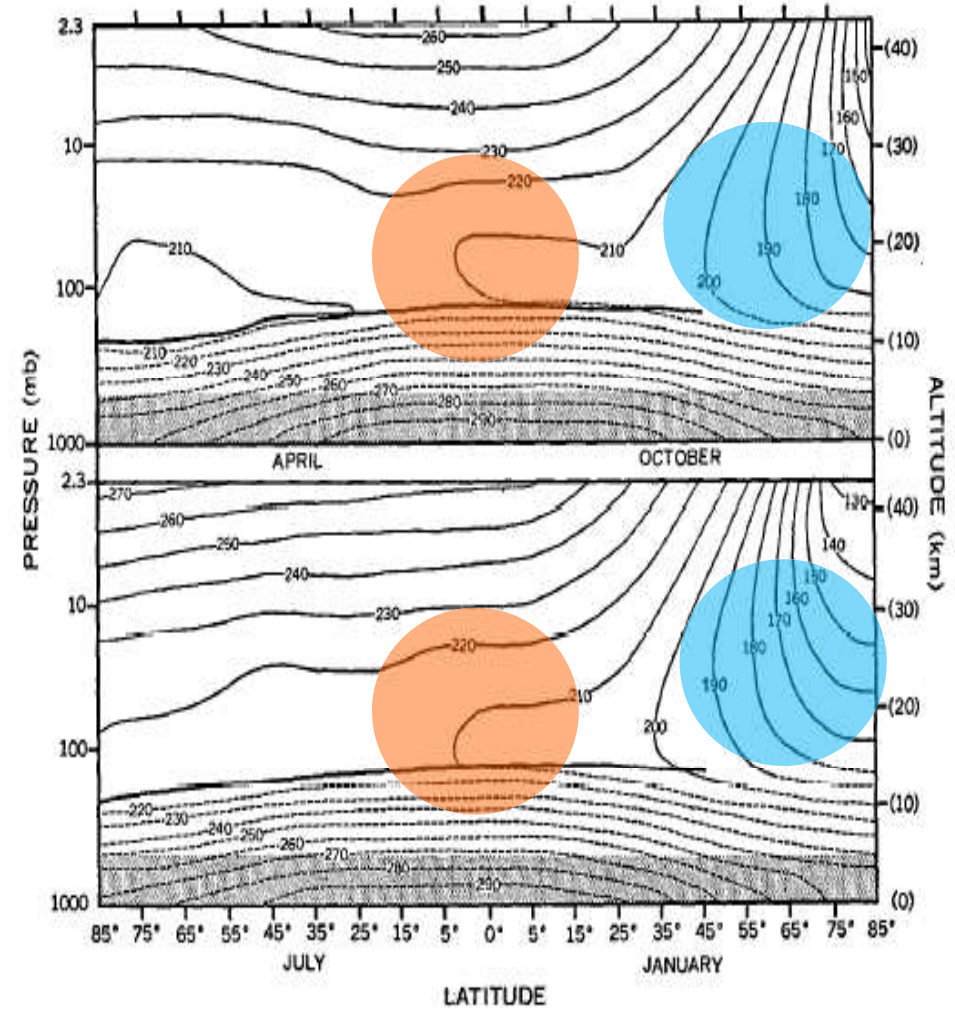


FIG. 13. The local radiative equilibrium temperature of the stratosphere. The shaded area is the region where the temperature was fixed at the observed value. Above the shaded area the state of the convective equilibrium, whose critical lapse rate for convective adjustment is deg km^{-1} , is shown. The region covered by solid lines is in local radiative equilibrium.

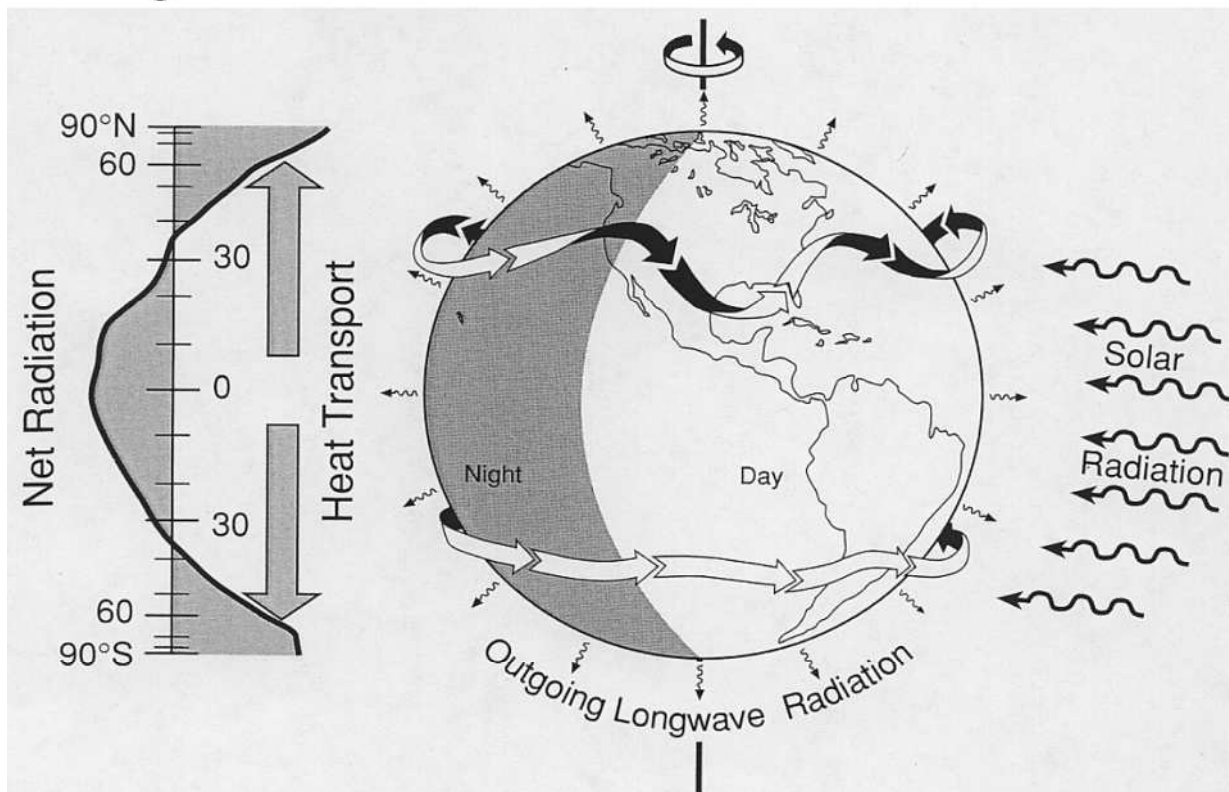
Horizontal Radiative Imbalance and Circulations



Imbalanced horizontal distribution of radiative heating

(1) Latitudinal Imbalance between Pole and Tropics Timescale=1 year

Driving Forces of Climate



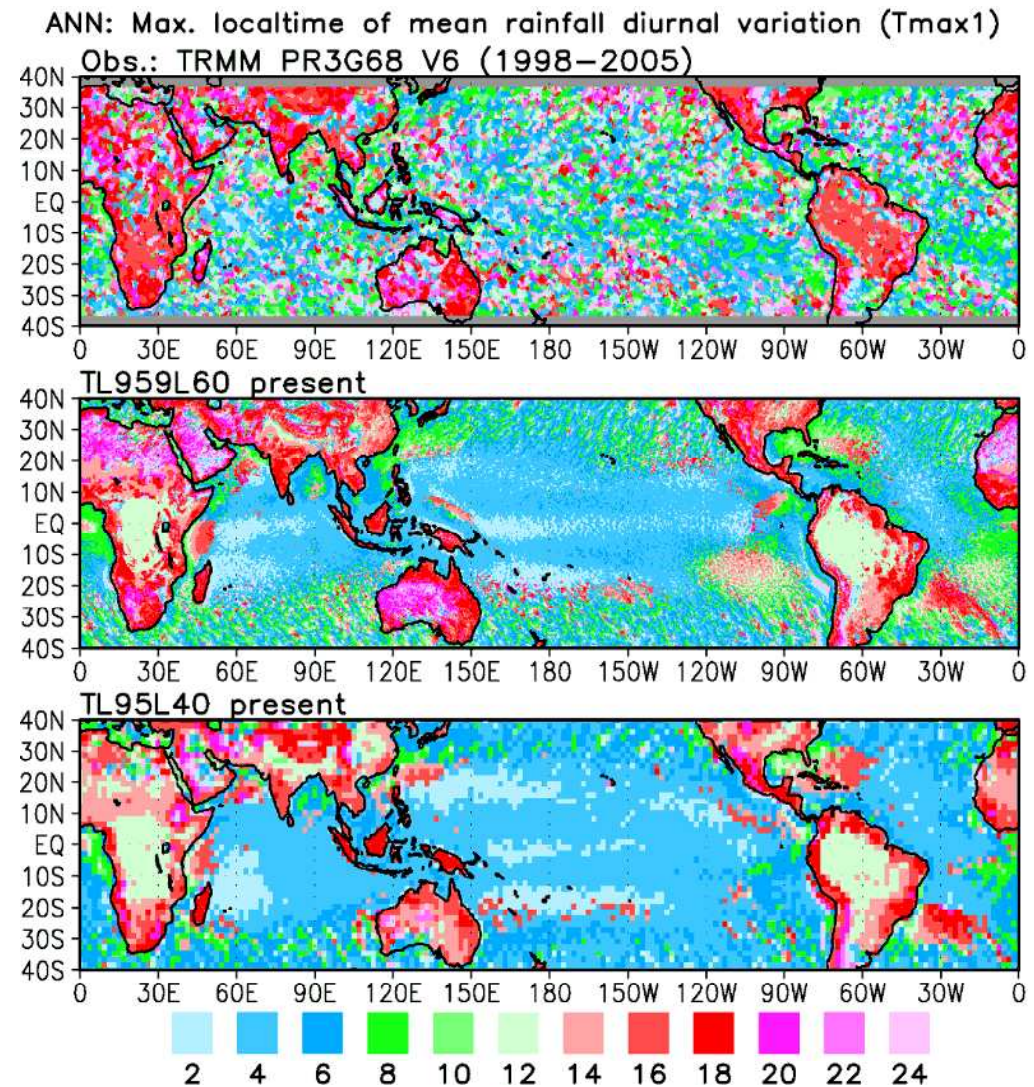
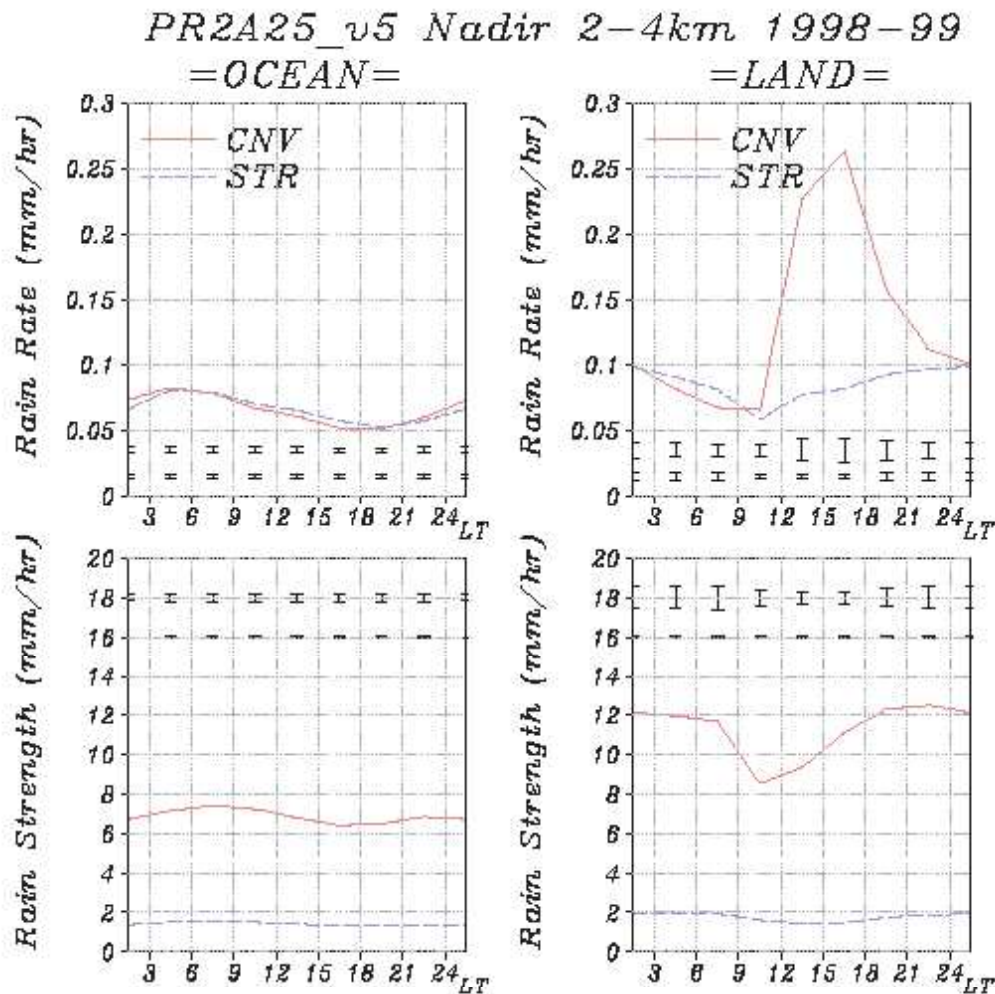
- ⌘ Relaxation time to radiative equilibrium temperature (radiative equilibrium timescale) is estimated as about **30 days**.
- ⌘ Radiative imbalance between Pole and Tropics drives global circulations.
- ⌘ Radiative imbalance between day and night has small influence on global circulations directly.

(2) Longitudinal Imbalance between Day and Night Timescale=1 day

Diurnal Cycle of Precipitation from TRMM

From Takayabu, Y.N., 2002: GEOPHYSICAL RESEARCH LETTERS, VOL. 29, NO. 12, 1584, 10.1029/2001GL014113.

From Arakawa, O. and A. Kitoh at MRI/JMA



Diurnal Precipitation near Coastal Area

Diurnal Precipitation Regimes in the Global Tropics*

KAZUYOSHI KIKUCHI AND BIN WANG[†]

Department of Meteorology, and International Pacific Research Center, University of Hawaii at Manoa, Honolulu, Hawaii

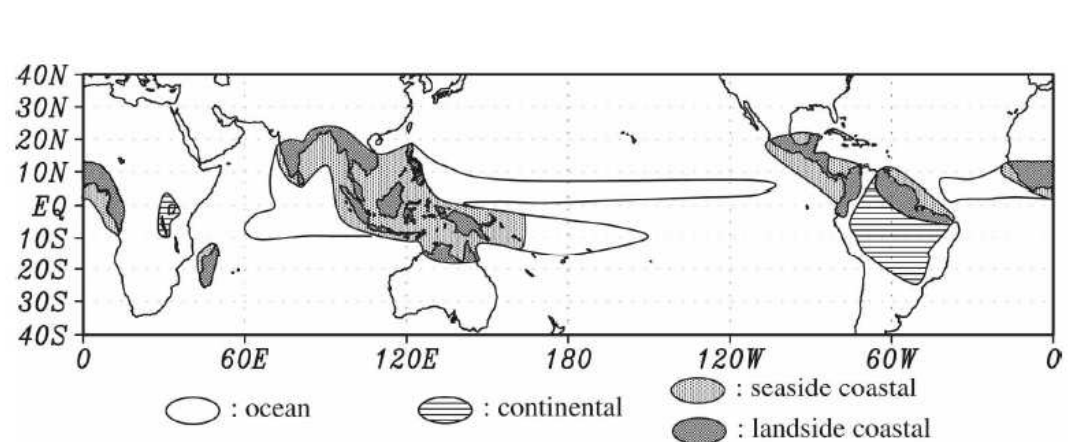
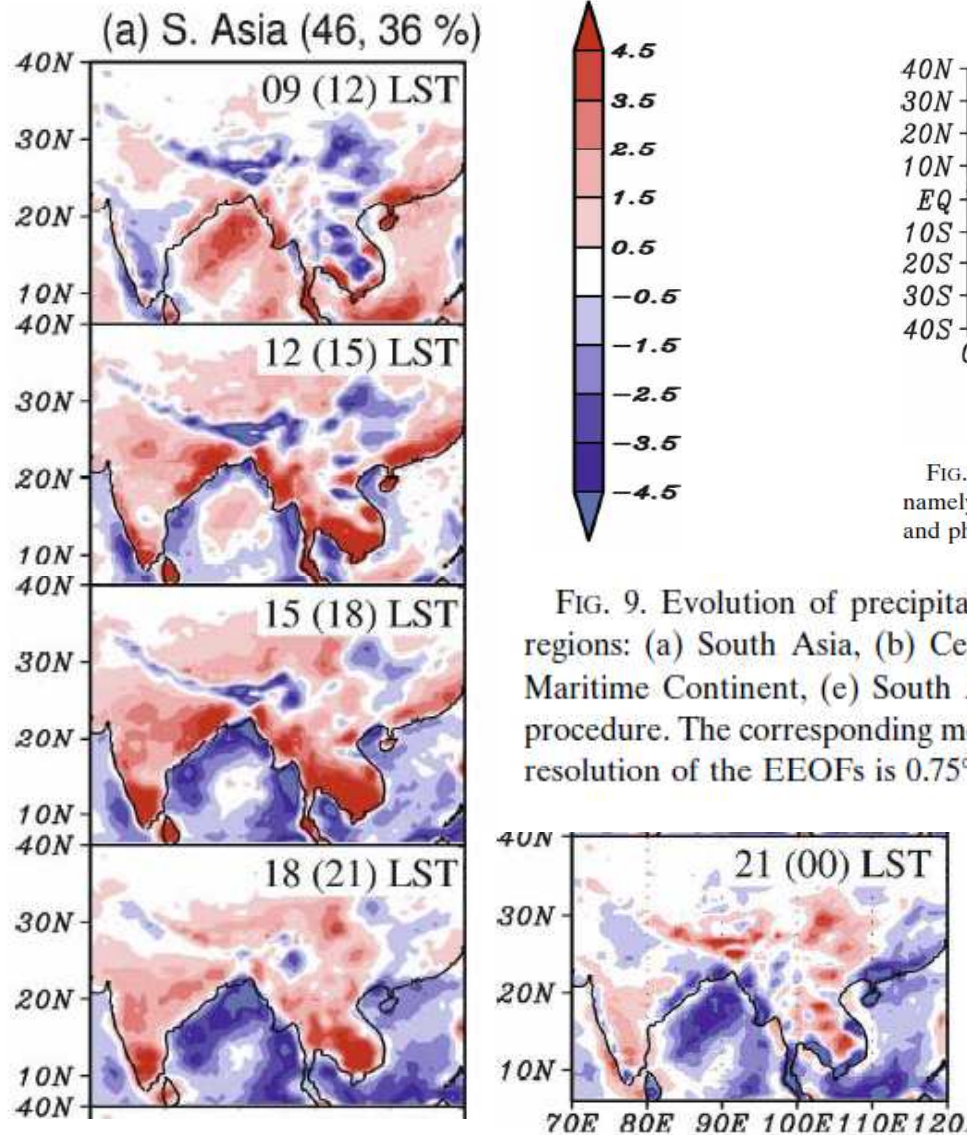
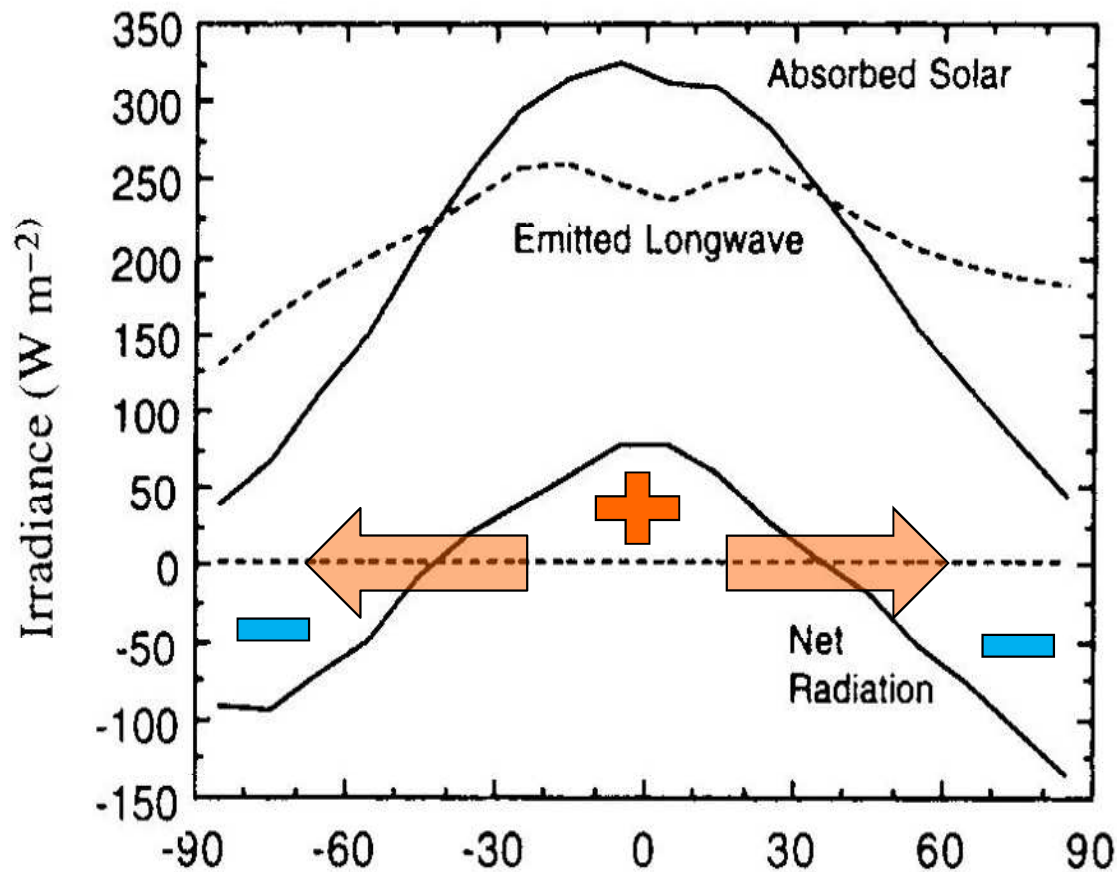


FIG. 10. Schematic diagram showing the global tropical diurnal precipitation regimes. Three regimes, namely oceanic, continental, and coastal regimes, are identified according to the amplitude, peak time, and phase propagation characteristics of the diurnal precipitation.

FIG. 9. Evolution of precipitation represented by the combination of EEOF₁ and EEOF₂ for the following regions: (a) South Asia, (b) Central America and northwest part of America, (c) West Africa, (d) Indonesia Maritime Continent, (e) South America, and (f) Madagascar. See the text for the complete description of the procedure. The corresponding modified LSTs are shown at the right corner of panels in (a) and (d). The horizontal resolution of the EEOFs is 0.75° × 0.75°.

Meridional distribution of Annual mean radiation balance



Hartmann (1994)

■ Solar radiation

- Global mean : 235 Wm^{-2}
- Low latitude : over 300 Wm^{-2}
- Poles : about 50 Wm^{-2}

■ Terrestrial radiation

- Global mean : 235 Wm^{-2}
- Less gradient between low latitudes and poles compared to that in solar radiation

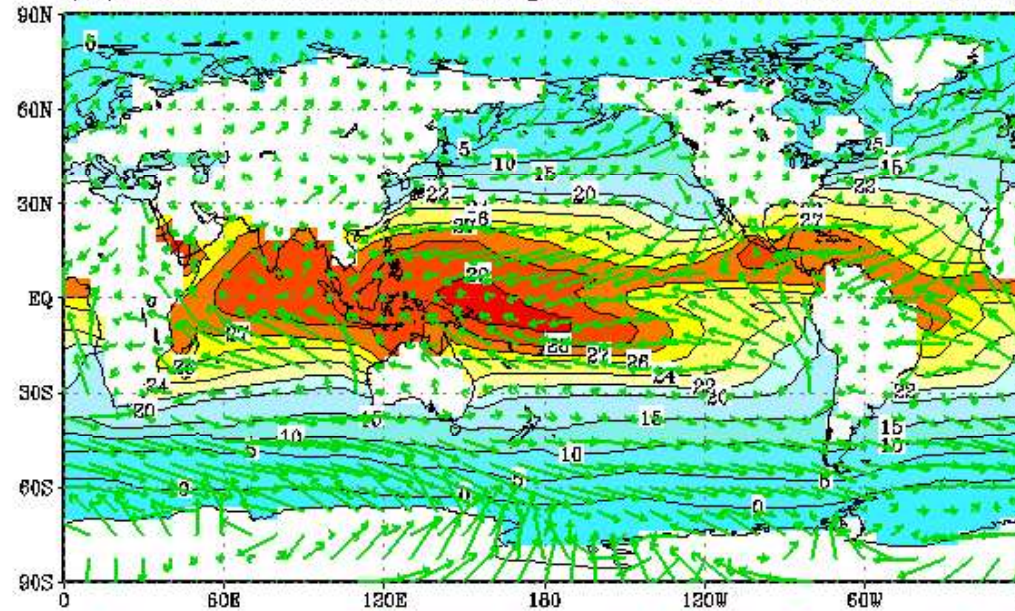
■ Net radiation

- Global mean : 0 Wm^{-2}
- Positive in low latitudes, negative in high latitudes

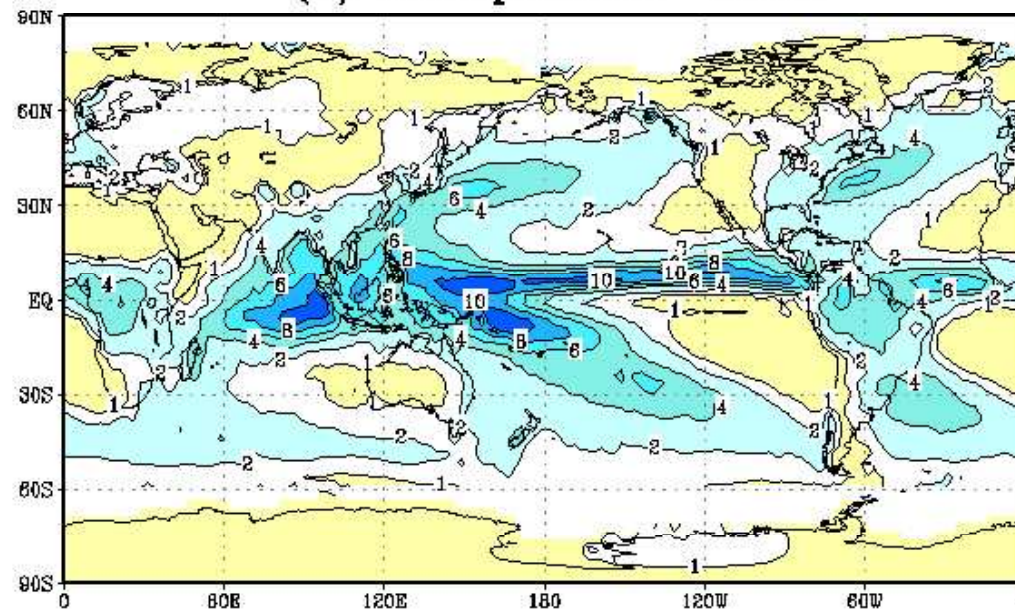
► Poleward heat transport by the atmosphere and ocean balances this meridional heat imbalance

Observed annual mean SST, surface wind, precipitation

(a) Sea Surface Temperature & Wind ANN

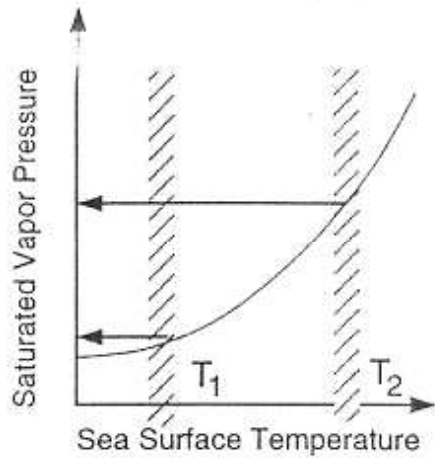


(b) Precipitation ANN₀

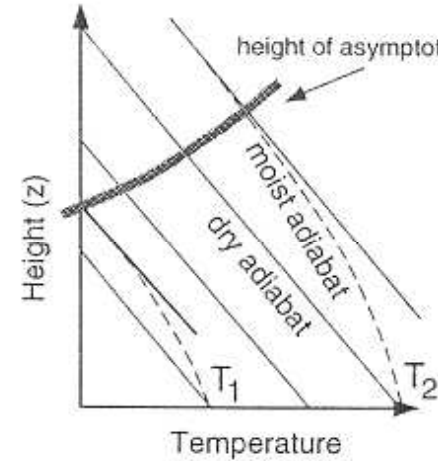


Sea surface temperature (SST) and Cumulus

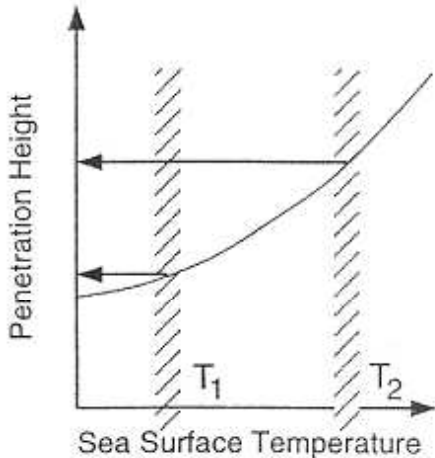
a Clausius-Clapeyron



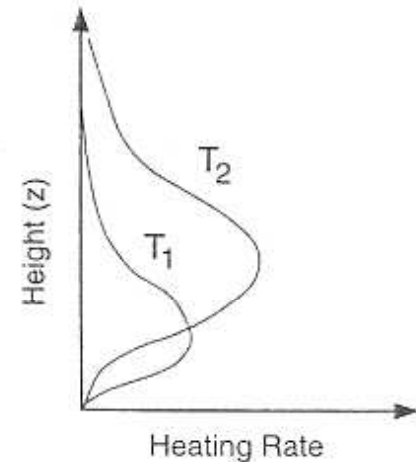
b Convective Penetration



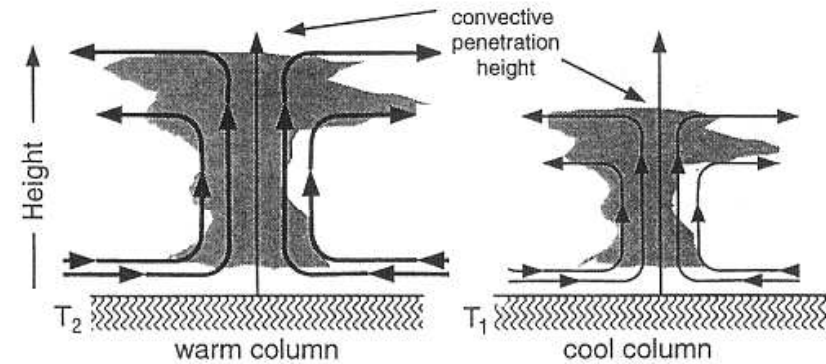
c Penetration(SST)



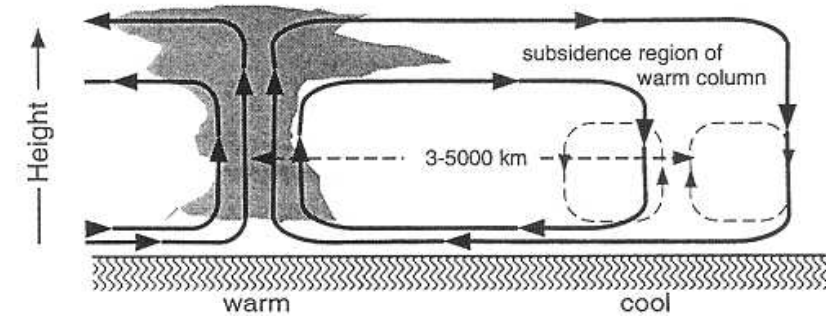
d Heating Profile (z)



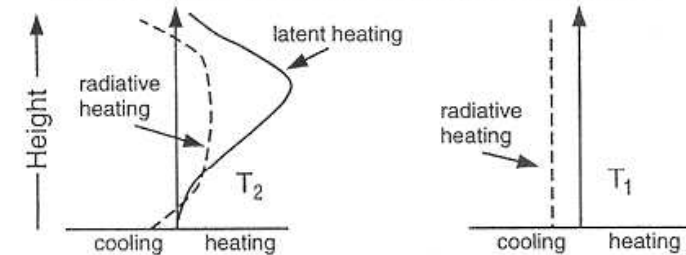
a Vertical Circulation in Columns of Temperature T_1 , and T_2 .



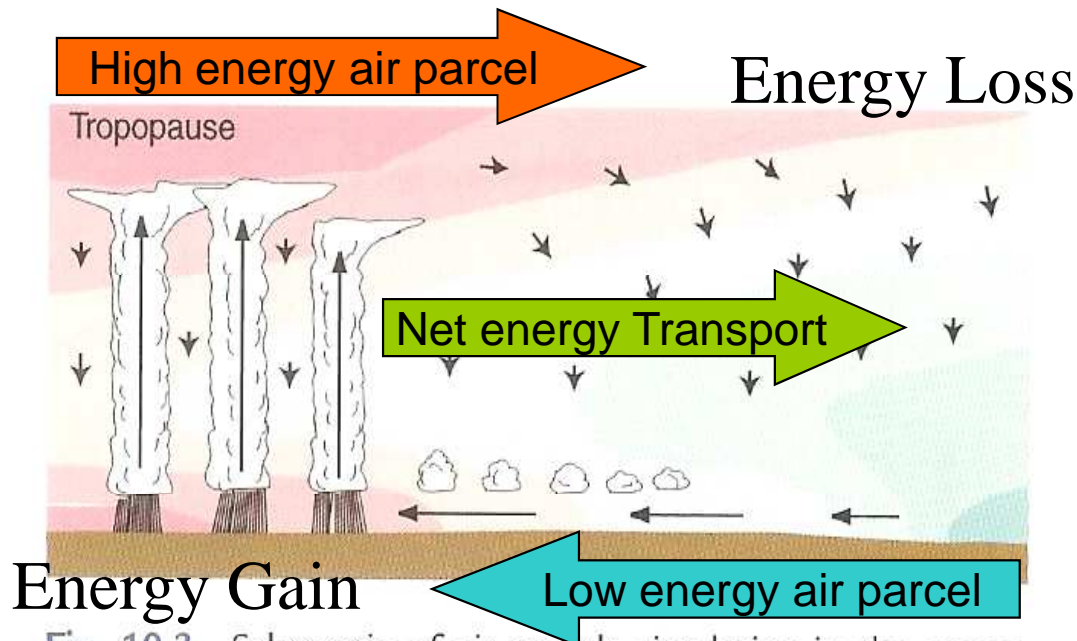
b Resulting Circulation Between Warm and Cool Columns



c Final Heating Profiles in Warm and Cool Columns



Energy Transport by Atmospheric Circulation



⌘ Moist Static Energy
 $H = C_p T + gZ + Lq$

T: Temperature

Z: Height

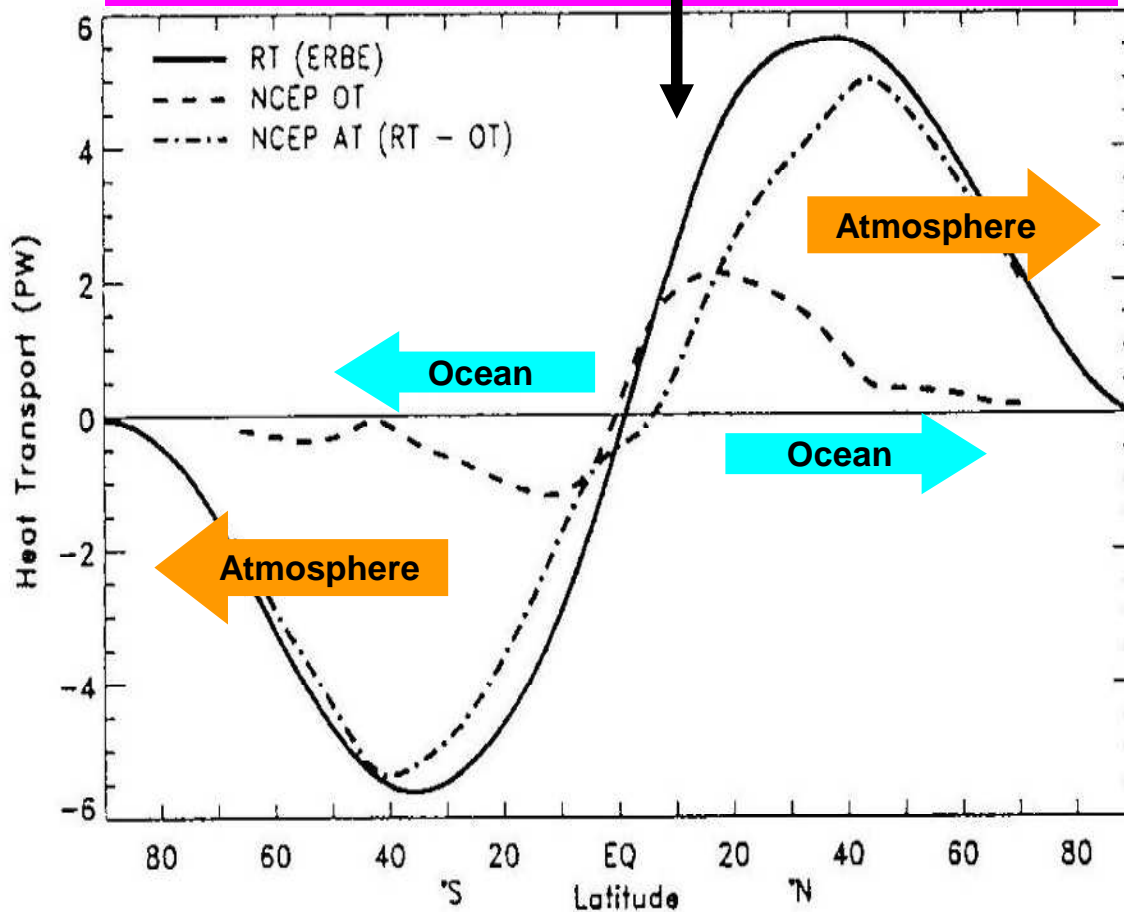
q: Specific Humidity

H of air parcels is conserved even through adiabatic process and/or condensation process, but, not conserved through the processes of radiation, heat and moisture supply from ground surface.

Fig. 10.3 Schematic of air parcels circulating in the atmosphere. The colored shading represents potential temperature or moist static energy, with pink indicating higher values and blue lower values. Air parcels acquire latent and sensible heat during the time that they reside within the boundary layer, raising their moist static energy. They conserve moist static energy as they ascend rapidly in updrafts in clouds, and they cool by radiative transfer as they descend much more slowly in clear air.

Heat transport by the atmosphere and ocean

Integration from the South Pole of Net radiation absorbed in the Earth



Trenberth and Caron (2001)

- Implied heat transport from top of atmosphere (TOA) radiation balance
 - Integrate net radiation from pole to pole
- Both the atmosphere and ocean are responsible for heat transport
- Atmospheric transport is larger, particularly in the mid and high latitudes
- Oceanic heat transport is large in low-latitudes

Atmospheric global circulations driven by latitudinal heating contrast

From Wallace, J.M. and P. V. Hobbs, 2006: Atmospheric Science. Academic Press, 483pp.

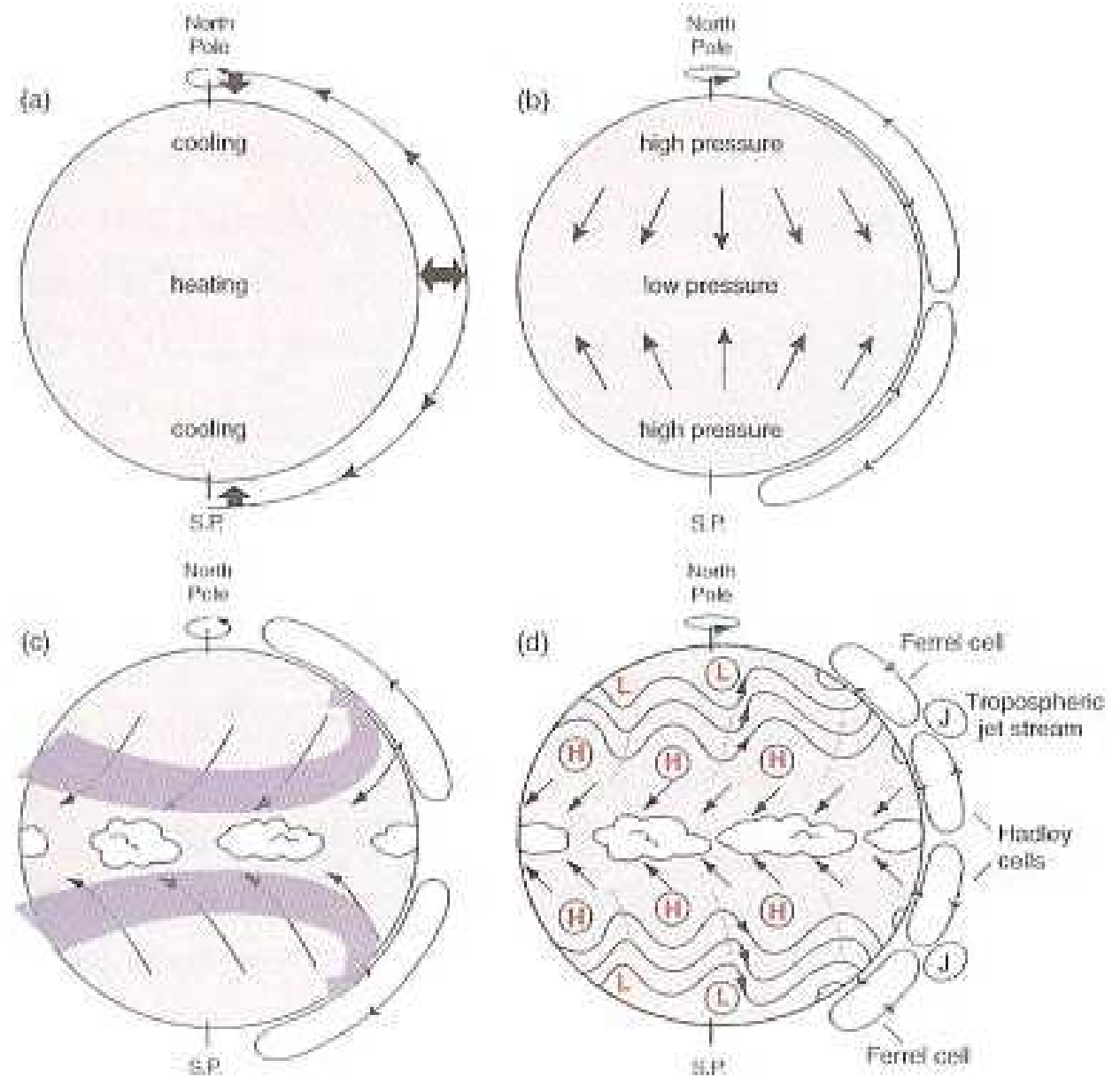
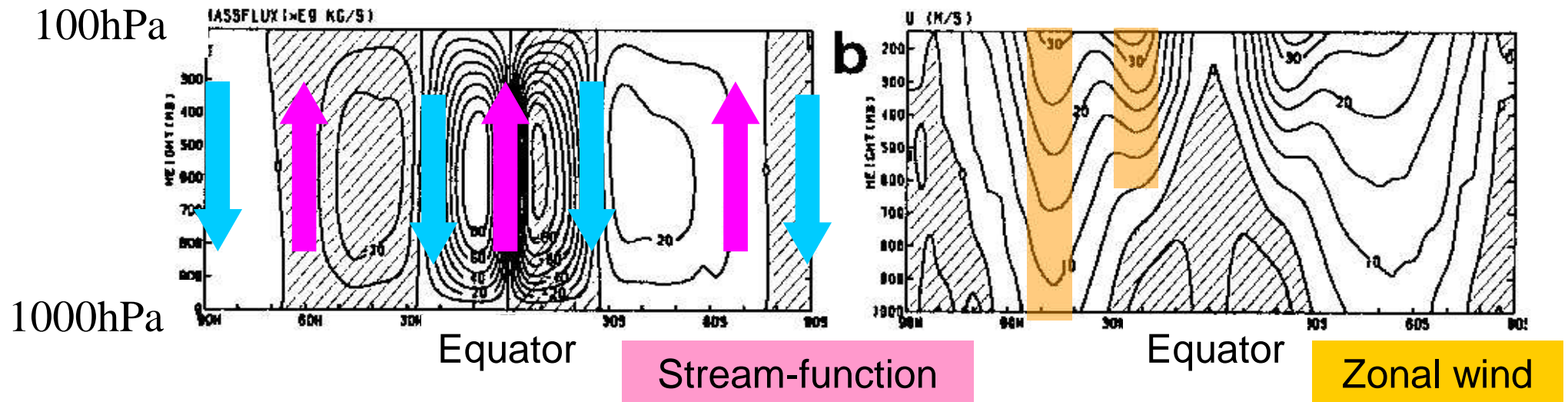


Fig. 7.21 Schematic depiction of the general circulation as it develops from a state of rest in a climate model for equinox conditions in the absence of land-sea contrasts. See text for further explanation.

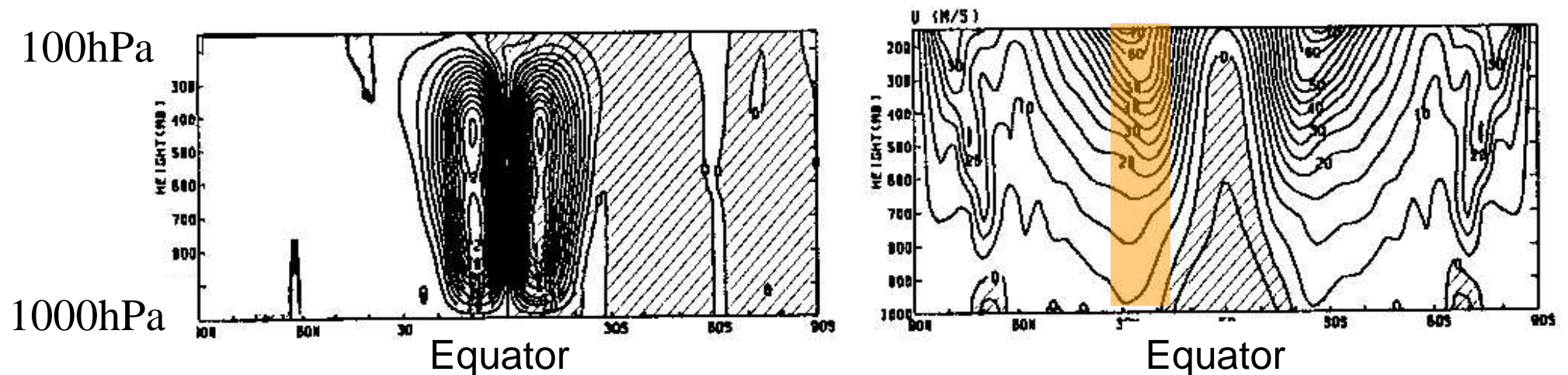
Hadley (direct) circulation

These are model results.

(1) There are two direct and one indirect circulations.

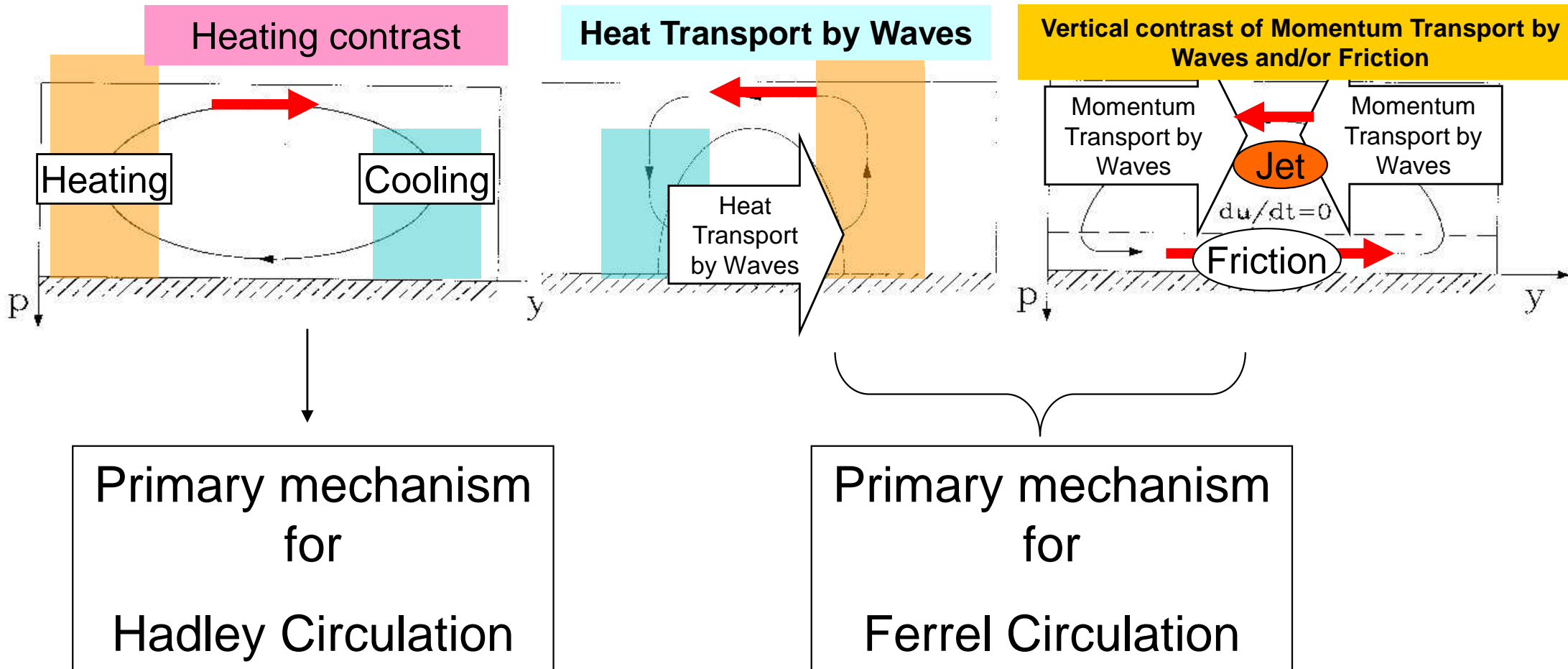


(2) After zonal waves are removed in the model, Hadley circulations and subtropical jets are left.



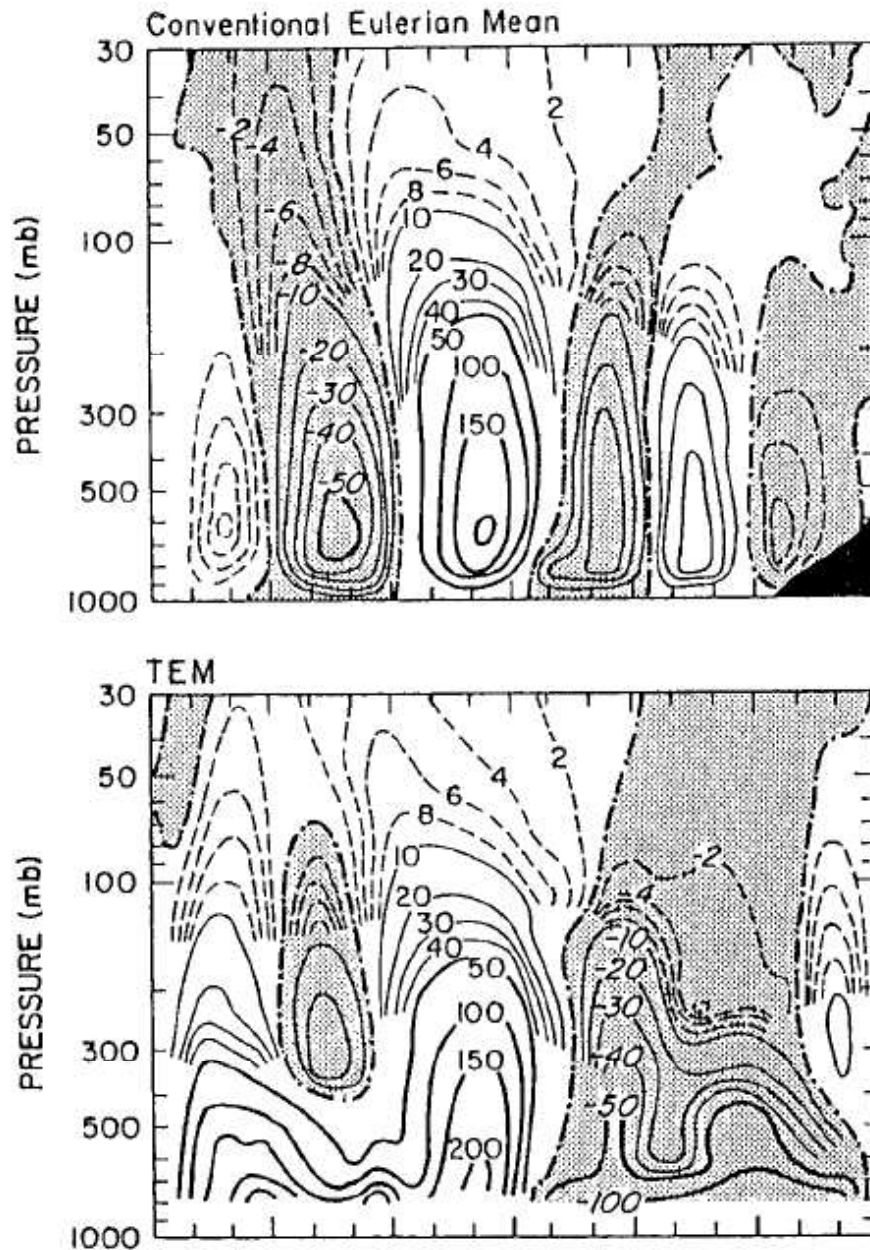
Ferrel (in-direct) circulation.

Three mechanisms to drive meridional mass circulations



Mean meridional Circulations depend on vertical coordinates.

Iwasaki, T., 1989: A diagnostic formulation for wave–mean flow interactions and Lagrangian-mean circulation with a hybrid vertical coordinate of pressure and isentropes. *J. Meteor. Soc. Japan*, **67**, 293–312.



Lagrangian Mean

Net mass transport including wave effect

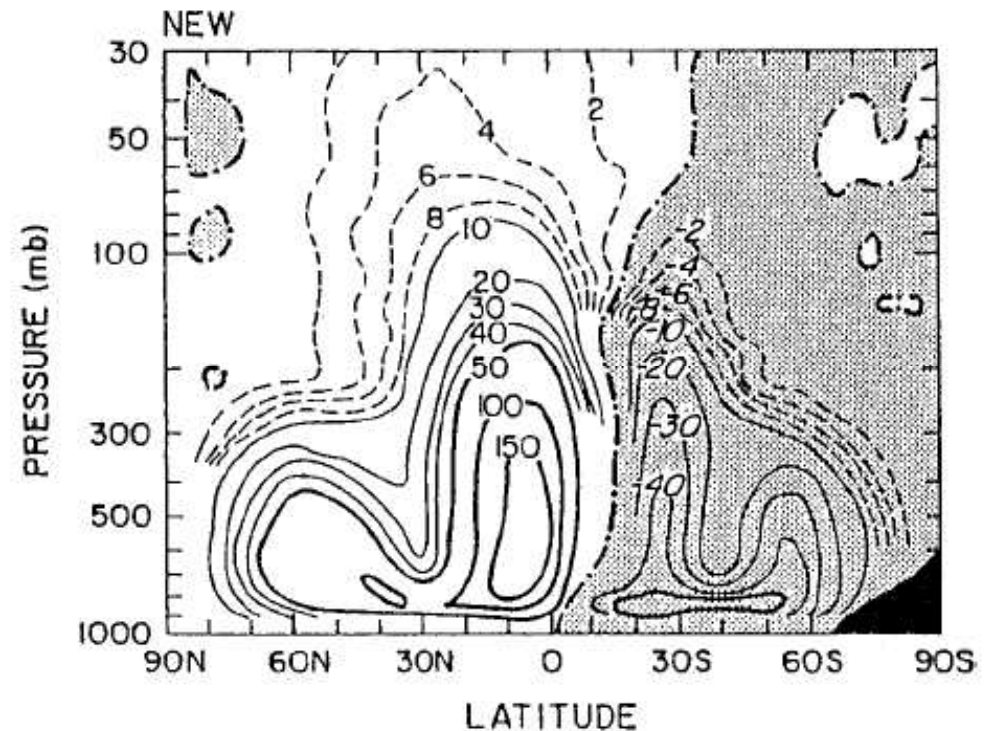
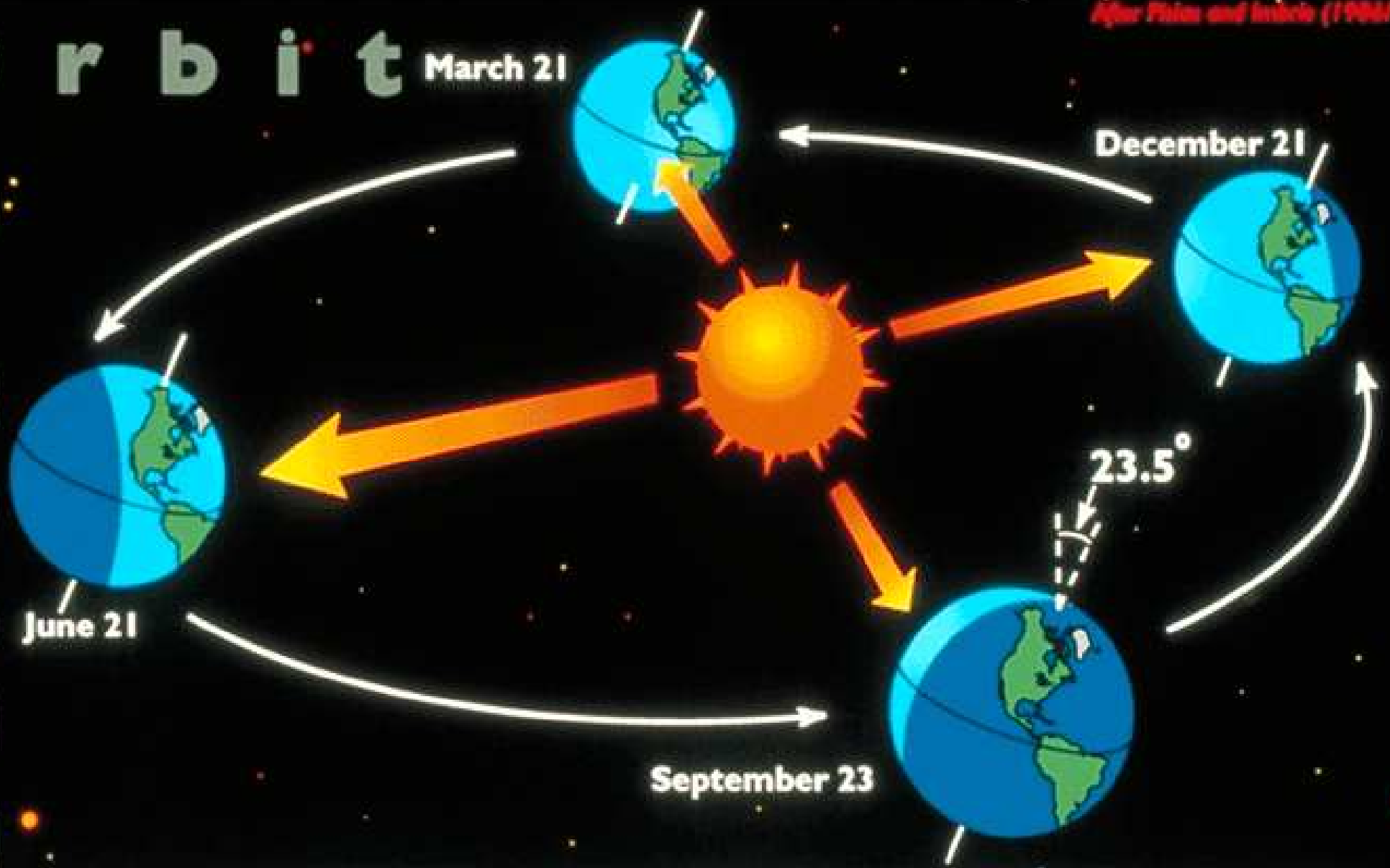


FIG. 1. Mass streamfunctions of the perpetual Jan simulation by the National Center for Atmospheric Research Community Climate Model version 1, diagnosed with the conventional Eulerian mean, the TEM, and the p_s analyses. Contour values are shown with units of $\times 10^9 \text{ kg s}^{-1}$ (after I89).

Seasonal Change

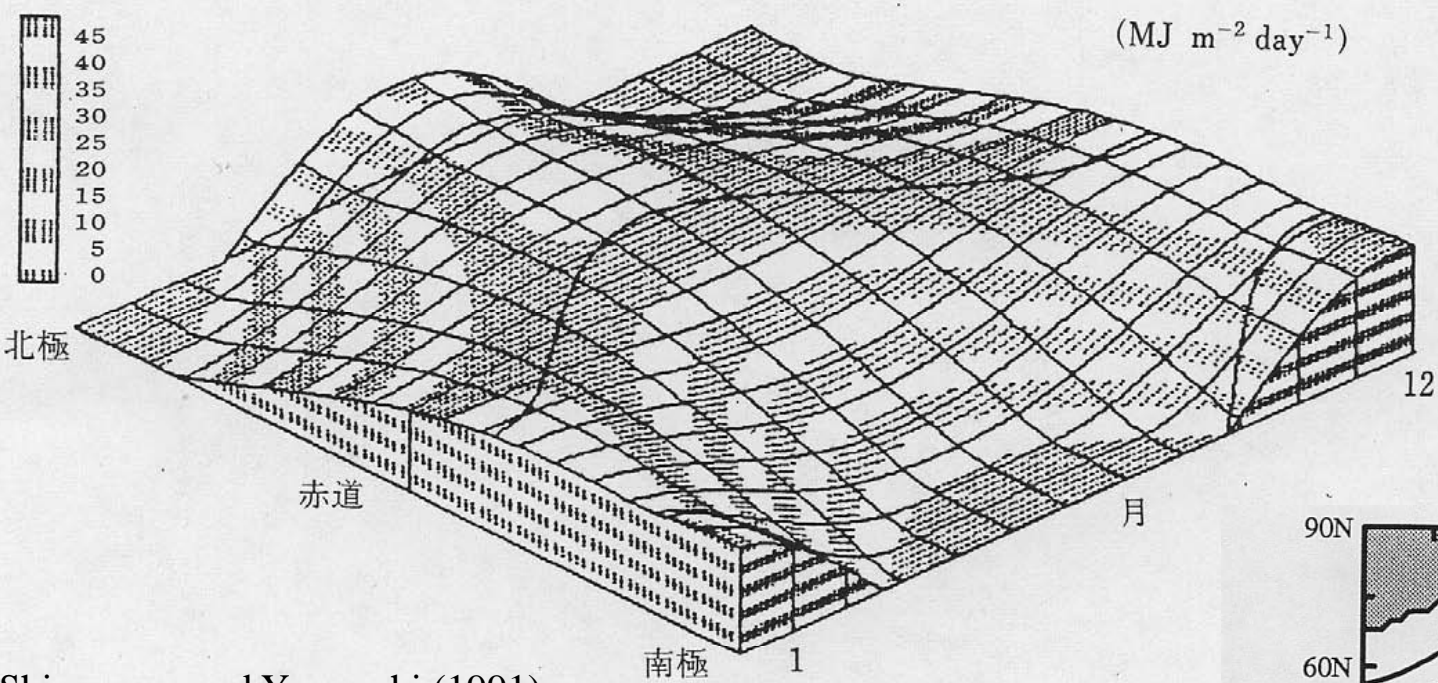
A thick, horizontal yellow brushstroke underline that spans the width of the page, positioned directly below the title.

E a r t h ' s O r b i t



Viewed in the present, the tilted Earth revolves around the Sun on an elliptical path. The orientation of the axis remains fixed in space, producing changes in the distribution of solar radiation over the course of the year. These changes in the pattern of radiation reaching Earth's surface cause the succession of the seasons. The Earth's orbital geometry, however, is not fixed over time. Indeed, long-term variations in the Earth's orbit help explain the waxing and waning of global climate in the last several million years.

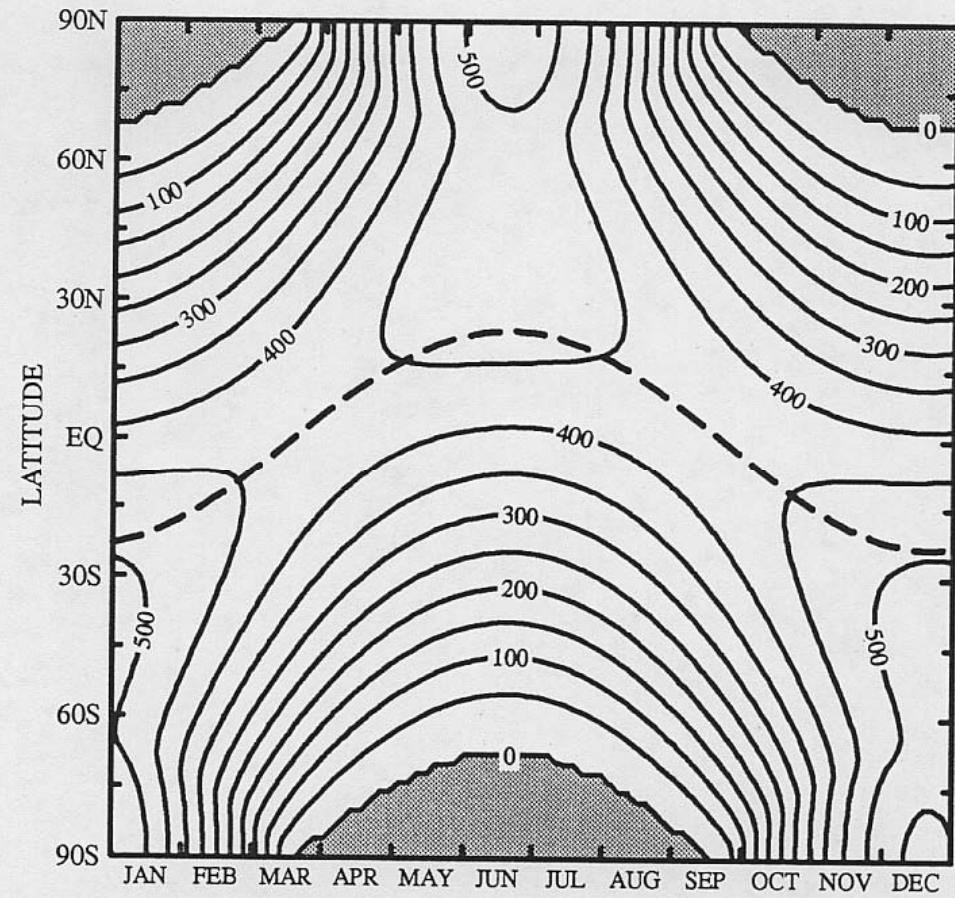
month-latitude diagram of TOA solar insolation



Hartmann (1994)

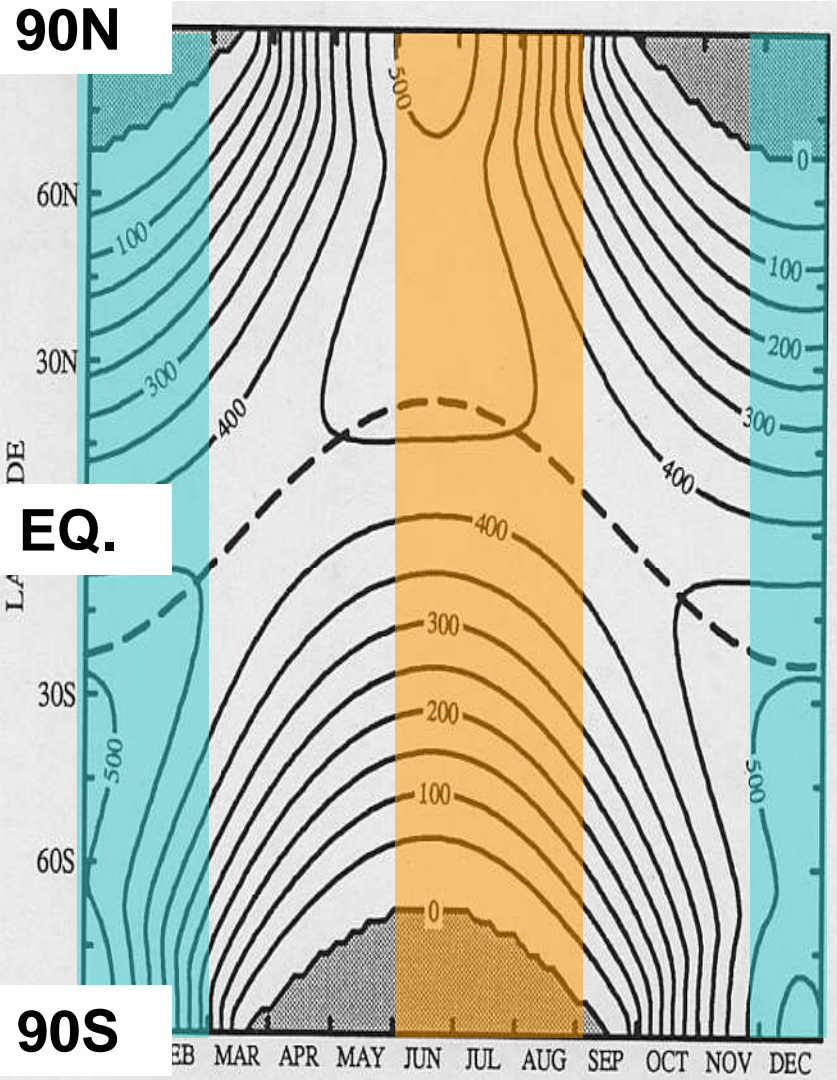
Shimamura and Yamauchi (1991)

Earth's orbit is not circular, and currently Earth is somewhat closer to the sun during SH summer than during NH summer. As a result, the maximum insolation in the SH is about 6.9% higher than that in the NH. Note that at the summer solstice the insolation in high latitudes is actually greater than that near the equator. This results from the very long days during summer and in spite of the relatively large solar zenith angles at high latitudes.

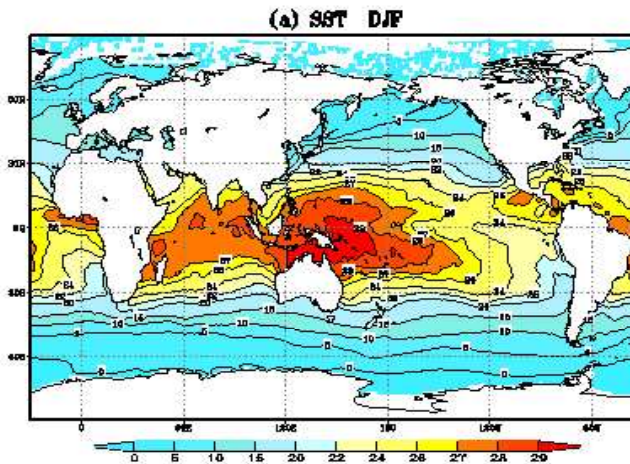


Seasonal Change of Sea Surface Temperature (SST)

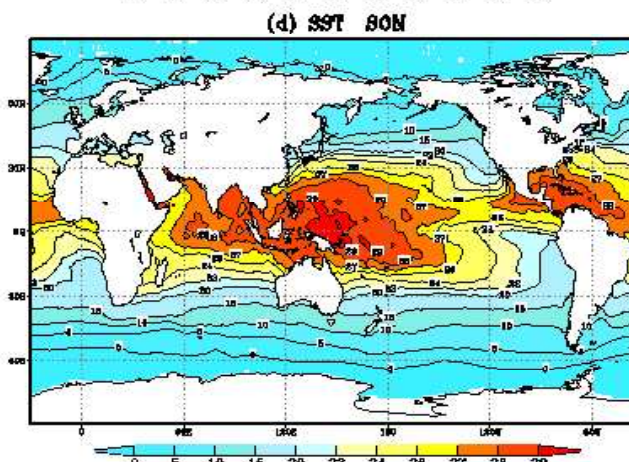
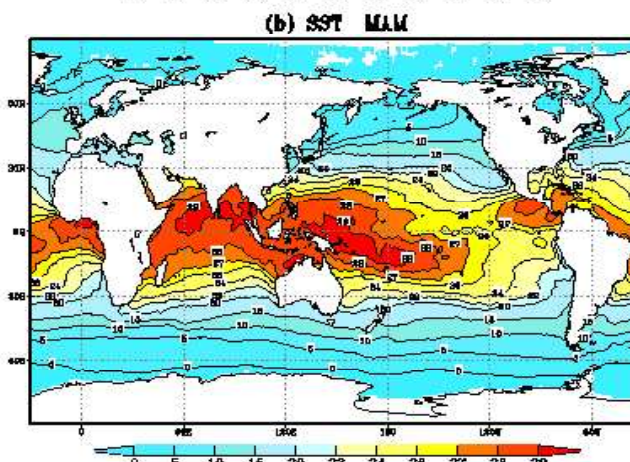
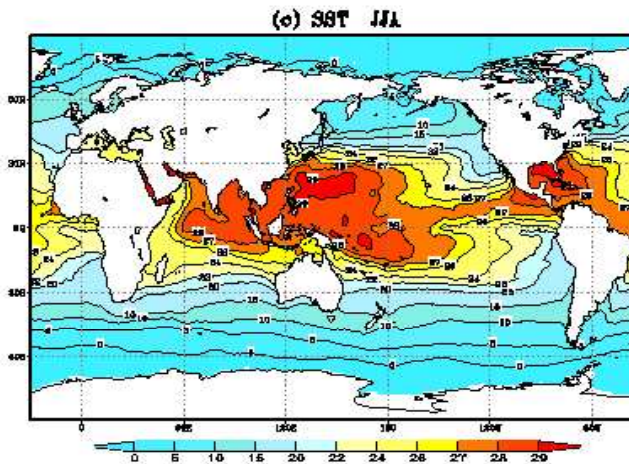
Solar Insolation



Dec.-Jan.-Feb.



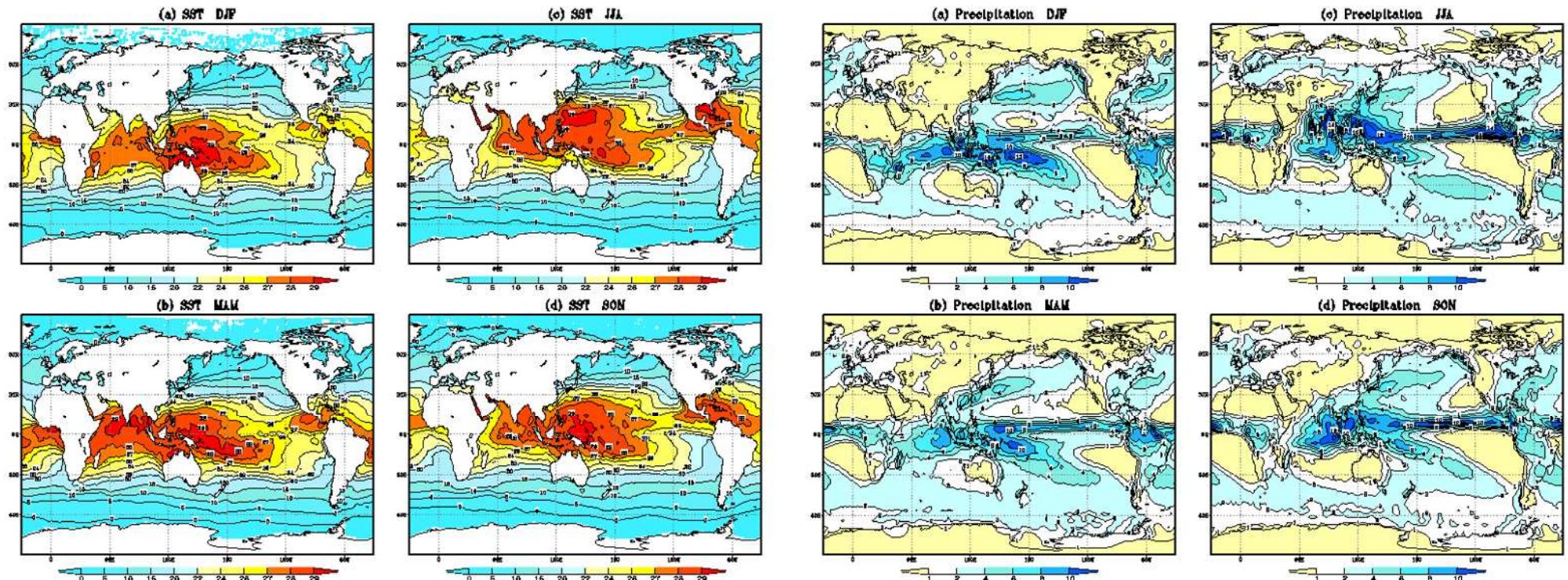
Jun-July-August



Mar.-Apr.-May

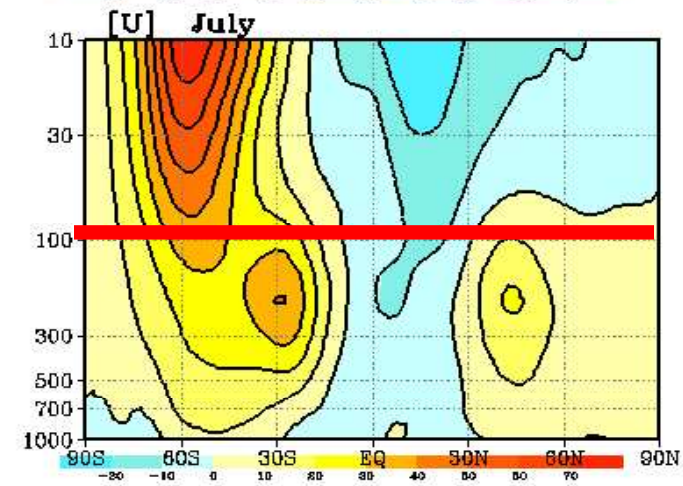
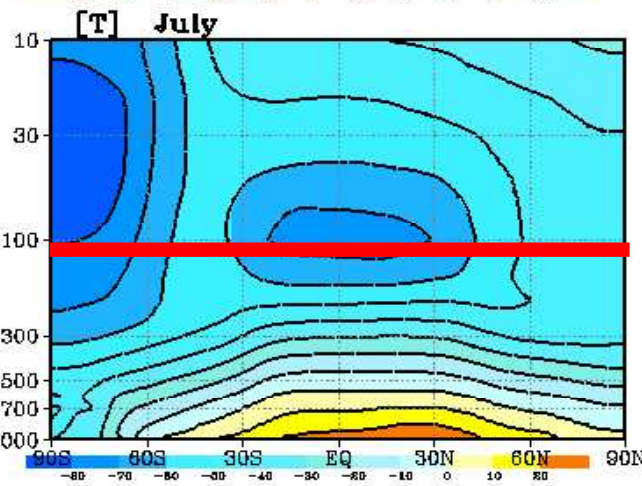
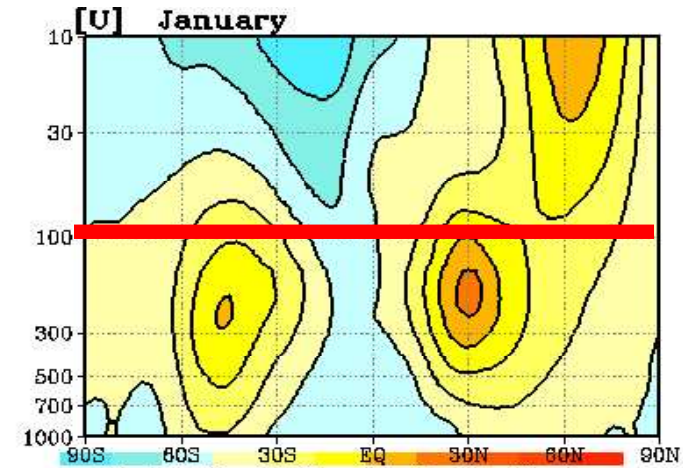
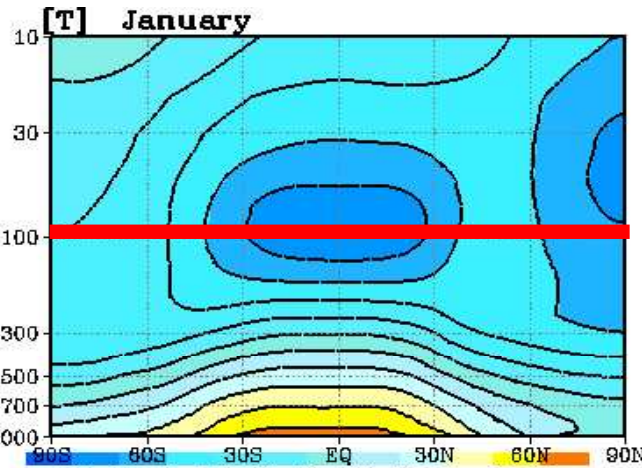
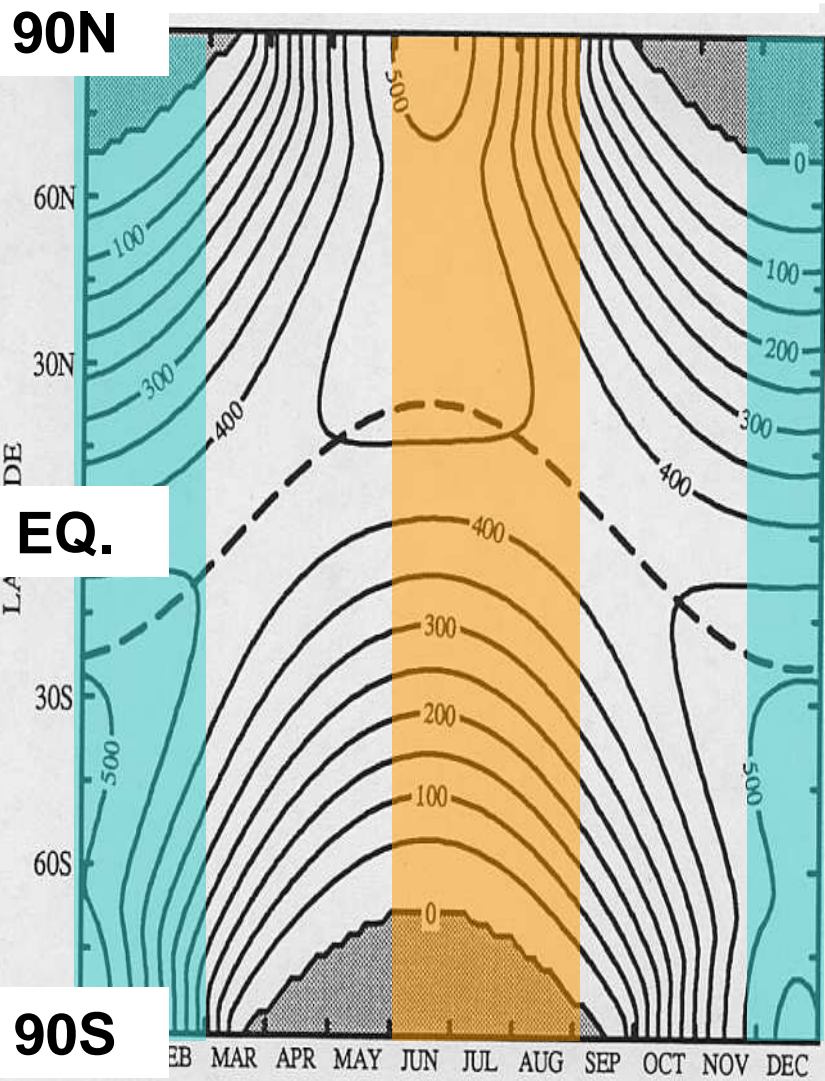
Sep.-Oct.-Nov.

SST and Precipitation in each season



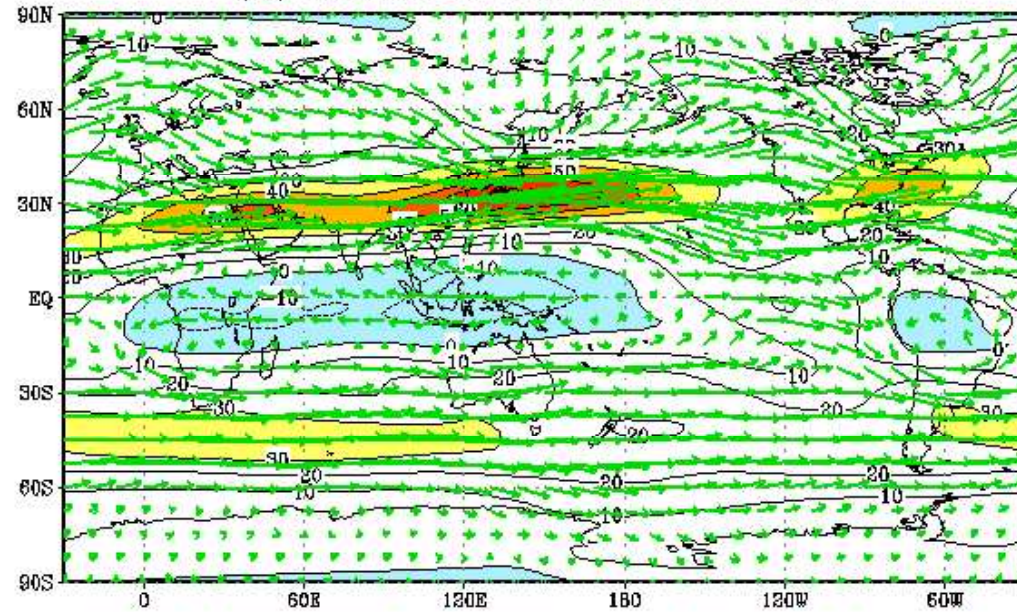
Seasonal Change of Temperature and Zonal Wind

Solar Insolation

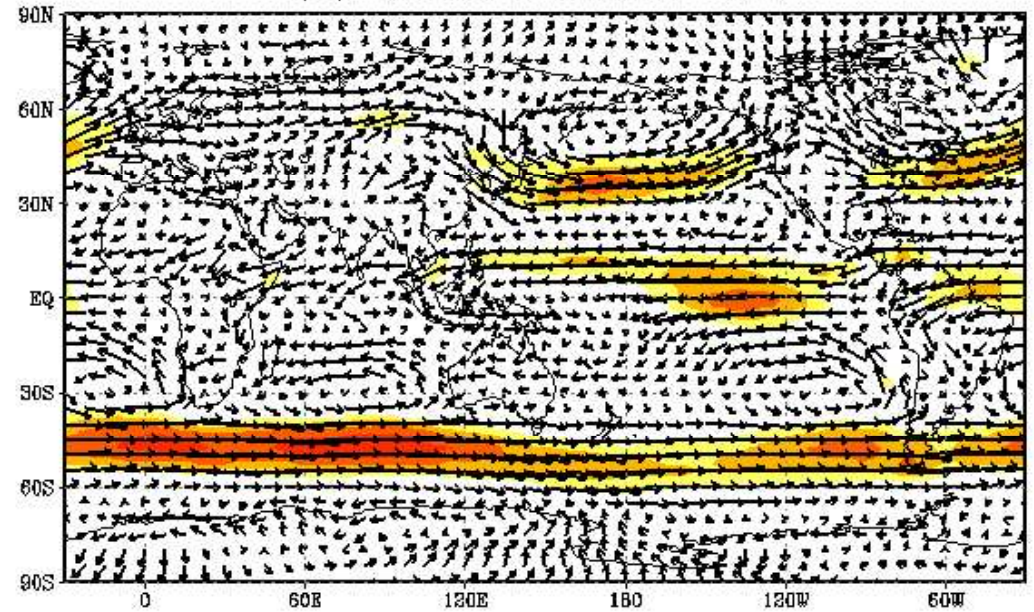


200 hPa and 850 hPa winds in JJA and DJF

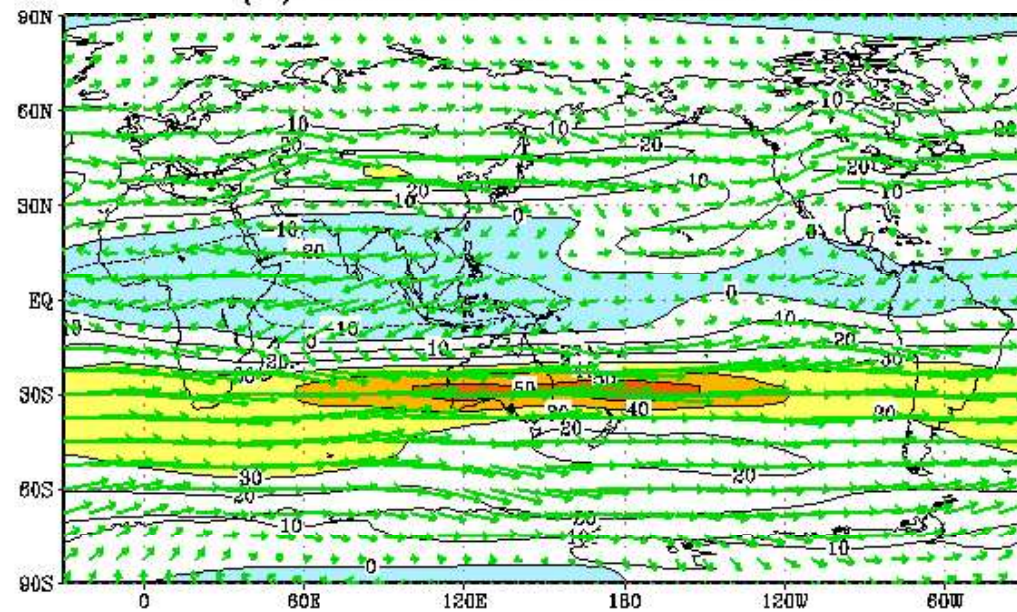
(a) 200hPa zonal wind DJF



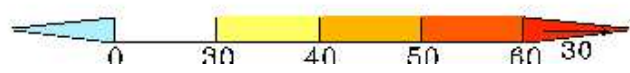
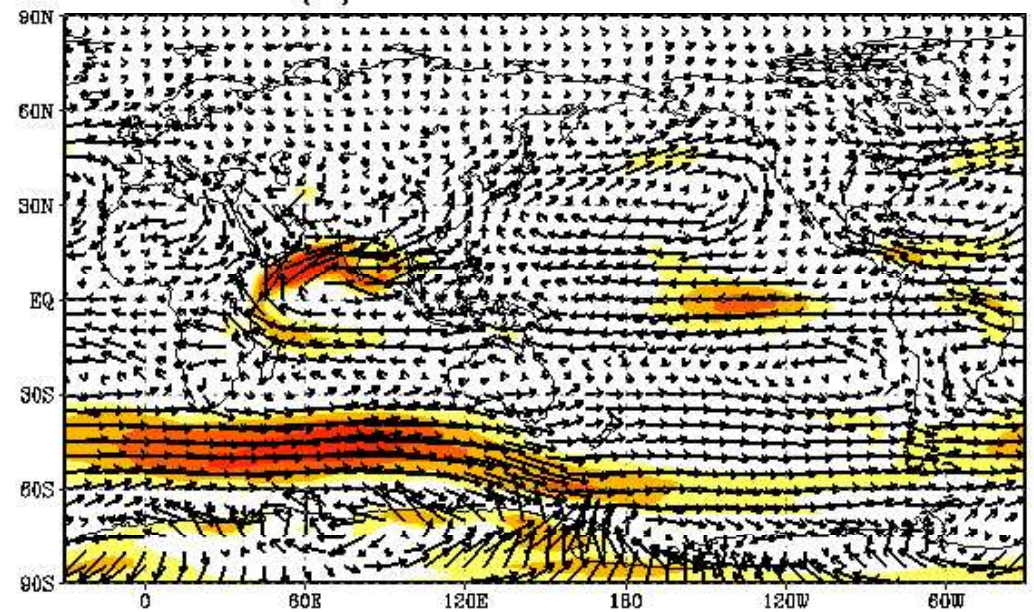
(a) 850hPa winds DJF



(b) 200hPa zonal wind JJA

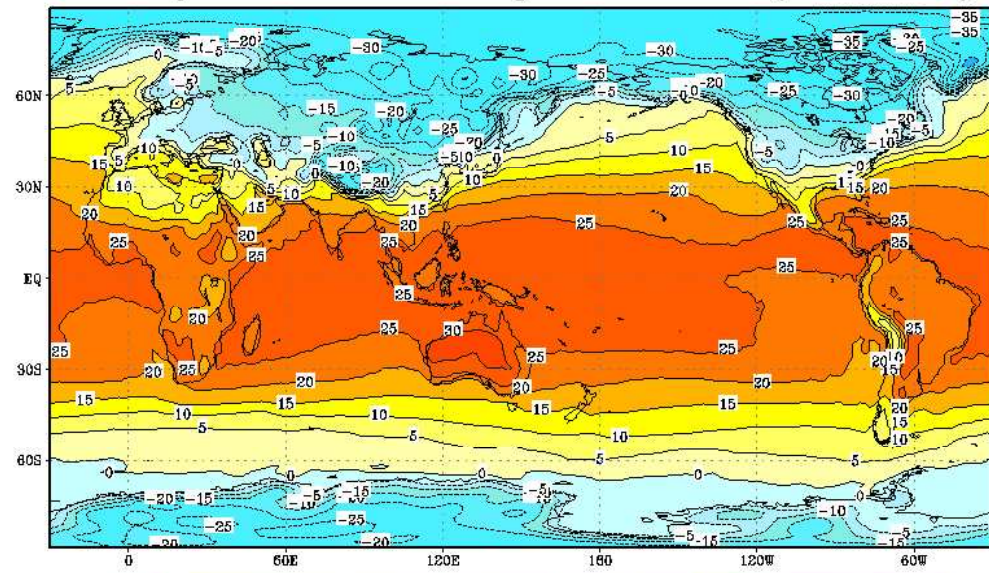


(b) 850hPa winds JJA

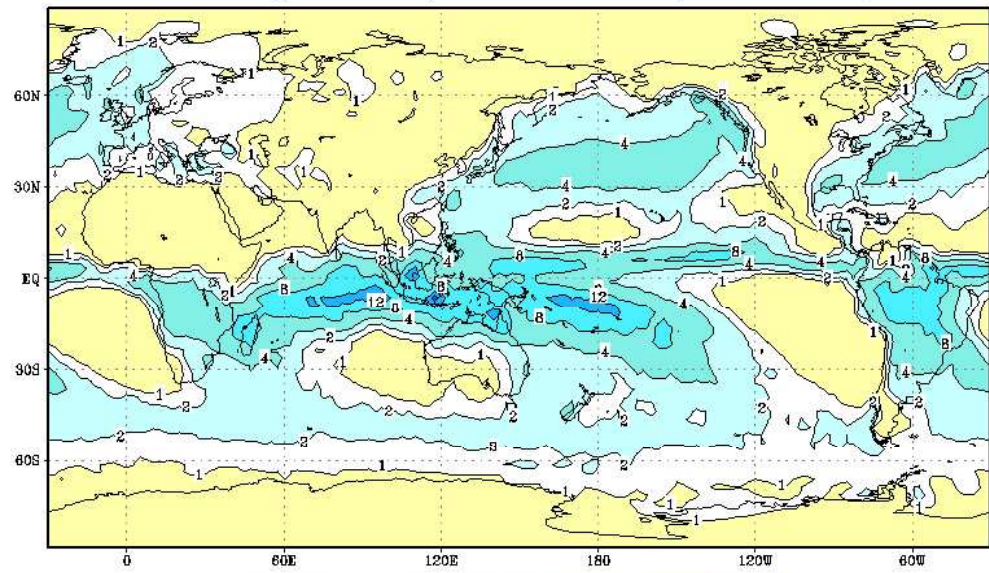


Jan-Jul contrast of surface temperature/precipitation

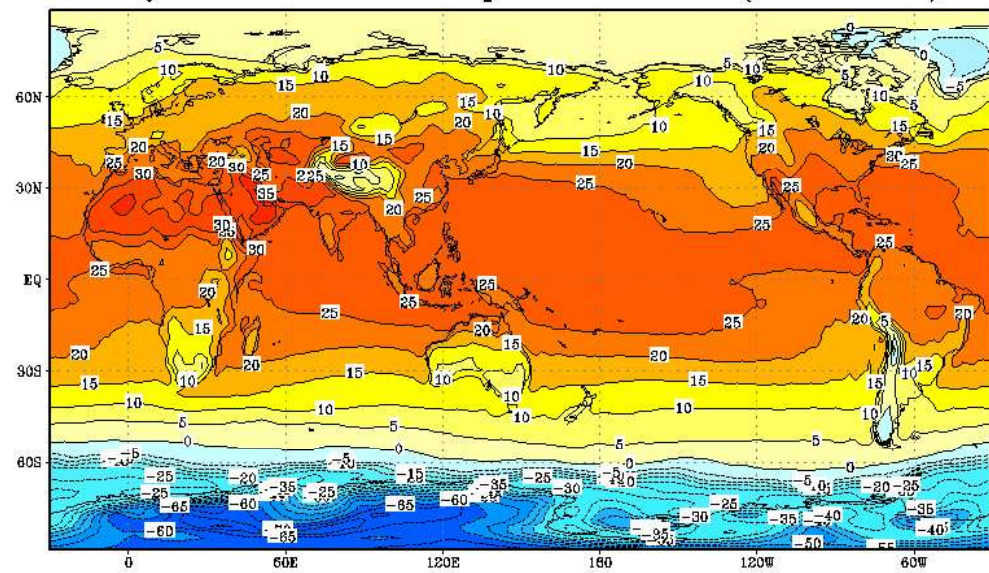
January Surface Air Temperature NCEP(1949-2000)



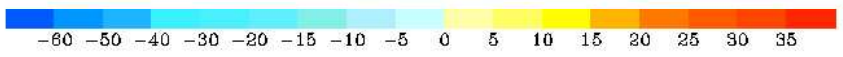
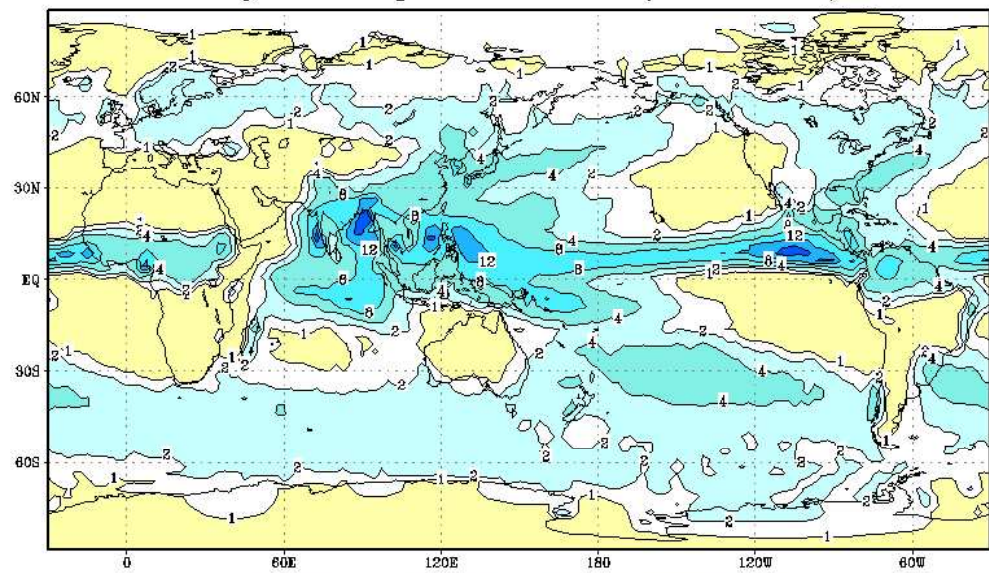
January Precipitation CMAP(1979-2001)



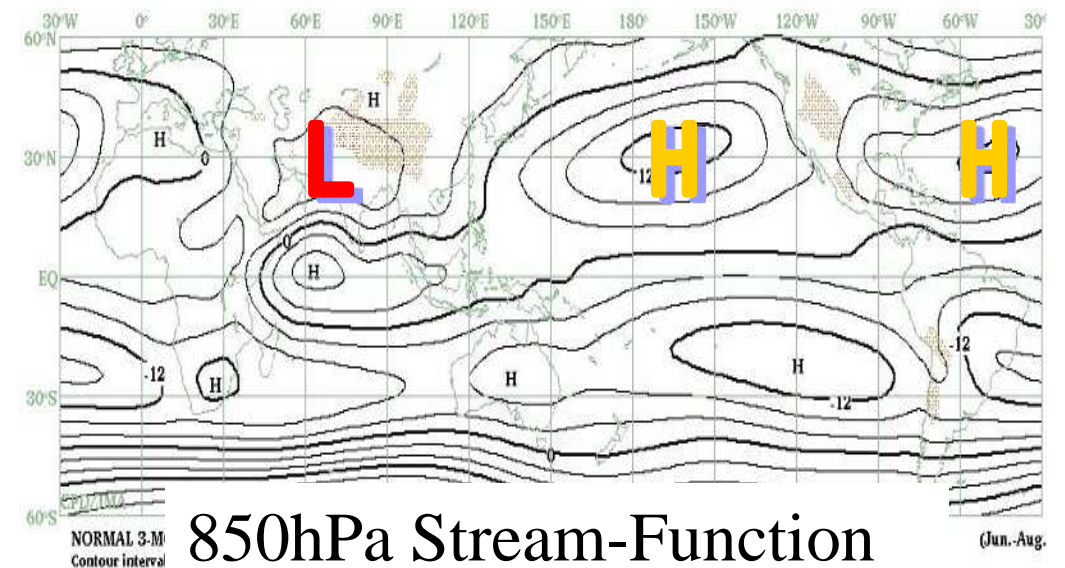
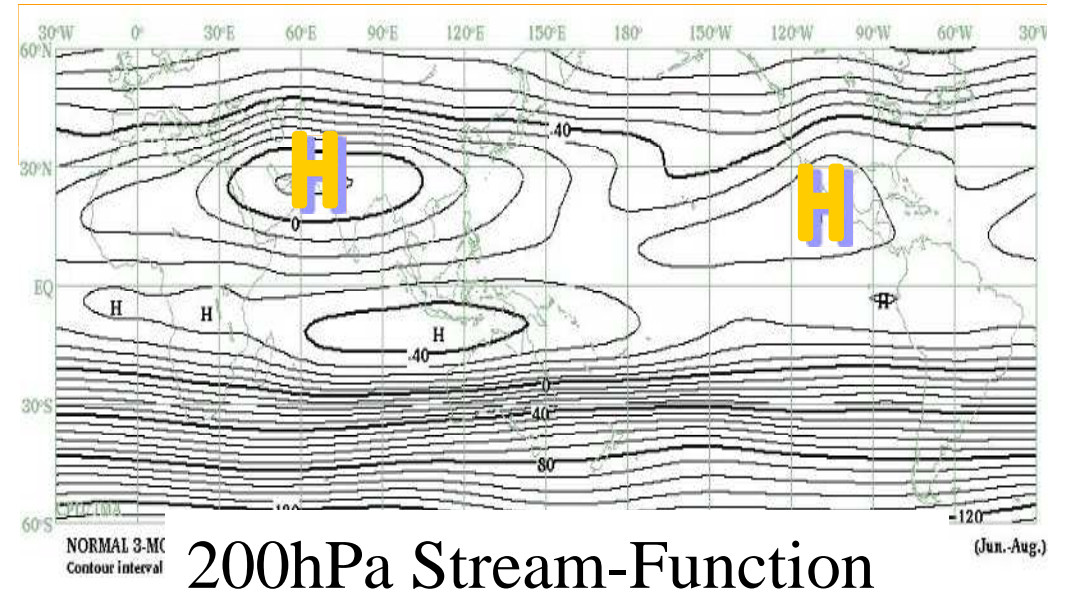
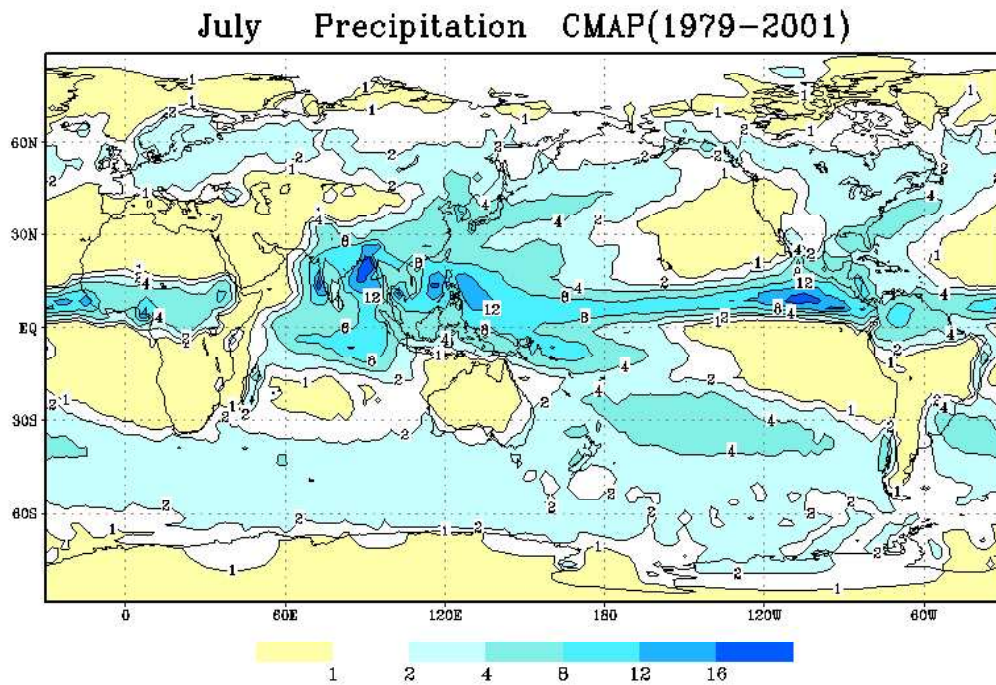
July Surface Air Temperature NCEP(1949-2000)



July Precipitation CMAP(1979-2001)

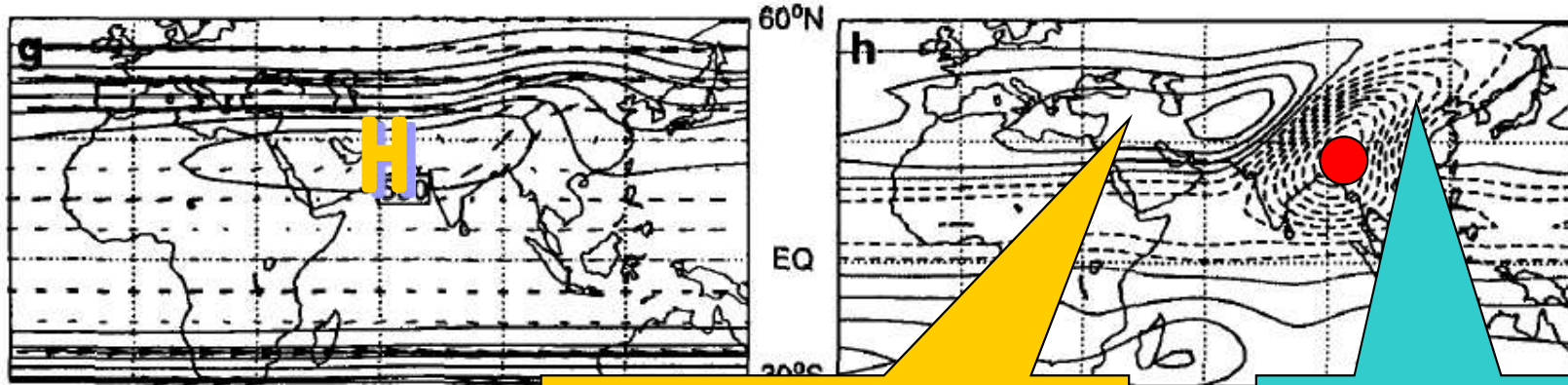


Northern Summer Monsoon



Q. J. R. Meteorol. SOC. (1996), 122, pp. 1385-1404 Monsoons and the dynamics of deserts. By MARK J. RODWELL' and BRIAN I. HOSKINS

25N
Precipitation



Downward motion => DRY

Upward motion => WET

10N
Precipitation

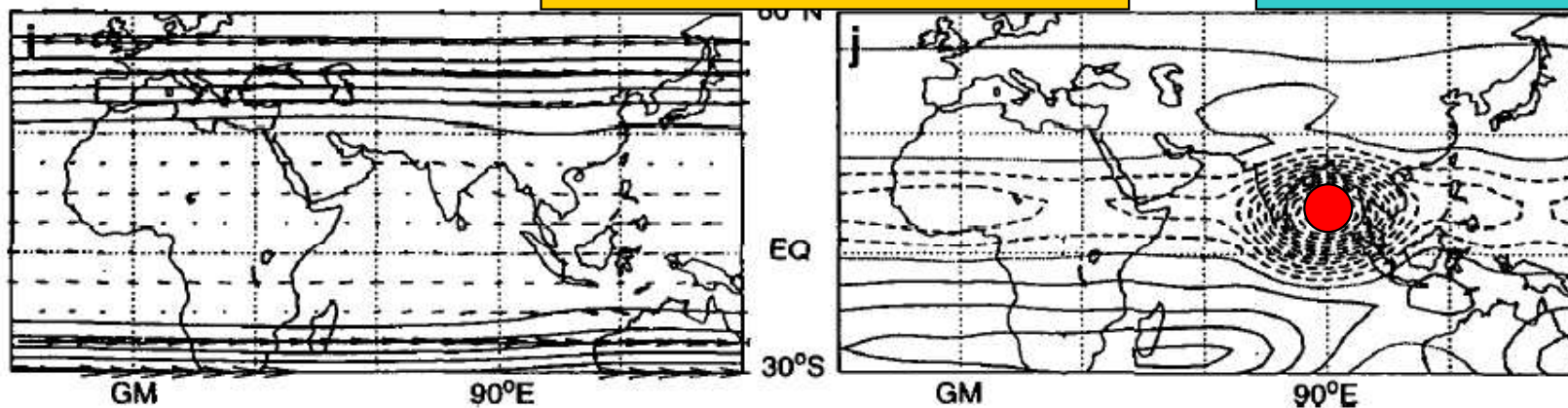


Figure 8. Day 11 of a series of integrations without orography. (a), (c), (e), (g) and (i) pressure and horizontal winds on the 325 K isentropic surface, with contour interval 40 hPa; (b), (d), (f), (h) and (j) vertical velocity at 477 hPa, with contour interval 0.25 hPa hr⁻¹; (a) and (b) integration linearized about a resting basic-state and forced with heating at 90°E, 25°N; (c) and (d) integration linearized about a resting basic-state and forced with heating at 25°N superimposed on the June to August zonal-mean flow; (e) and (f) integration linearized about the zonal-mean basic-state and forced with heating at 25°N; (g) and (h) non-linear integration forced with heating at 25°N; (i) and (j) nonlinear integration forced with heating at 90°E, 10°N.

NOTES AND CORRESPONDENCE

Role of Narrow Mountains in Large-Scale Organization of Asian Monsoon Convection*

SHANG-PING XIE,⁺ HAIMING XU,[#] N. H. SAJI, AND YUQING WANG⁺*International Pacific Research Center, SOEST, University of Hawaii at Manoa, Honolulu, Hawaii*

W. TIMOTHY LIU

Jet Propulsion Laboratory, Pasadena, California

Precipitation and Mountain

15 JULY 2006

NOTES AND CORRESPONDENCE

3421

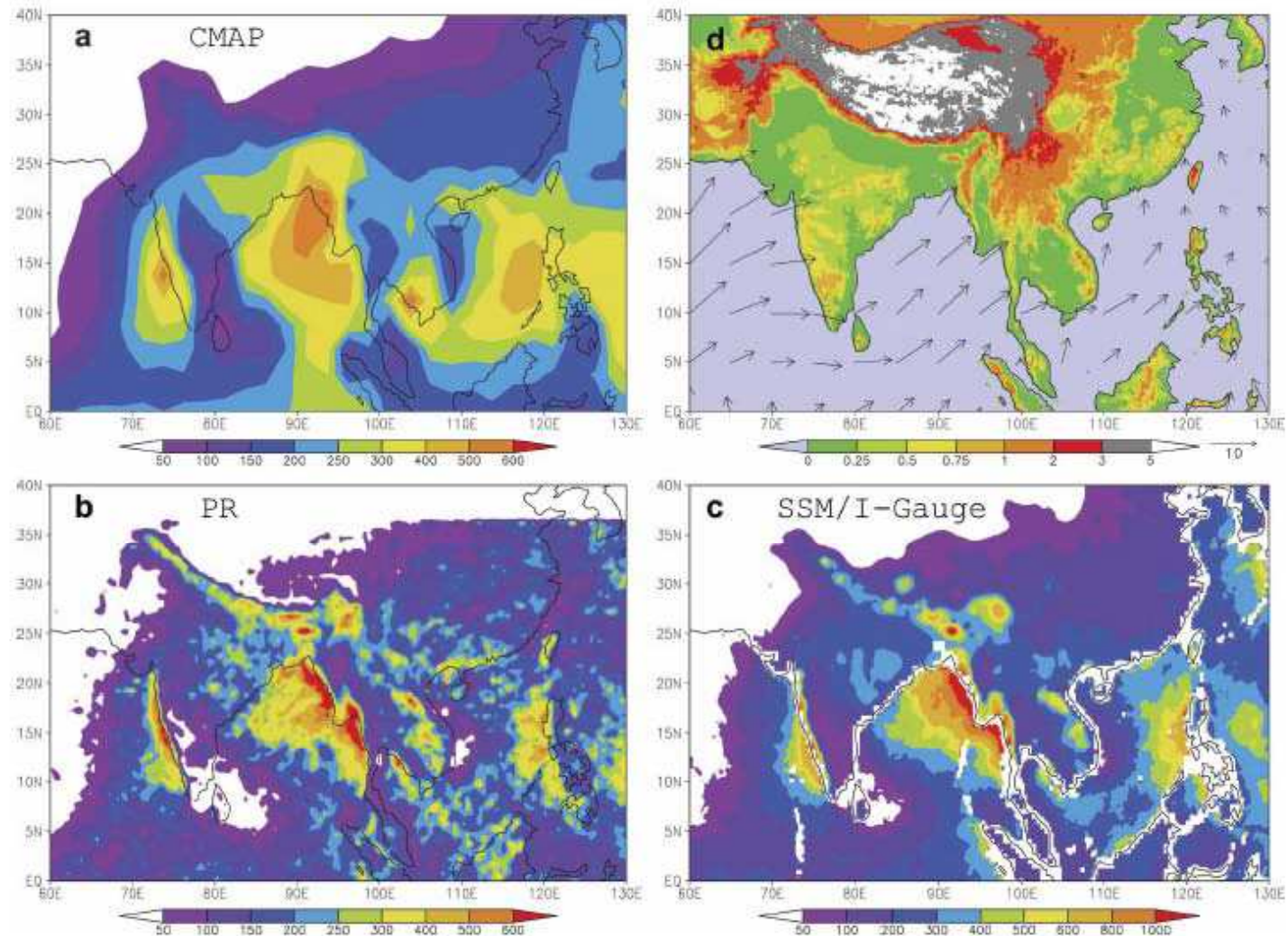
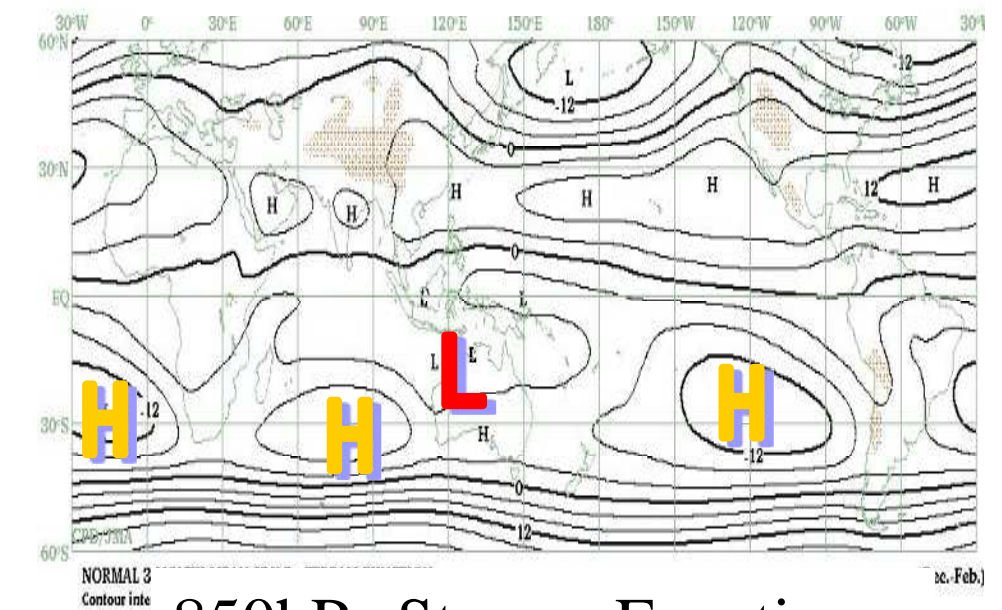
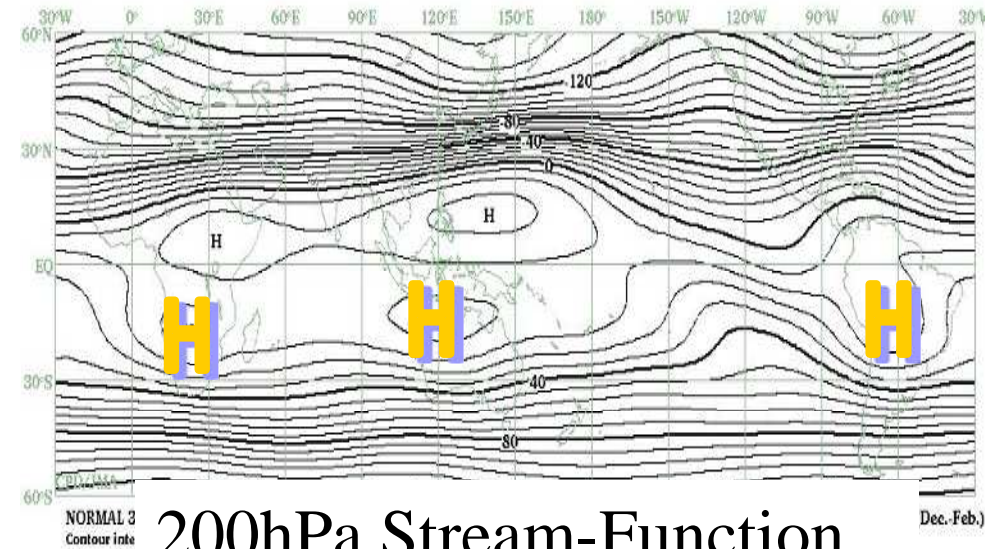
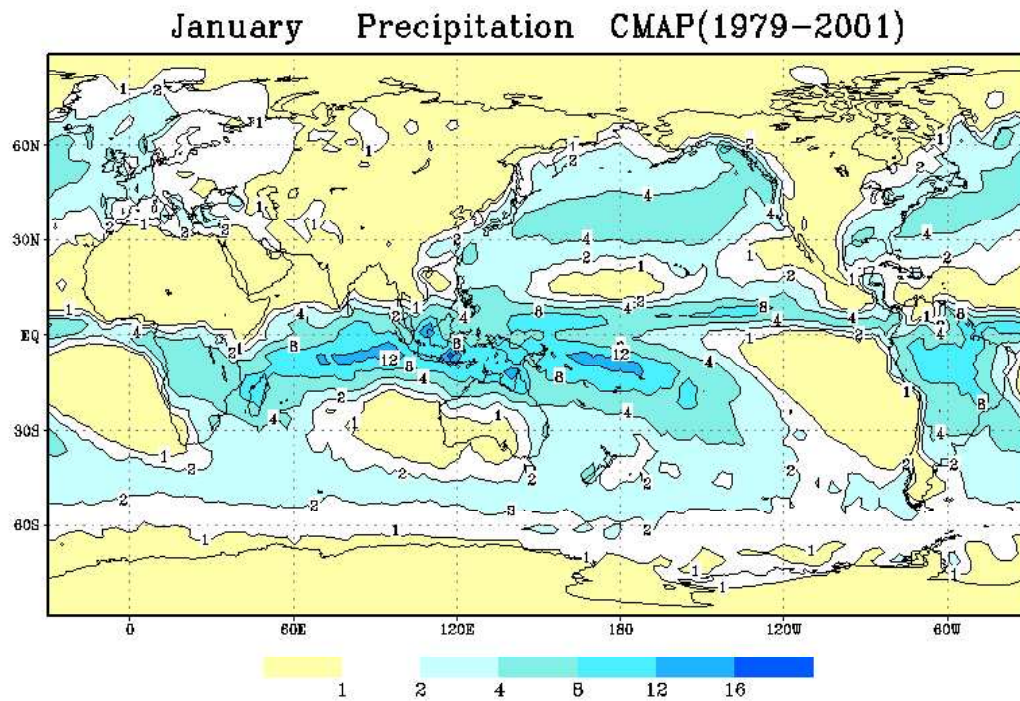


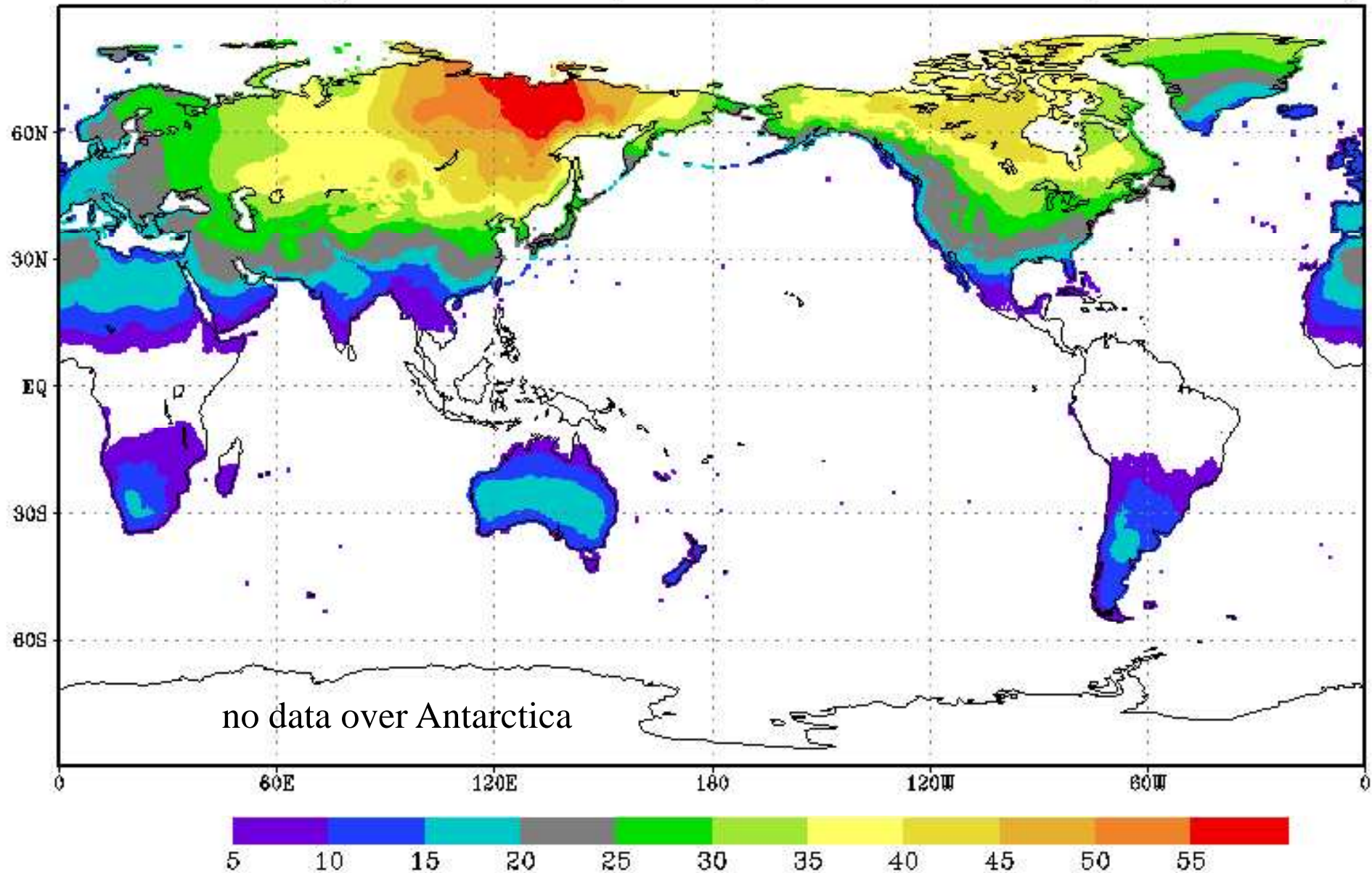
FIG. 1. Jun–Aug climatologies of surface precipitation (mm month^{-1}) based on (a) CMAP, (b) TRMM PR, and (c) SSM/I-gauge merged products. (d) Land orography (km) and QuikSCAT surface wind velocity (m s^{-1}).

Southern Summer Monsoon



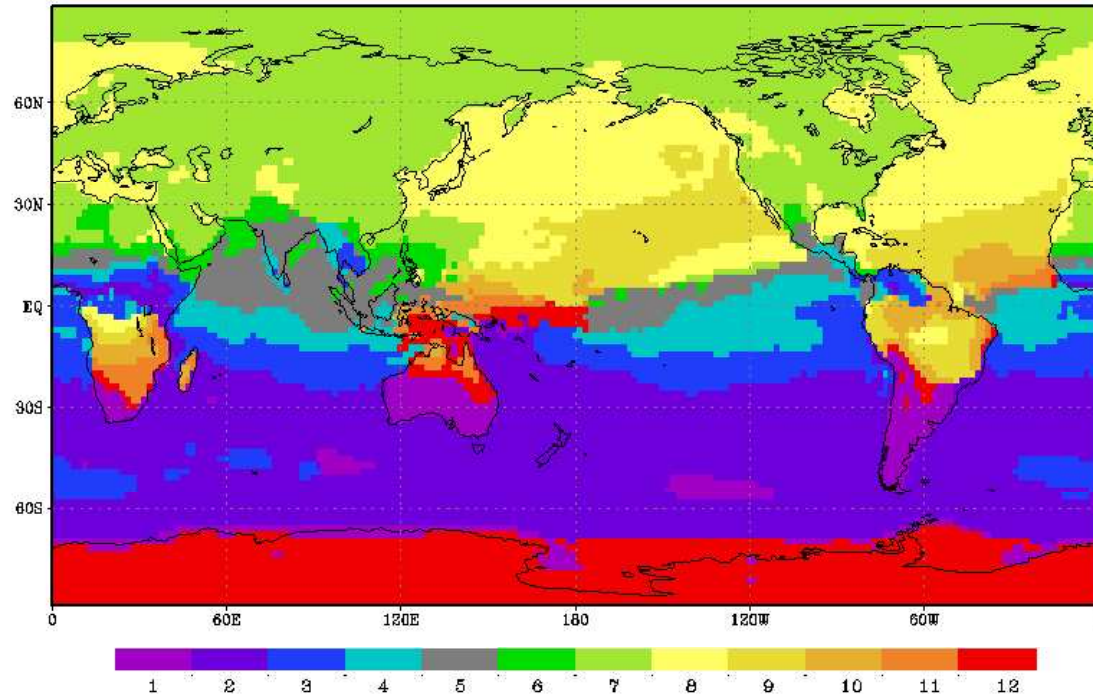
Annual temperature range

Annual Range of Monthly Temperature CRU(1901-1998)

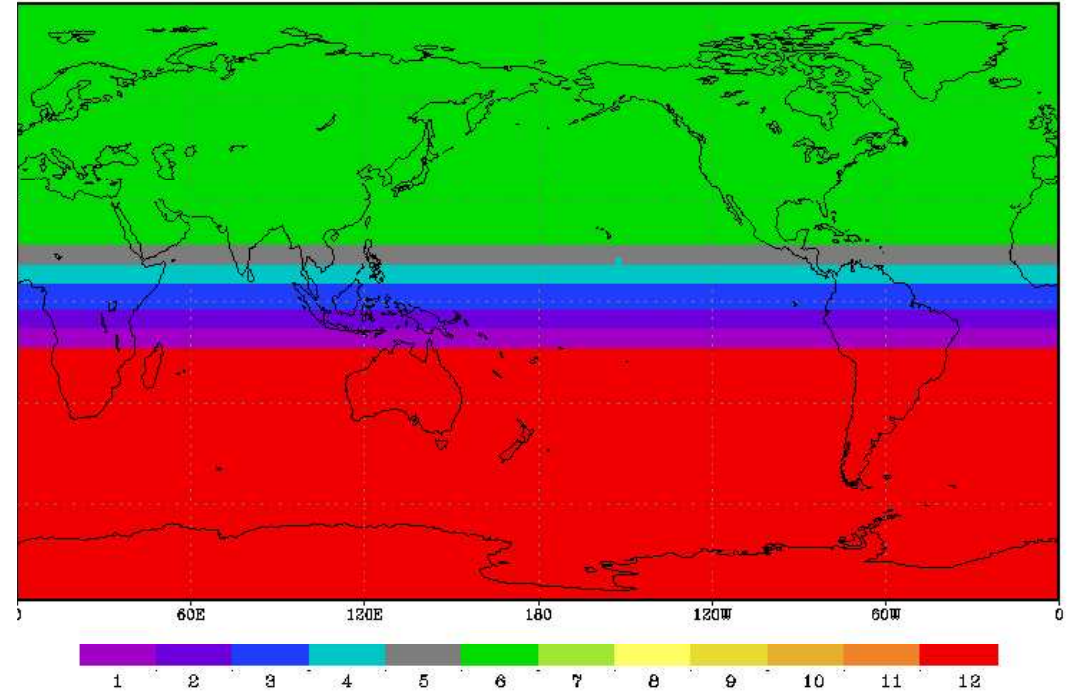


Month of maximum monthly mean temperature

Month of Maximum T2m NCEP(1949–2000)



Month of Maximum Downward Solar Radiation Flux at top

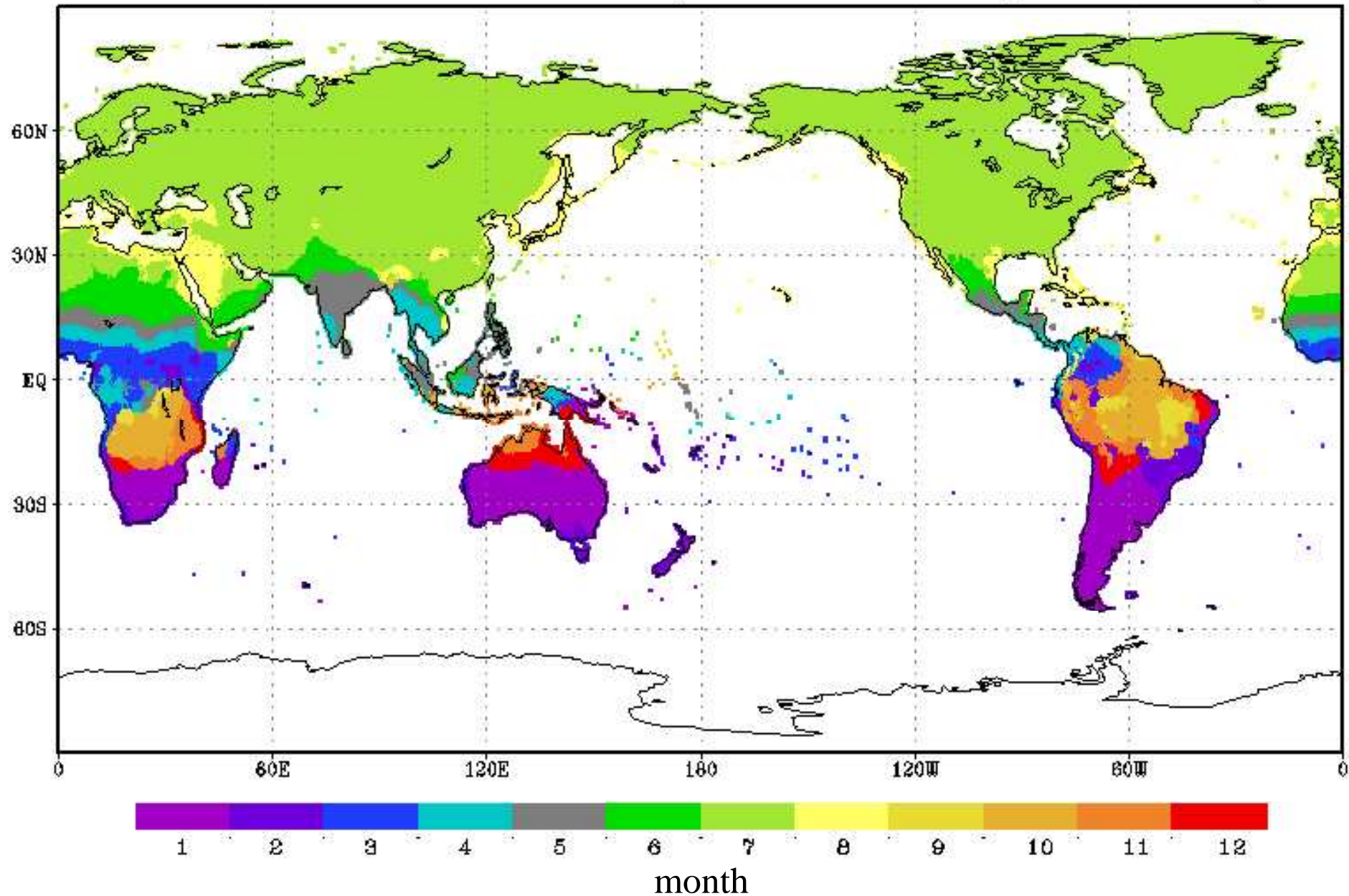


(Right) Downward solar radiation at the top of the atmosphere is maximum in June (December) poleward of about 15° latitude in the NH (SH). In the tropics, it is January, February, March, April and May at 10° S, 4° S, 2° N, 8° N and 14° N, respectively.

(Left) Actual month of maximum monthly mean temperature is quite different due to inertia of atmosphere, land and ocean. It is July over the continents and August over the oceans in the NH, but its distribution is not simple.

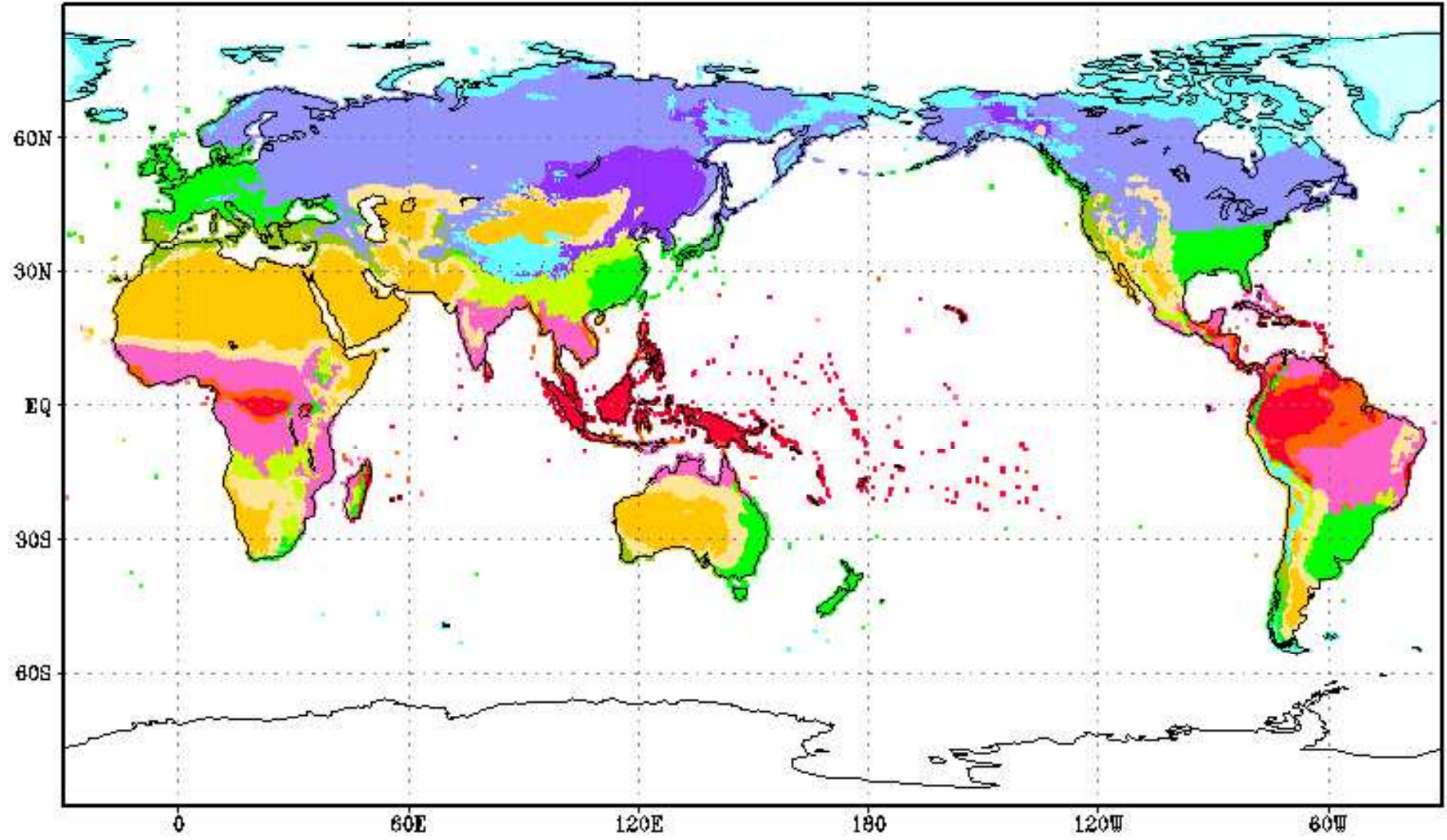
Month of maximum monthly mean temperature

Month of Maximum Temperature CRU(1901-1998)



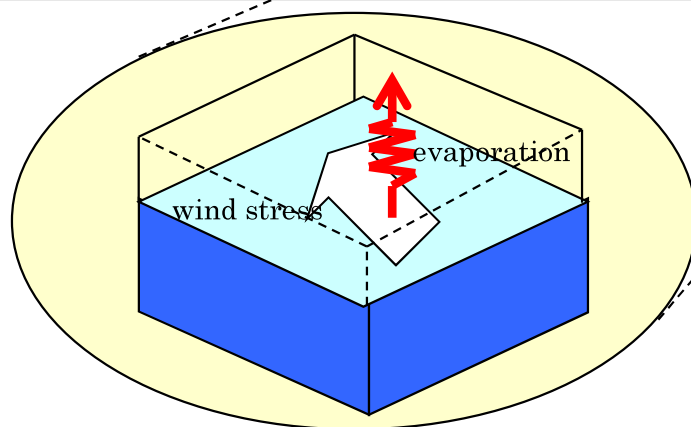
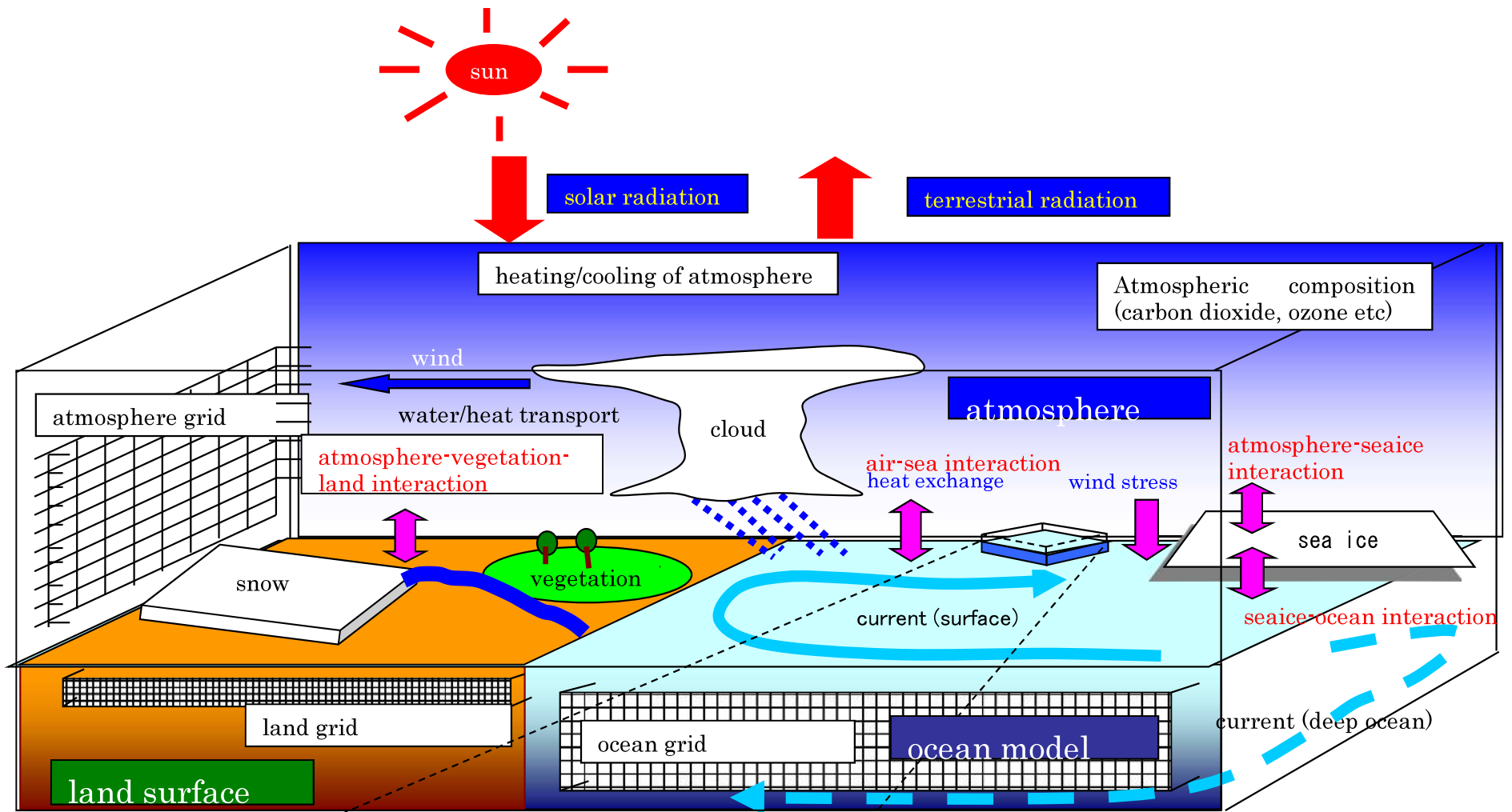
Koppen climate classification

Observation



Climate Modeling

A thick, horizontal yellow brushstroke underline that spans the width of the slide, positioned directly below the title text.

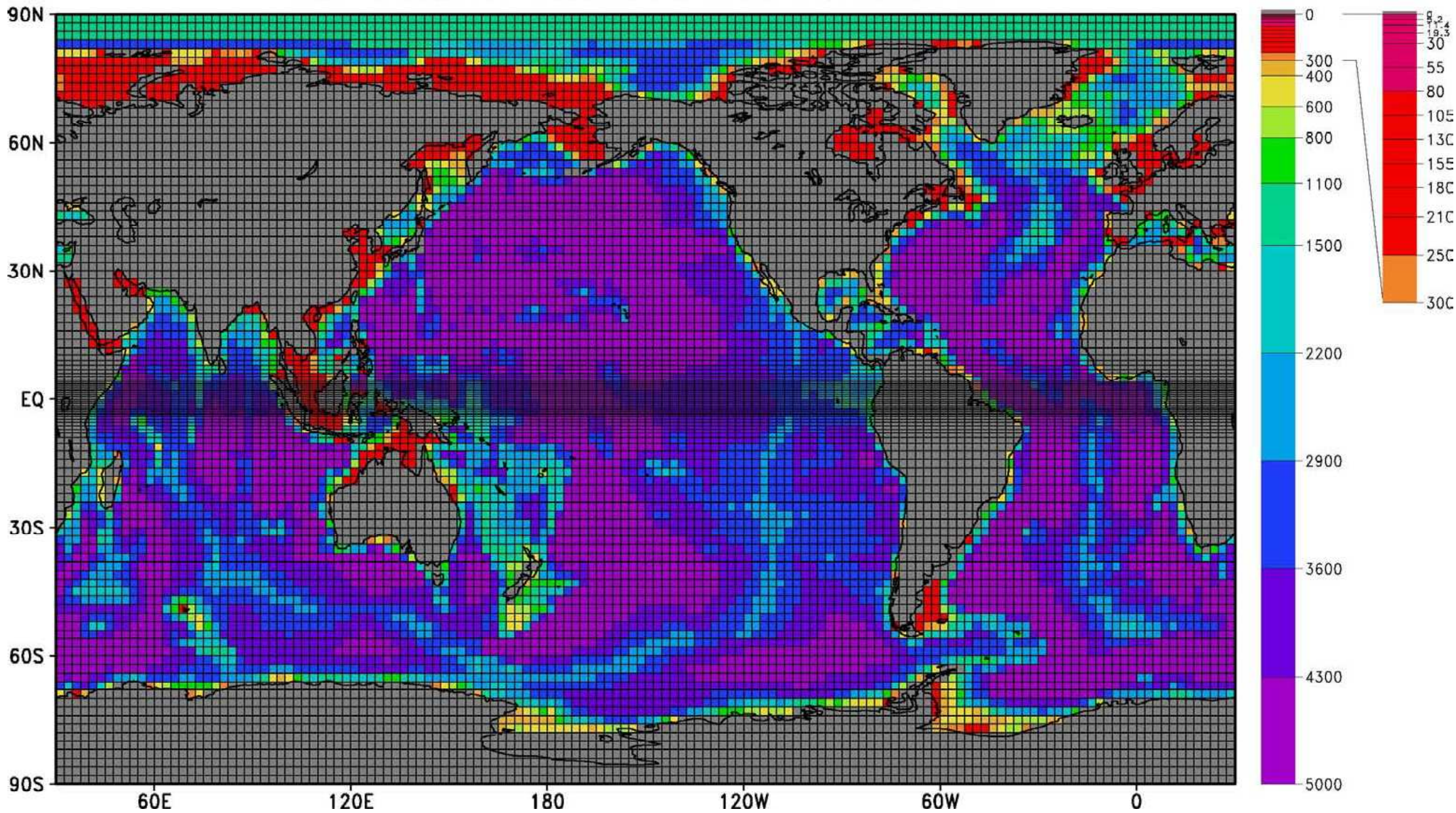


Schematic of climate model

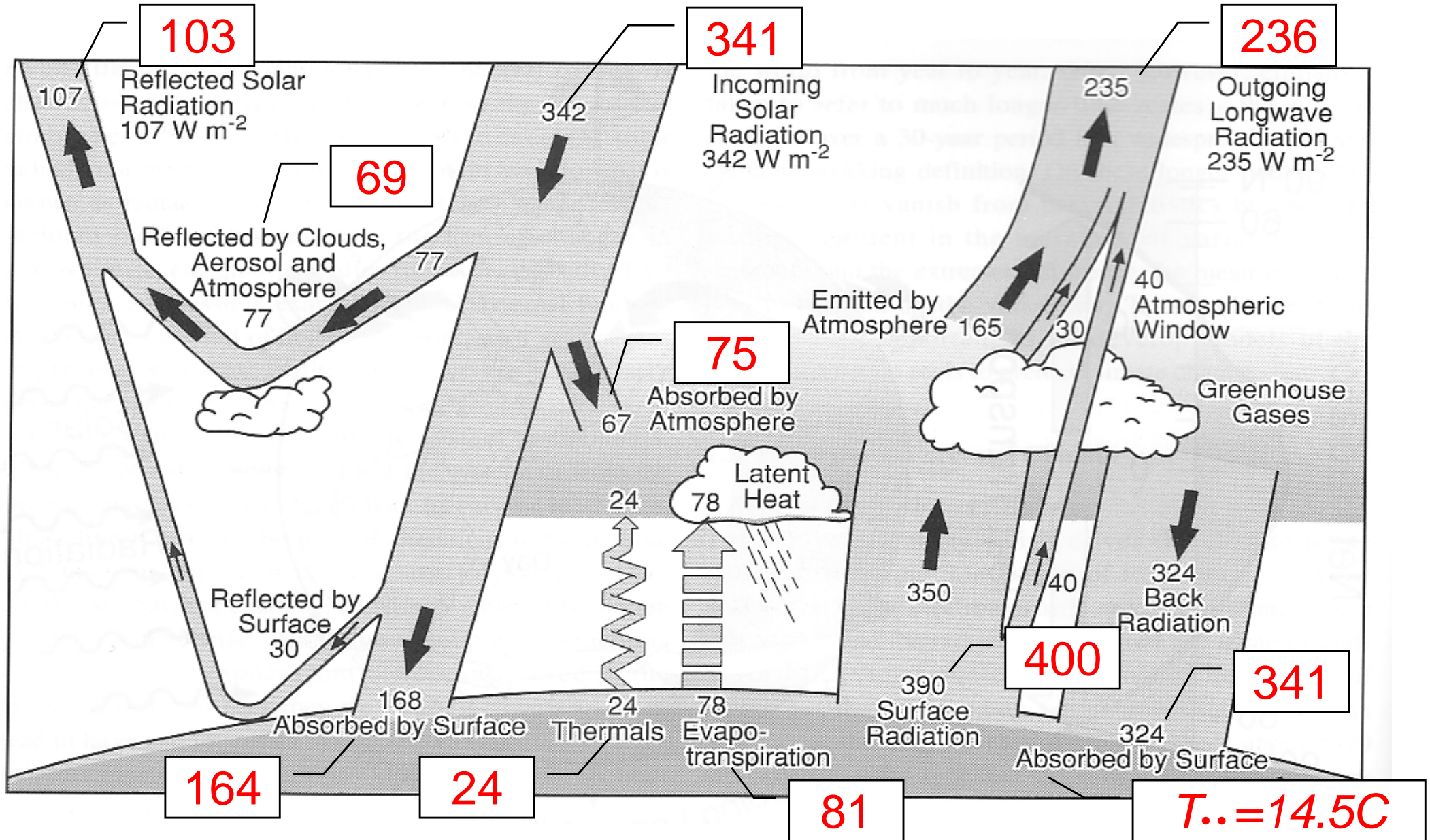
MRI Coupled Atmosphere-Ocean General Circulation Model (MRI-CGCM2)

- AGCM
 - MRI/JMA98
 - T42 (2.8x2.8), L30 (top at 0.4 hPa)
 - Longwave radiation - Shibata and Aoki (1989)
 - Shortwave radiation - Shibata and Uchiyama (1992)
 - Cumulus - Prognostic Arakawa-Schubert type
 - PBL - Mellor and Yamada level 2 (1974)
 - Land Surface - L3SiB or MRI/JMA_SiB
- OGCM
 - Resolution : 2.5x(0.5-2.0), 23layers
 - Eddy mixing : Isopycnal mixing, GM
 - Seaice : Mellor and Kantha (1989)
- Coupling
 - Time interval : 24hours
 - Flux adjustment: used “with” or “without”

MRI-CGCM2.2 OCEAN BOTTOM TOPOGRAPHY

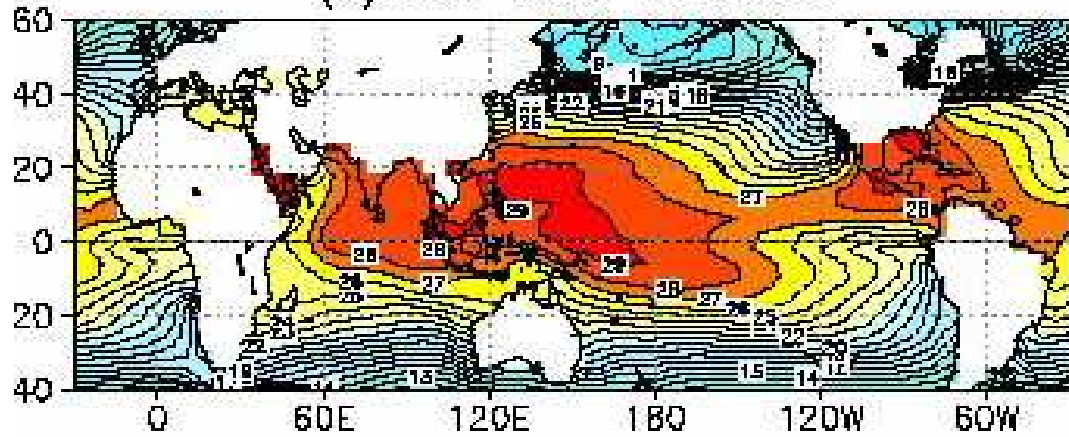


Climate Model Evaluation: Global Energy Balance

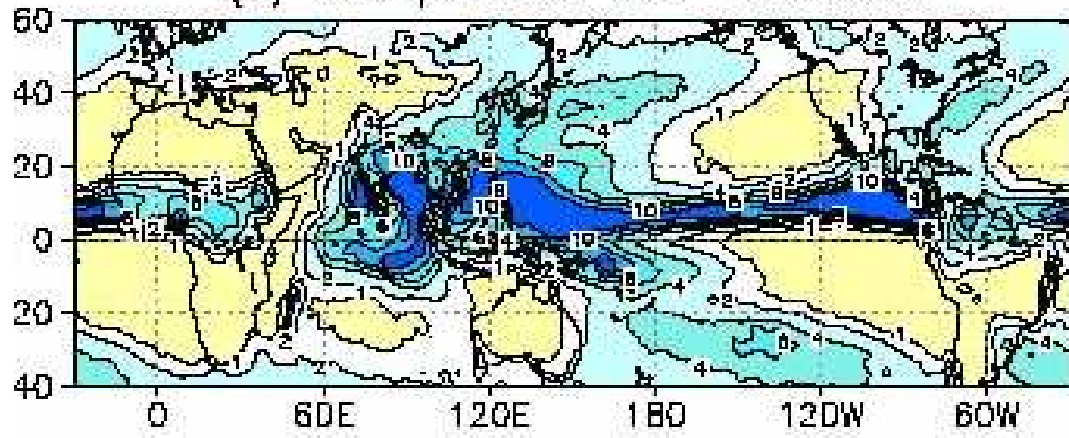


Obs

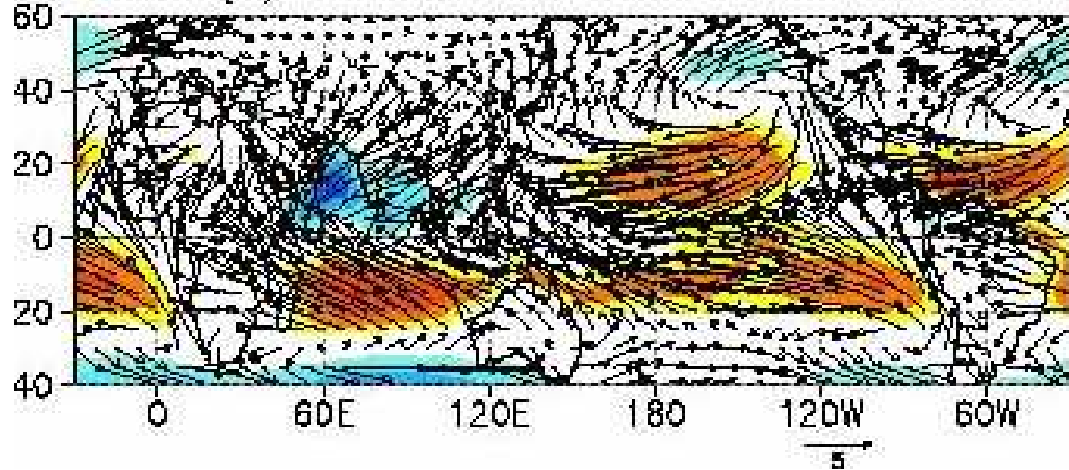
(a) SST JJA Observed



(b) Precipitation JJA Observed

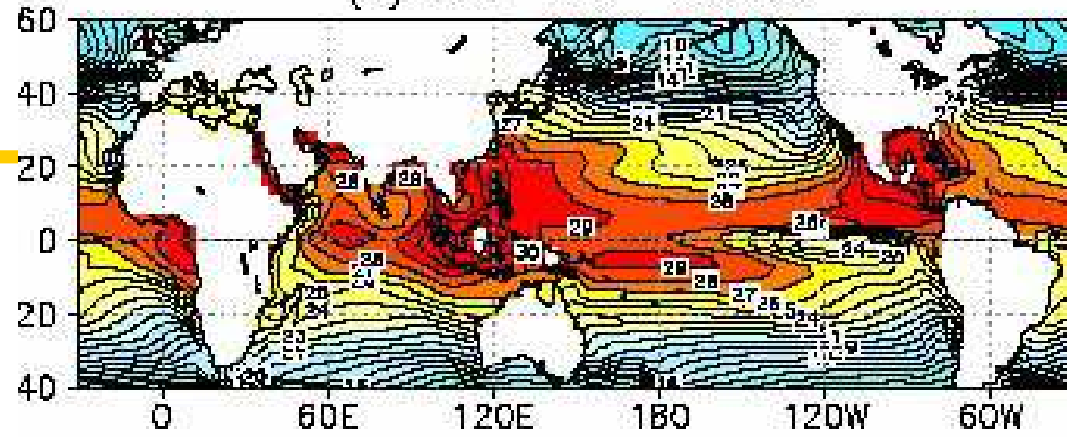


(c) Surface Wind JJA Observed

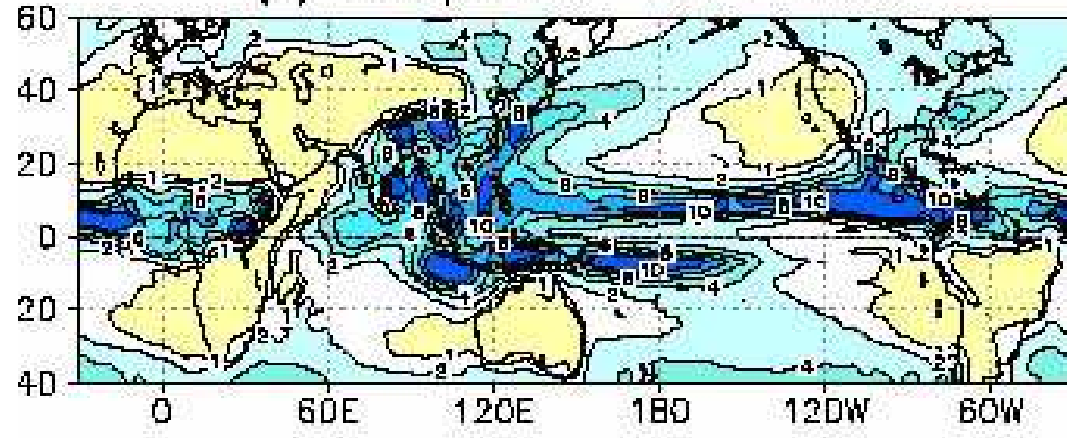


Model

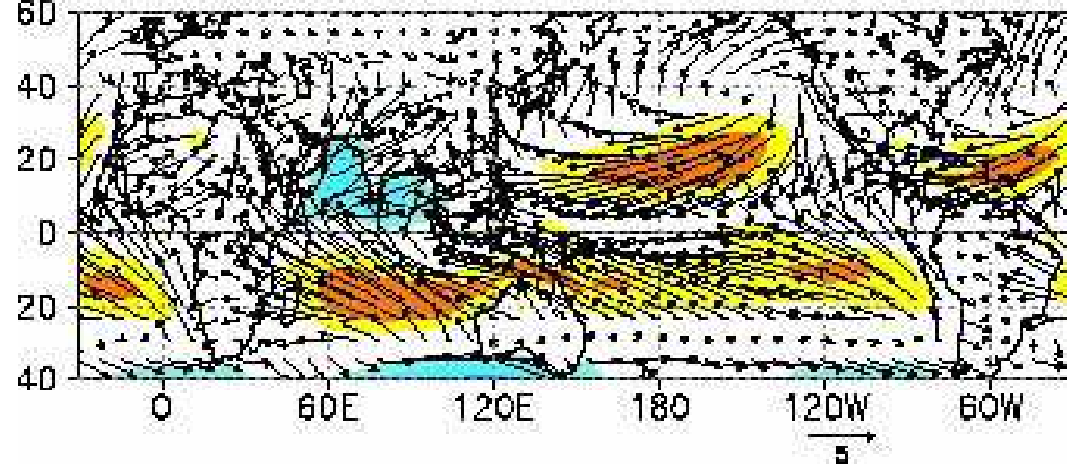
(a) SST JJA CGCM2



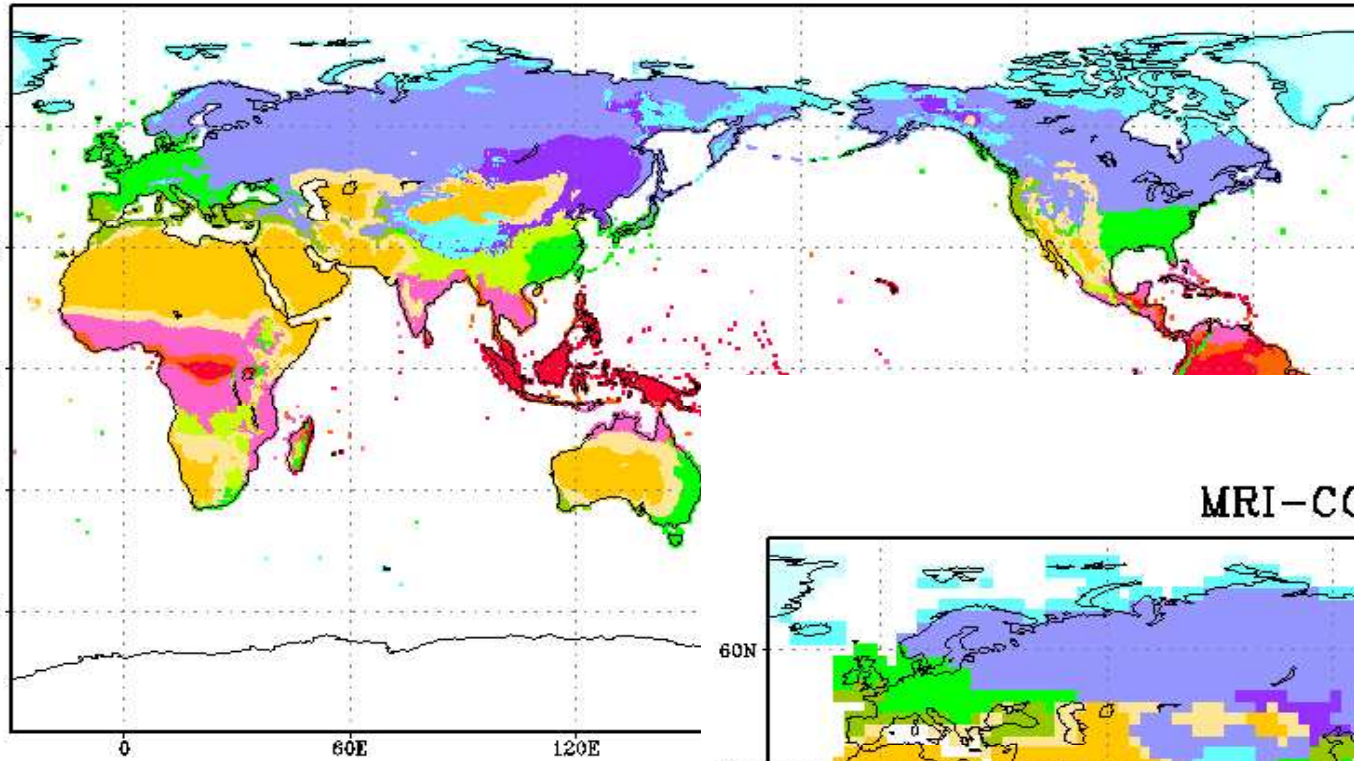
(b) Precipitation JJA CGCM2



(c) Surface Wind JJA CGCM2

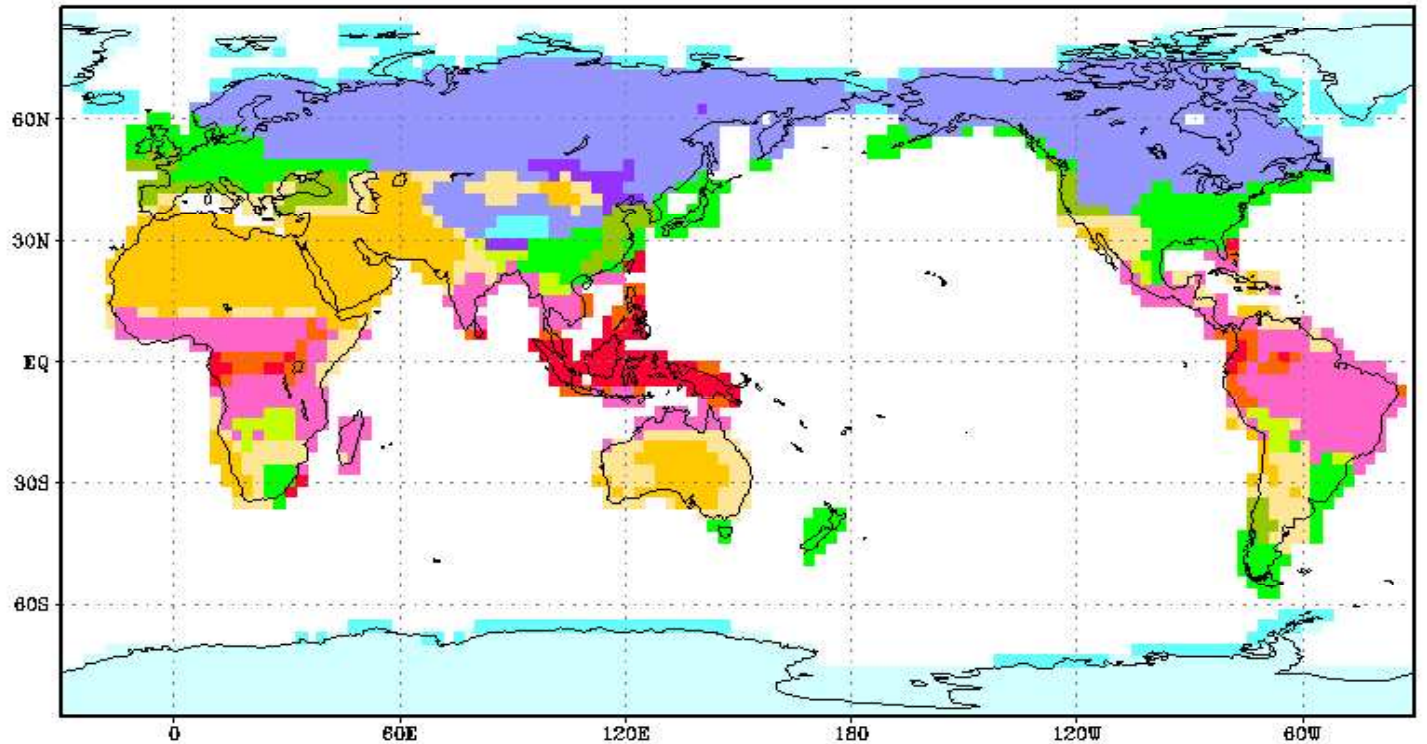


Observation



Koppen climate

MRI-CGCM2.2 control



Onset Pentad: the Julian pentad in which the relative climatological pentad mean rainfall rate exceeds 4 mm/day.

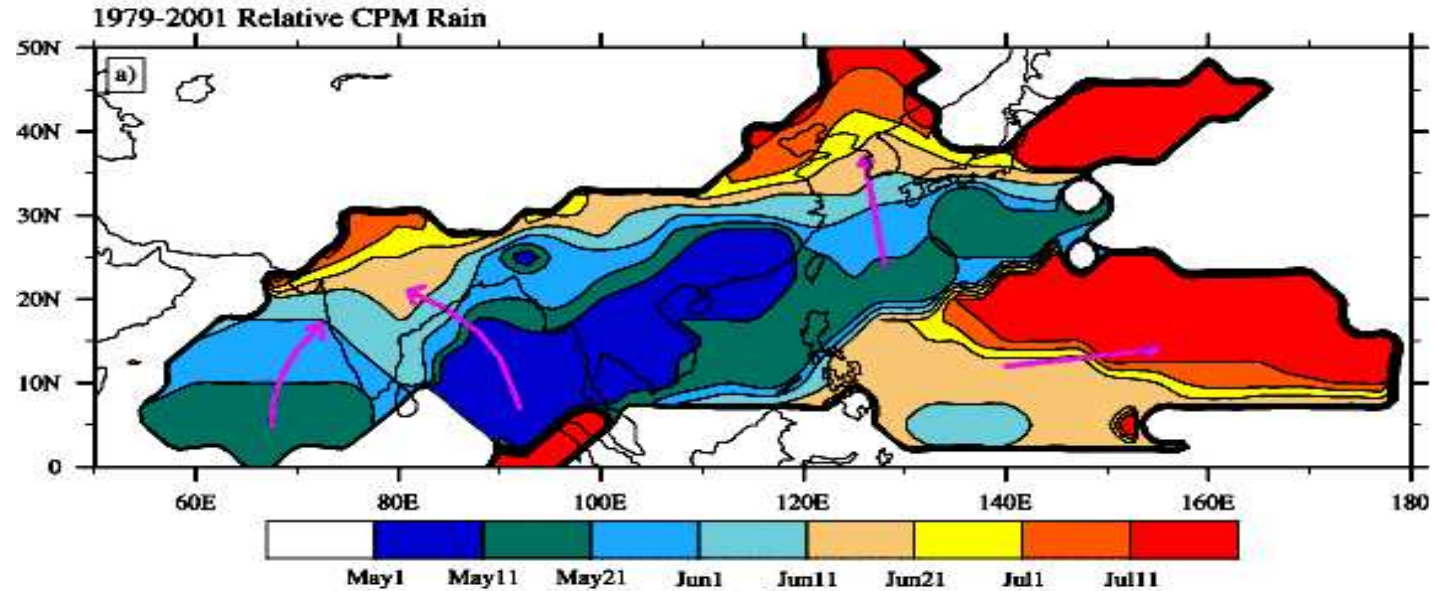
Indian region

- Northeastward progression over AS and the northwestward progression over the Bay of Bengal are well reproduced.

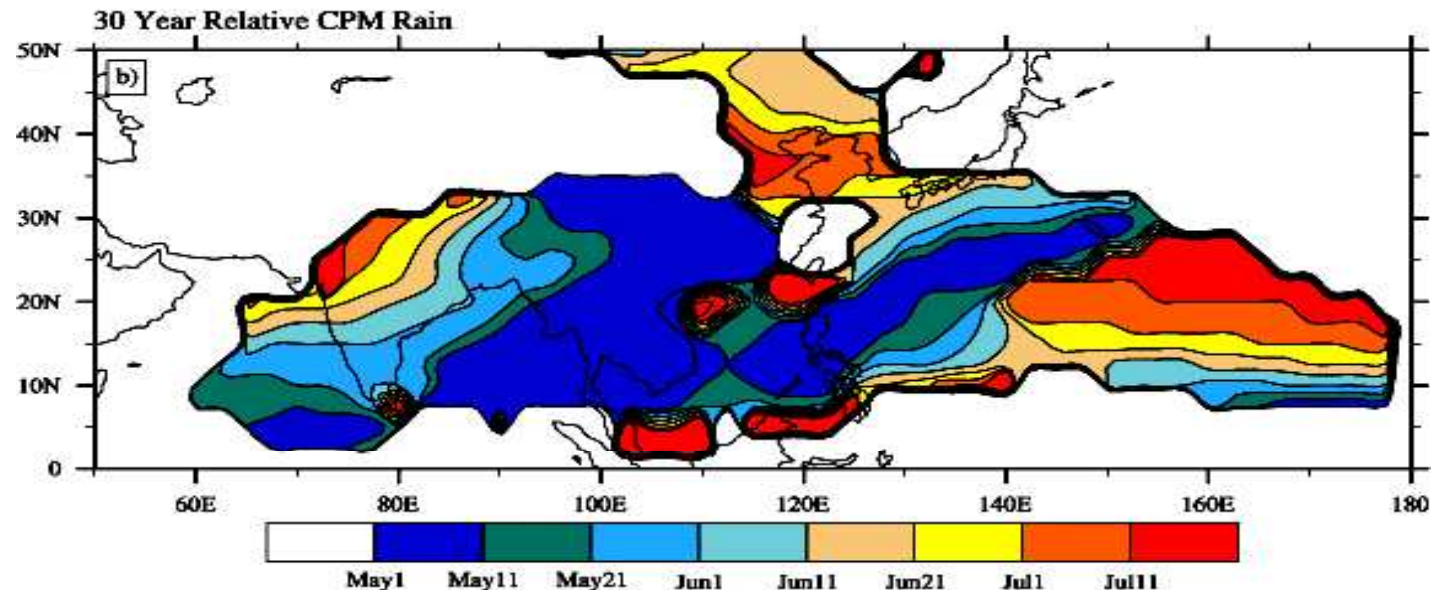
East Asia

- The model simulates earlier monsoon onset over southeast Asia.
- Onset over Indochina in early May, the mid-May onset over the SCS & later northward progression due to Meiyu/Baiu rainband are all simulated, although the precise timings differ slightly.
- In northern China, onset is earlier and precipitation is heavier.

Monsoon Onset Date Xie-Arkin Observation



MRI CGCM2.2.2 Simulation



Mean Evolution of Monsoon: Withdrawal

Withdrawal Date of Rainy Season

Withdrawal Pentad: the transitional pentad in which rainfall drops below 4 mm/day.

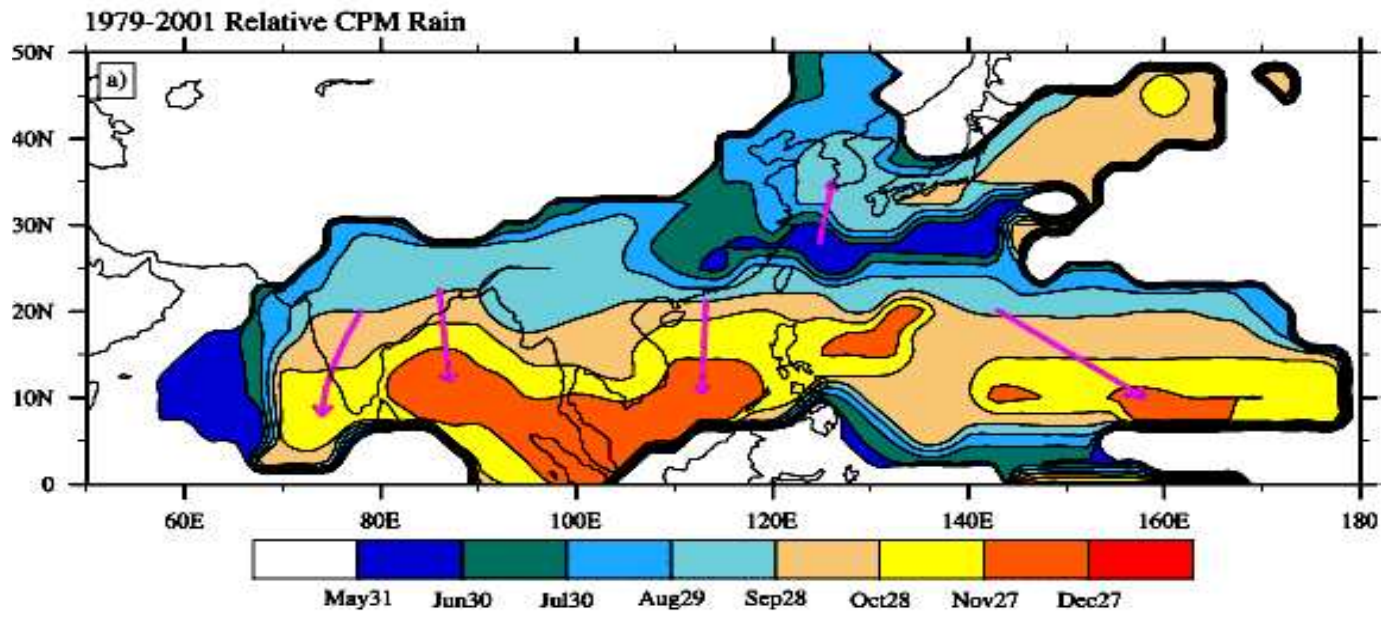
Observation shows:

➤ southward retreat of monsoon over India, southeast Asia and Western north Pacific

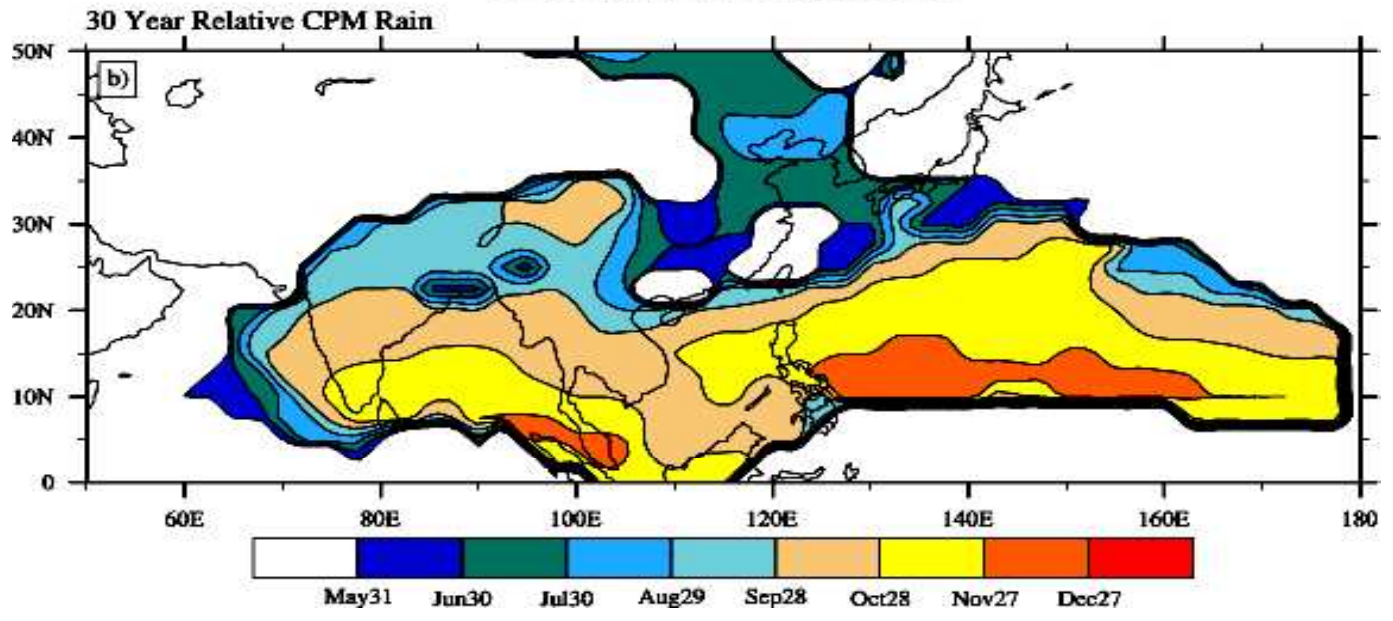
➤ northward retreat over East Asia.

Simulation close to observation.

Xie-Arkin Observation



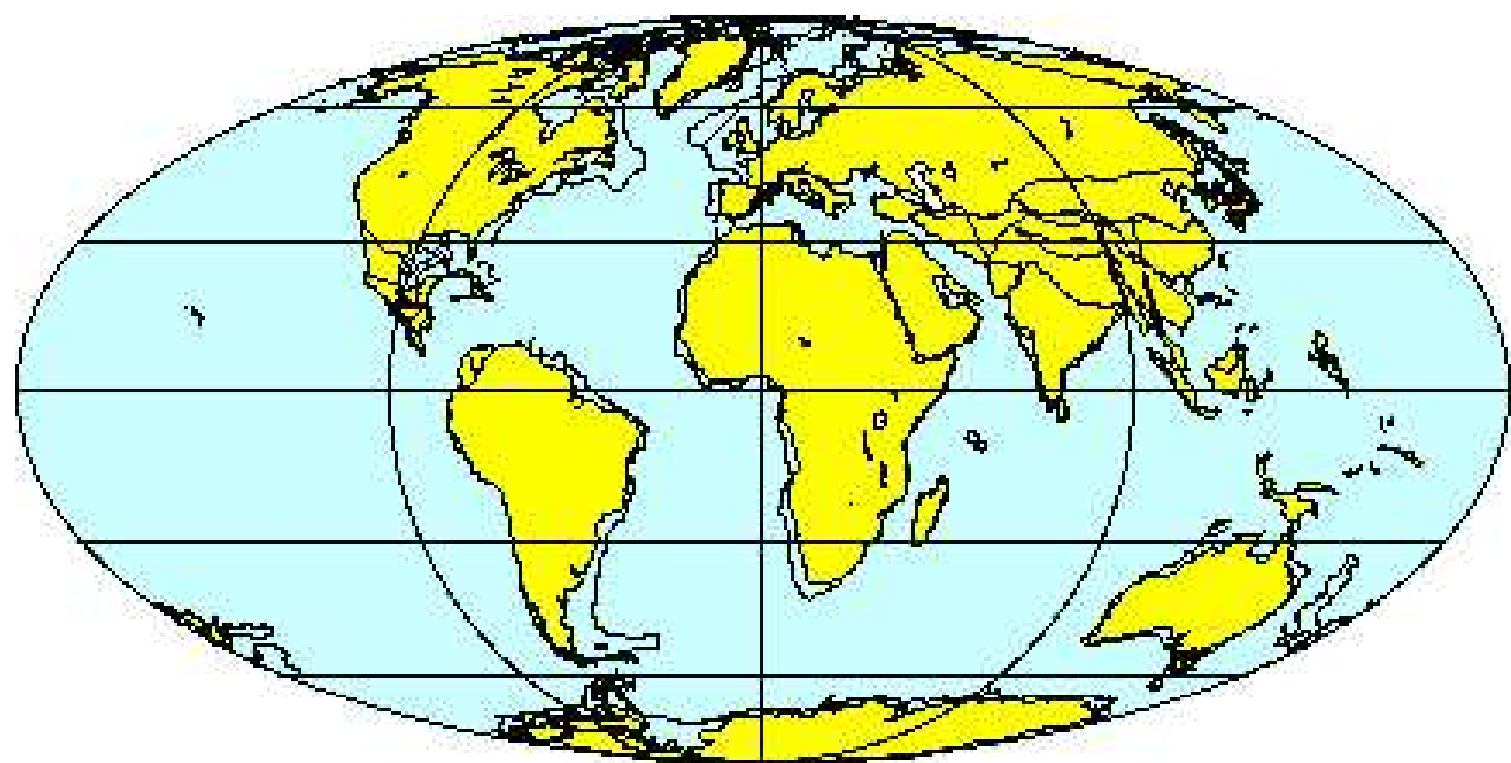
MRI CGCM2.2.2 Simulation



Role of orography on climate

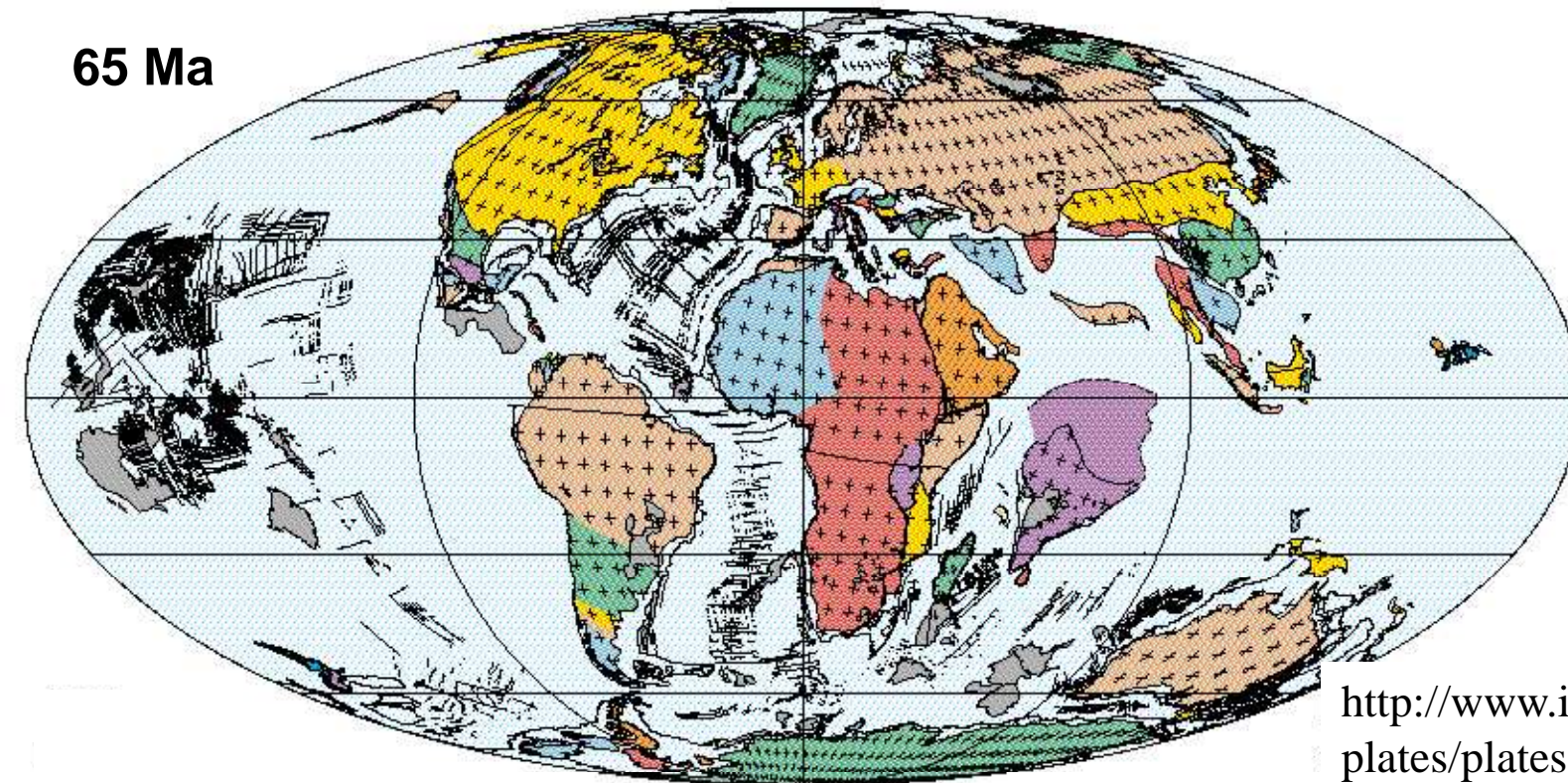


Plate Reconstruction

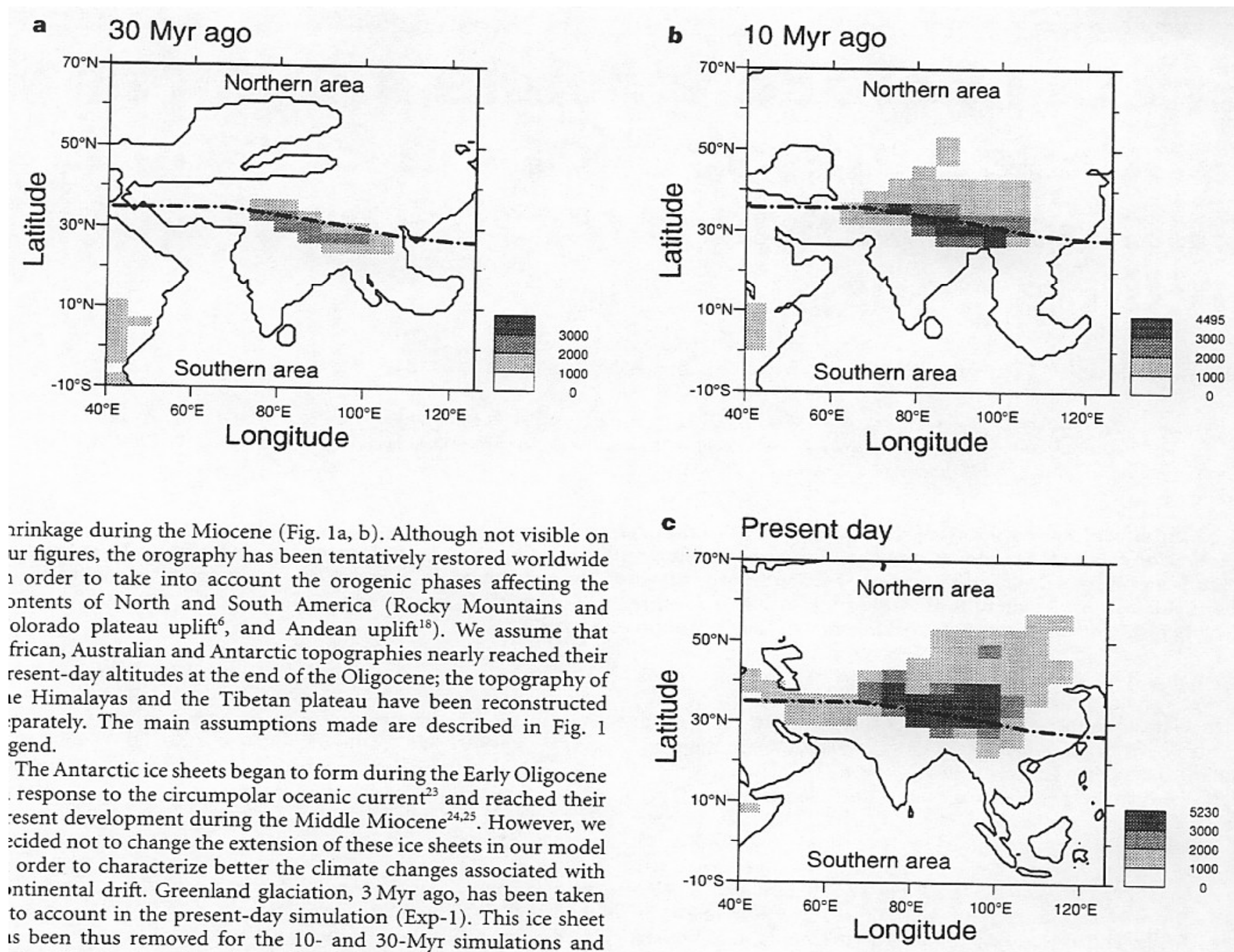


30 Ma

65 Ma



<http://www.ig.utexas.edu/research/projects/plates/plates.htm>



rinkage during the Miocene (Fig. 1a, b). Although not visible on our figures, the orography has been tentatively restored worldwide in order to take into account the orogenic phases affecting the contents of North and South America (Rocky Mountains and Colorado plateau uplift⁶, and Andean uplift¹⁸). We assume that African, Australian and Antarctic topographies nearly reached their present-day altitudes at the end of the Oligocene; the topography of the Himalayas and the Tibetan plateau have been reconstructed separately. The main assumptions made are described in Fig. 1 legend.

The Antarctic ice sheets began to form during the Early Oligocene in response to the circumpolar oceanic current²³ and reached their present development during the Middle Miocene^{24,25}. However, we decided not to change the extension of these ice sheets in our model in order to characterize better the climate changes associated with continental drift. Greenland glaciation, 3 Myr ago, has been taken into account in the present-day simulation (Exp-1). This ice sheet has been thus removed for the 10- and 30-Myr simulations and

Effect of mountains on climate

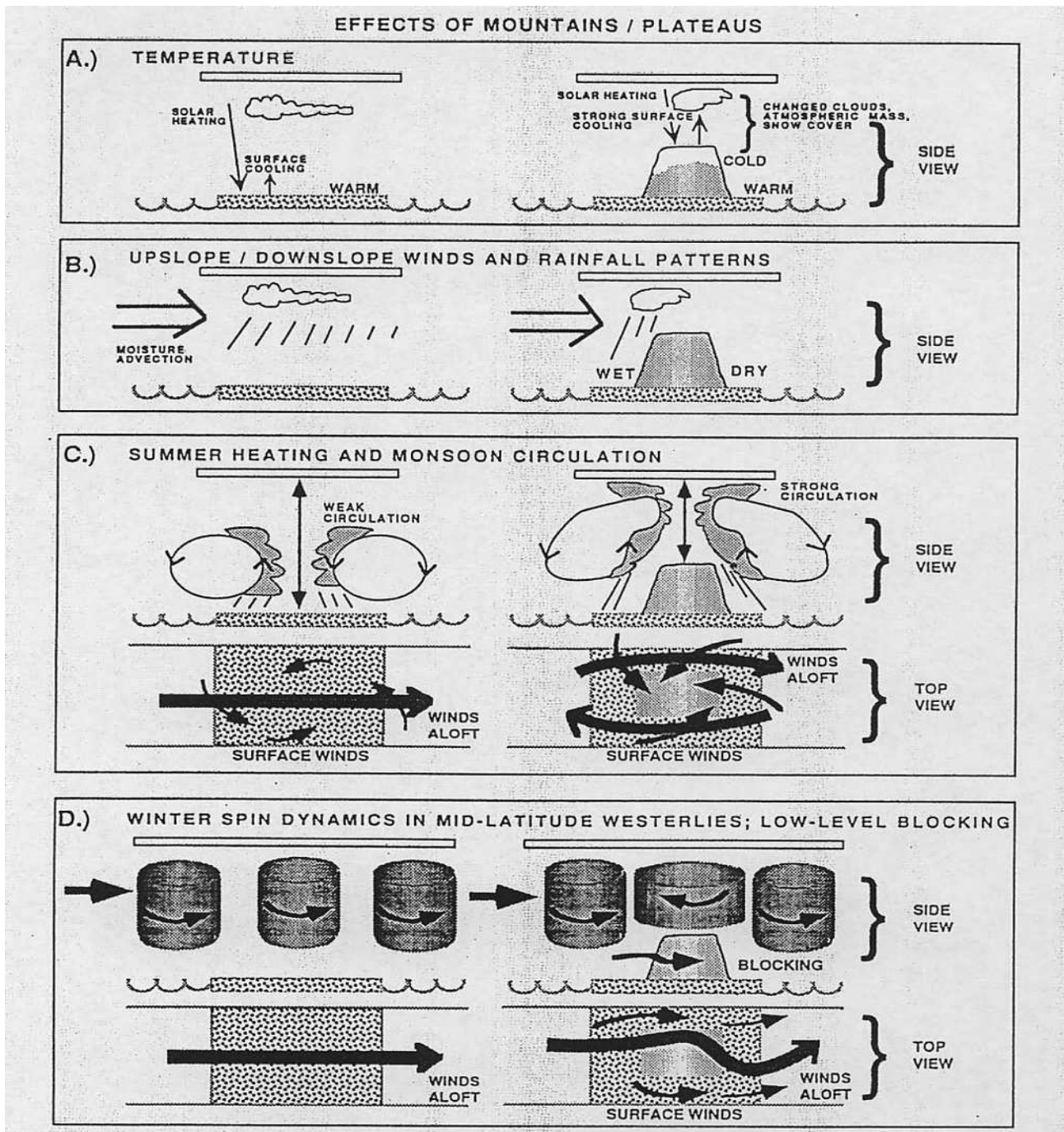
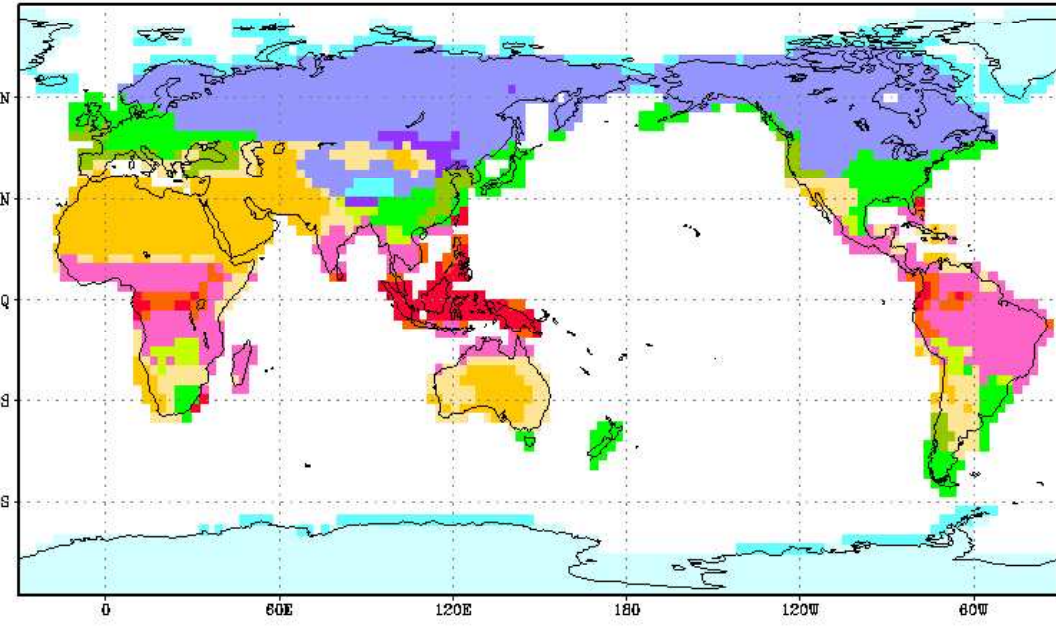


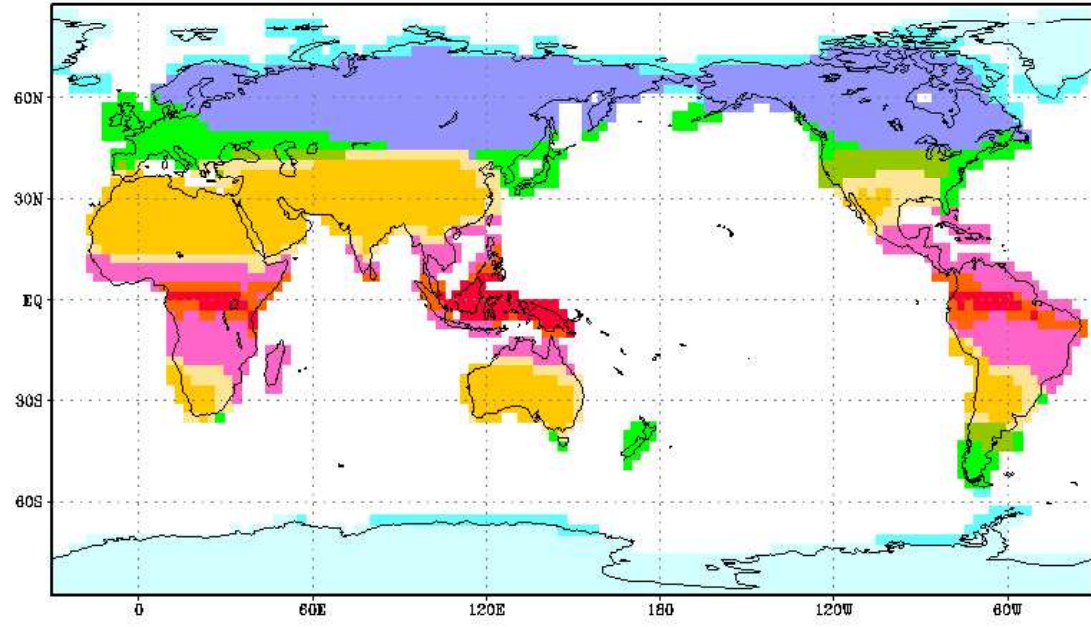
Figure 1. Effects of mountains/plateaus on climate: (a) temperature, (b) upslope/downslope winds and rainfall patterns, (c) summer heating and monsoon circulation, and (d) winter spin dynamics in mid-latitude westerlies, and low-level blocking. See text for explanation.

Effect of mountain: Koppen climate

MRI-CGCM2.2 control



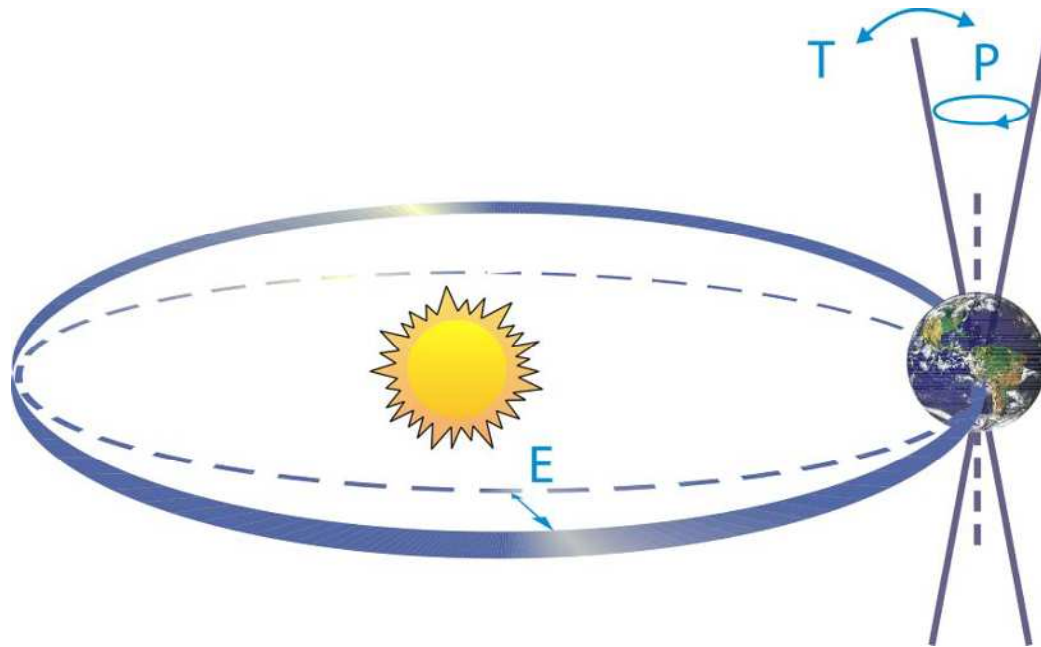
MRI-CGCM2.2 no-mountain



Paleo climate

A thick, horizontal yellow brushstroke underline that spans most of the width of the slide, positioned directly below the title text.

Orbital parameters

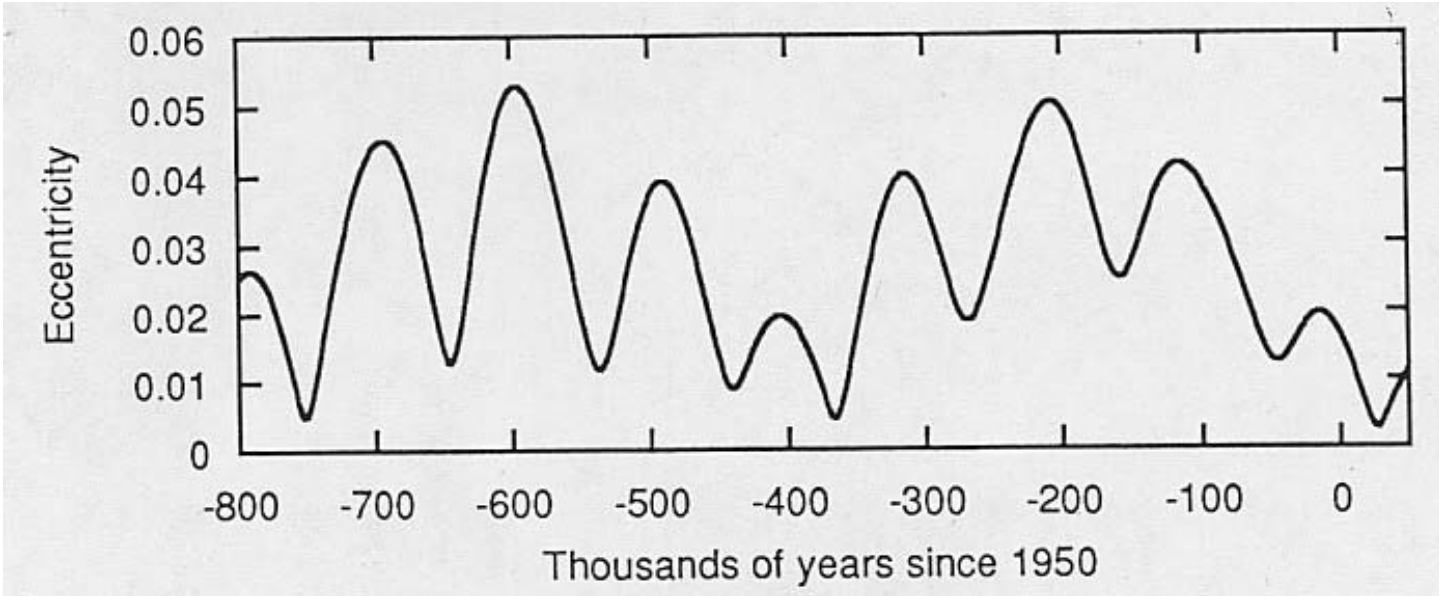


There are three fundamental ways the Earth's radiation balance can change, thereby causing a climate change:

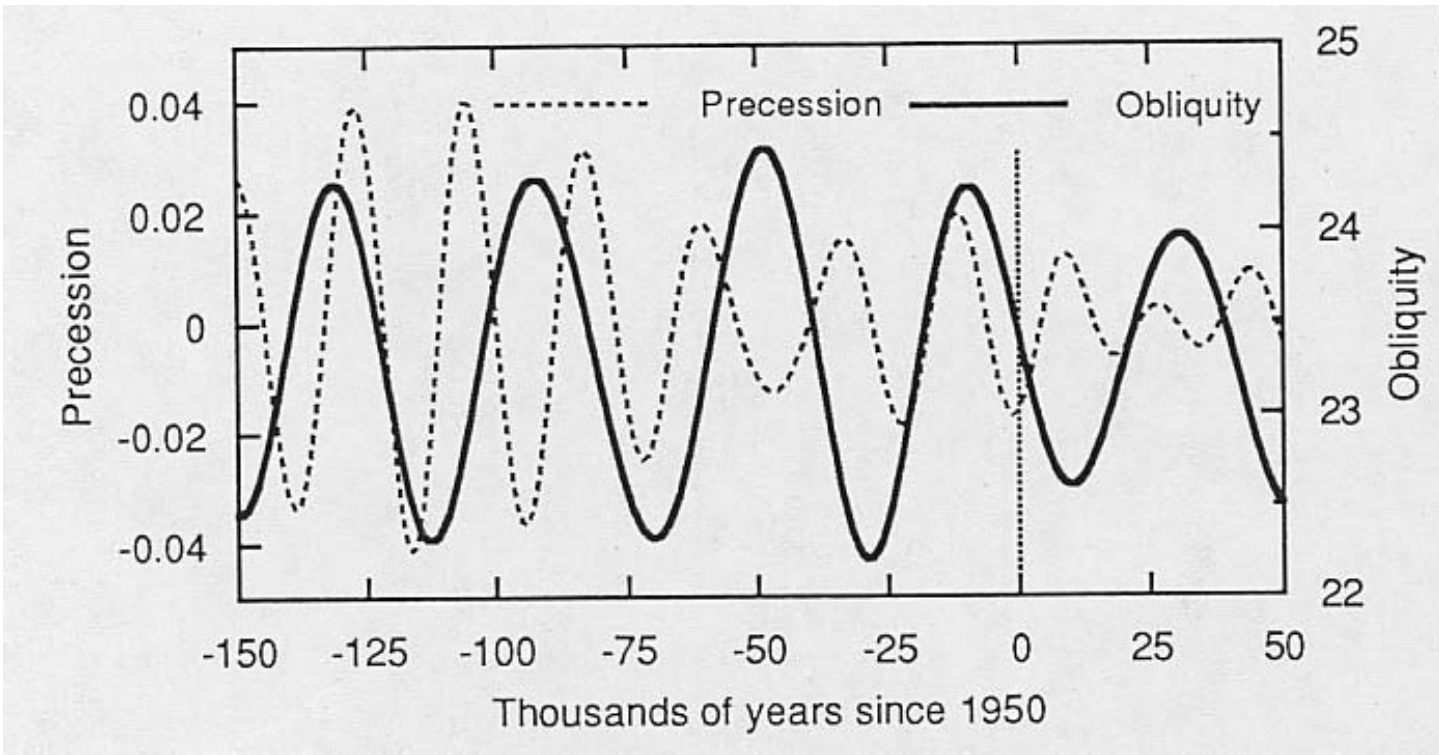
- (1) changing the incoming solar radiation (e.g., by changes in the Earth's orbit or in the Sun itself),
- (2) changing the fraction of solar radiation that is reflected (this fraction is called the albedo – it can be changed, for example, by changes in cloud cover, small particles called aerosols or land cover), and
- (3) altering the longwave energy radiated back to space (e.g., by changes in greenhouse gas concentrations).
- (4) local climate also depends on how heat is distributed by winds and ocean currents.

Schematic of the Earth's orbital changes (Milankovitch cycles) that drive the ice age cycles. 'T' denotes changes in the tilt (or obliquity) of the Earth's axis, 'E' denotes changes in the eccentricity of the orbit (due to variations in the minor axis of the ellipse), and 'P' denotes precession, that is, changes in the direction of the axis tilt at a given point of the orbit. Source: Rahmstorf and Schellnhuber (2006).

Eccentricity, Obliquity and Precession

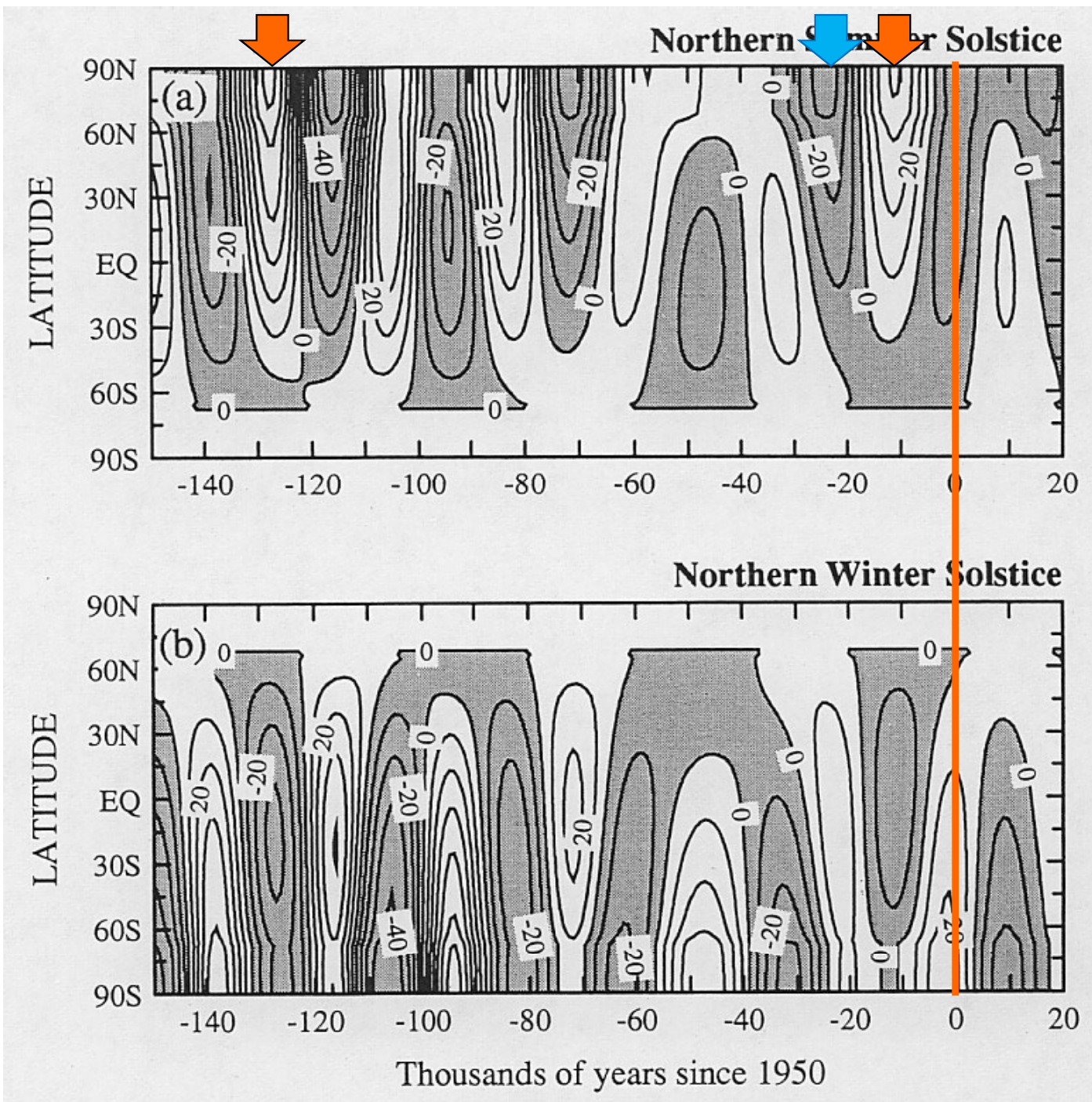


Eccentricity has a dominant period of 100,000 years



The obliquity and the precession have dominant periodicity of 40,000 years and 20,000 years, respectively

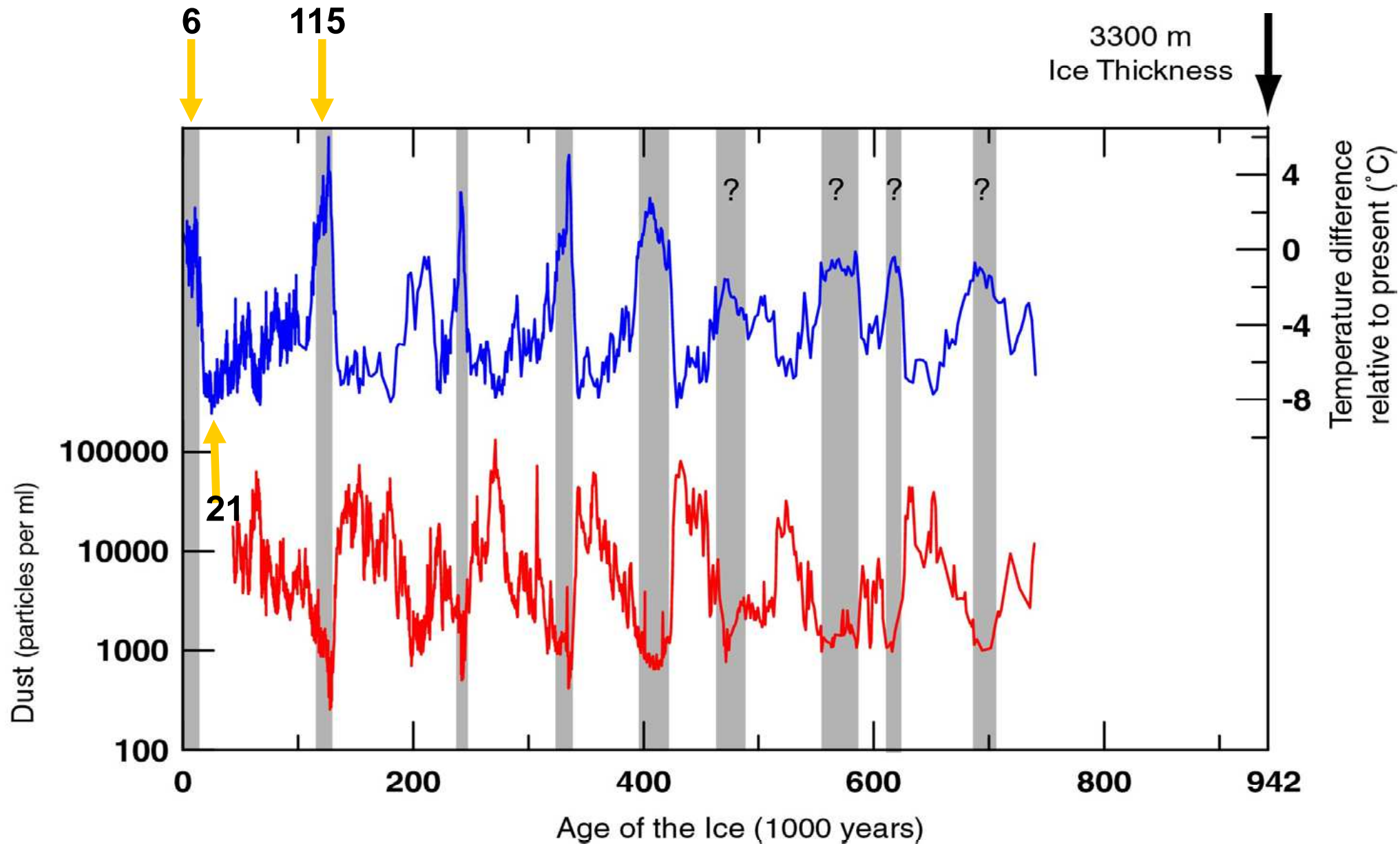
Insolation anomalies from 150,000 years ago until 20,000 years in the future



Insolation variations at NH summer solstice show amplitudes as large as 60 $W m^{-2}$ near the pole.

Large positive anomalies at 125,000 ya and 10,000 ya correspond fairly well with the times of the last two interglacial periods. The last glacial maximum about 20,000 ya was preceded by a relative minimum in NH summertime insolation.

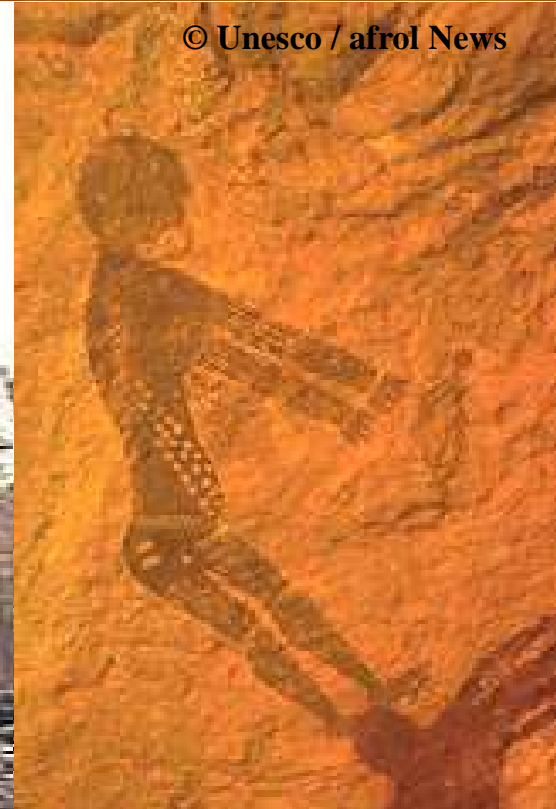
Dome Concordia (Antarctica): 740,000 years of climate change



(EPICA Members, 2004)

Mid-Holocene: 6ka

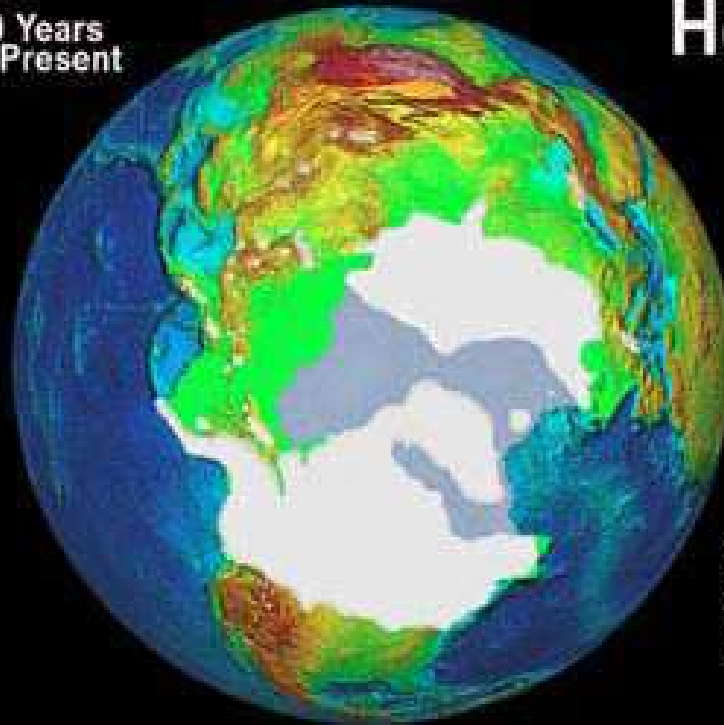
Tassili n'Ajjer, Algeria
- Sahara was greener



© Unesco / afrol News

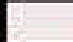
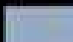

Last Glacial Maximum: 21ka

18,000 Years
Before Present

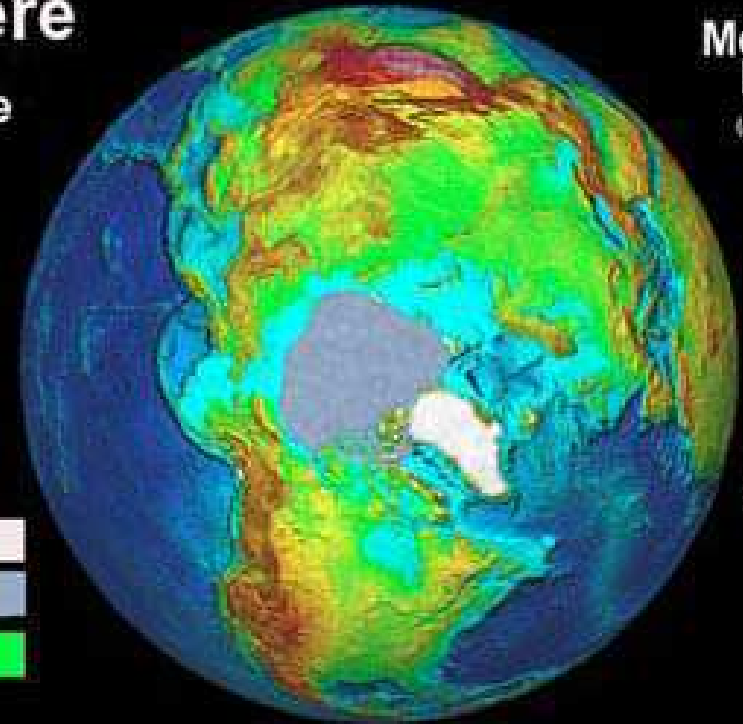


Northern Hemisphere Ice Coverage

Legend

Continental Ice	
Sea Ice	
Land Above Sea Level	

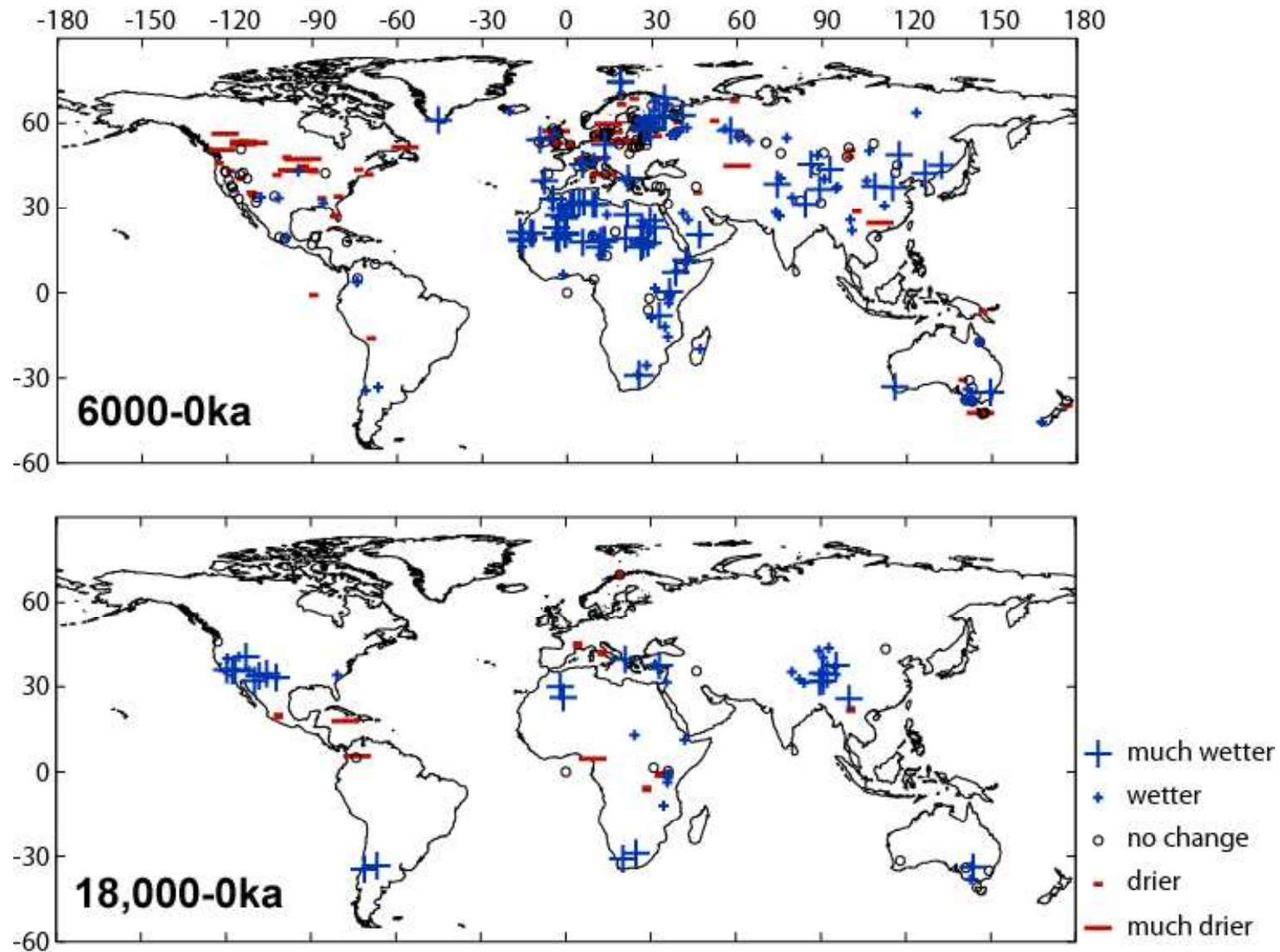
Modern
Day
(August)



Note: Modern sea ice
coverage represents
summer months.



PMIP data: global lake status



Jul-Aug-Sep Precipitation difference (6ka–0ka) with 4 CGCMs

